

**Investigation of TET protein function in  
safeguarding pluripotency through  
embryonic dormancy**

Inaugural-Dissertation

to obtain the academic degree

Doctor rerum naturalium (Dr. rer. nat.)

submitted to the Department of Biology, Chemistry, Pharmacy  
of Freie Universität Berlin

by Maximilian Stötzel

2024

Research work for this dissertation was performed under the supervision of Dr. Aydan Bulut-Karslioglu at the Max Planck Institute for Molecular Genetics in Berlin, Germany, from October 2019 to December 2023. This dissertation was submitted to the Department of Biology, Chemistry, Pharmacy of the Freie Universität Berlin in February 2024.

1<sup>st</sup> reviewer: Dr. Aydan Bulut-Karslioglu

Department of Genome Regulation

Max Planck Institute for Molecular Genetics, Berlin, Germany

2<sup>nd</sup> reviewer: Prof. Dr. Sigmar Stricker

Institute of Chemistry and Biochemistry, Laboratory of Biochemistry and Genetics

Freie Universität Berlin

Date of disputation: 25.04.24

# Table of contents

Acknowledgments.....	8
Declaration of Independence .....	9
List of Figures .....	10
List of Abbreviations .....	14
Abstract.....	16
Zusammenfassung.....	16
1. Introduction.....	18
1.1 Early embryonic development in the mouse .....	18
1.2 Transcription factors and signalling pathways of pluripotency.....	19
1.3 The chromatin state and epigenetics of pluripotency .....	20
1.4 DNA methylation .....	21
1.5 TET DNA demethylases and DNA hydroxymethylation.....	23
1.6 Cis-regulatory elements.....	25
1.5 Embryonic diapause .....	26
1.6 Embryonic diapause in <i>Mus musculus</i> .....	26
1.7 Molecular regulation of diapause in vivo and mTOR inhibition-induced model systems.....	28
Thesis Rationale and Aims .....	30
2. Results.....	31
2.1 Increased methylation is a feature of in vivo diapaused embryos, ex-vivo diapaused embryos, and mouse embryonic stem cells.....	31
2.1.1 Dormant ESCs and embryos show increased methylation.....	31
2.1.2 Activity of TETs is crucial to successfully establish a dormant state .....	32
2.1.3 Generation of a feeder-free system using E14 mESCs.....	35
2.2 TETs are required for ex vivo- and in vivo-diapause.....	39
2.2.1 Validation of the <i>Tet1/2</i> DKO dormancy phenotype in vivo .....	39

2.2.2 Pharmacological modulation of TET activity in ex vivo diapause .....	43
2.3 Epigenetic profiling of wild-type and <i>Tet1/2</i> double knock-out mESCs.....	46
2.3.1 <i>Tet1/2</i> DKO ESCs show global defects in DNA accessibility and transcription but not DNA methylation .....	46
2.4 TET dormancy targets.....	52
2.4.1 TETs demethylate enhancers and LINE elements in dormancy.....	52
2.4.2 TET dormancy targets are characterized by low methylation and enrichment of transcription factor motifs .....	53
2.5 TET activity facilitates the enrichment of transcription factors at dormancy targets ....	56
2.5.1 Dormancy targets show enrichment of the transcription factors KLF4, YY1, TFE3, ZFP57, SMAD3 and MYOD1.....	56
2.5.2 TFE3 accumulation is TET-dependent and dormancy specific.....	58
2.5.3 TFE3 and YY1 co-immunoprecipitate with TET1 .....	60
2.5.4 Knock-down of TFE3 prevents ESCs from entering a dormant state .....	61
2.6 TET dormancy targets are bookmarked .....	62
2.6.1 TET regulation of dormancy targets does not influence transcription of associated genes .....	62
2.6.2 Bookmarking of CREs and LINE1 repeats in dormancy .....	63
2.6.3 The dormant epigenetic signature is stably propagated.....	67
2.6.4 Reactivated wild-type ESCs show a homogeneous pluripotent phenotype .....	69
2.7 LINES are transiently upregulated and interact with TETs .....	70
2.7.1 Evolutionary young L1Md subfamilies are transiently upregulated in dormancy ..	70
2.7.2 L1Md repeats directly interact with TET proteins .....	72
3. Discussion.....	76
3.1 Dormancy and Methylation.....	76
3.2 TETs counteract increasing methylation and remodel the chromatin .....	78
3.3 A unique state of hypotranscription and globally increased DNA accessibility during the transition into dormancy .....	79

3.4 TETs facilitate transcription factor binding through demethylation .....	81
3.5 TETs as dormancy-specific transcription factor hubs .....	82
3.6 Bookmarking in the context of dormancy .....	82
3.7 Outlook: Dormancy type bookmarking in aging and disease.....	83
4. Methods.....	85
4.1 Cell lines and culture conditions .....	85
4.2 Animal experimentation .....	85
4.3 In vitro diapause .....	85
4.4 Embryo transfer and in vivo diapause induction .....	86
4.5 Flow-assisted cell sorting (FACS).....	86
4.8 Proliferation curves.....	87
4.9 Overexpression of wild-type or catalytically-dead TET1 and/or TET2.....	87
4.10 Generation of Tet1/2 DKO mESCs .....	87
4.11 Immunofluorescence (IF) imaging and quantifications.....	88
4.12 Western blotting .....	89
4.13 RNA-sequencing .....	90
4.14 ATAC-seq.....	90
4.15 Whole Genome Bisulfite Sequencing (WGBS) .....	91
4.16 CUT&Tag.....	92
4.17 Pathway expression analysis .....	94
4.18 Motif enrichment analysis .....	94
4.19 TF footprinting analysis.....	94
4.20 Definition of mESC enhancer sets.....	94
4.21 Generation of <i>Tet</i> KO embryos via Cas9-assisted gene editing .....	95
4.22 Guide RNA sequences.....	95
4.23 qPCR primers .....	96
4.24 FLASH.....	96

4.25 Immunoprecipitation (IP)-mass spectrometry .....	97
4.25 Enhancer and LIMd gene contact analysis .....	99
4.26 Gene knockdowns.....	99
5. Bibliography .....	100

# Acknowledgments

I thank Dr. Aydan Bulut-Karslioglu for granting me the opportunity to conduct my research in a remarkable academic environment. Aydan's dedication to scientific inquiry has been a constant source of inspiration for me. I express my gratitude for always guiding my pursuit of knowledge with your insightful mentorship and your infectious enthusiasm for science. I am excited to follow the scientific outputs that will emerge from the Bulut-Karslioglu laboratory.

I thank Prof. Dr. Alexander Meissner and Prof. Dr. Martin Vingron for their valuable feedback during my thesis advisory committee meetings.

I thank Prof. Dr. Sigmar Stricker for co-supervising this work.

I thank my mother for her unlimited support for the pursuit of my goals, for her guidance whenever it was needed and for believing in me. I thank my father for being a voice of reason, his support and his constructive feedback upon difficult decisions. I thank my sister for her support, her company for 25 years and valuable discussions alongside this journey.

I extend my gratitude to my whole family including my grandfather, grandmother, uncles, aunts, cousins and nephews. All together my family is an invaluable source of stability.

I thank my dear friend Vahid Asimi for inspiring discussions, honesty and unconditional friendship. You are among the outstanding brilliant minds I have met on this journey.

A special thanks goes to my best friends Konrad Klein, Jannik Weber, Florian Bockheim, Alexander Berlet, Julia Pawlick and Marco D'Aloia. I am deeply thankful for your unwavering support and encouragement during this journey. I look back at inspirational discussions and adventures that created life-time memories. I am looking forward to adventures that lie ahead. I consider all of you life-long friends with whom nothing is impossible.

# Declaration of Independence

Herewith, I certify that I have prepared and written my thesis independently and that I have not used any sources and aids other than those indicated by me.

Intellectual property of other authors has been marked accordingly. I also declare that I have not applied for an examination procedure at any other institution and that I have not submitted the dissertation in this or any other form to any other faculty as a dissertation.

Date: 23.02.2024

Signature:



# List of Figures

**Figure 1:** Early embryonic development and pluripotency

**Figure 2:** Derivation of ESCs, TSCs, and XEN cells from the epiblast, trophectoderm, and primitive endoderm, respectively.

**Figure 3:** DNA methylation and TETs.

**Figure 4:** Schematic overview of TETs and their promiscuous functions

**Figure 5:** Differences and commonalities of the proliferating and diapaused mouse embryo.

**Figure 6:** Immunofluorescence staining and quantification for 5mC and 5hmC in proliferating and mTORi treated mESCs.

**Figure 7:** Immunofluorescence staining and quantification for 5mC of E4.5, ex-vivo paused, in vivo diapaused, and reactivated (48h post in vivo diapause) mouse blastocysts.

**Figure 8:** Tet TKO does not sustain a pluripotent culture under mTORi conditions.

**Figure 9:** Rescue of *Tet* TKO dormancy defect via overexpression of wild-type, but not catalytic-dead (cd), *Tet1* or *Tet2*.

**Figure 10:** Mutations that lead to a catalytic dead version of Tet1 and Tet2.

**Figure 11:** Rescue of *Tet* TKO dormancy defect in the absence of DNA methyltransferase activity.

**Figure 12:** Schematic visualization of the *tet1* and *tet2* knock-out strategy.

**Figure 13:** PCR followed by gel-electrophoresis indicates successful deletion of *tet1* and *tet2*, respectively.

**Figure 14:** Western blot against Tet1 (left) and Tet2 (right) and Gapdh as a housekeeping control.

**Figure 15:** Bright field images and survival curves of wild-type and Tet1/2 DKO ESCs (E14 cells, feeder-independent) treated with the mTOR inhibitor INK128.

**Figure 16:** Alkaline phosphatase staining of an independently generated, feeder independent *Tet1/2* DKO ESC line in normal and mTORi conditions.

**Figure 17:** Flow cytometry analysis of SSEA1 expression levels (a pluripotency marker) in wild-type and *Tet1/2* DKO cells in normal and mTORi conditions.

**Figure 18:** Flow cytometry analysis of apoptosis levels in wild-type and *Tet1/2* DKO cells in normal and mTORi conditions.

**Figure 19:** Overview of genetic and pharmacological TET loss-of-function experiments.

**Figure 20:** Schematics of Cas9-assisted *Tet* deletions via zygotic electroporation.

**Figure 21:** Phenotype of *Tet* TKO vs control embryos collected at E8.5 after retransfer.

**Figure 22:** RT-qPCR showing expression levels of *Tet1/2/3* RNAs in control vs. targeted embryos.

**Figure 23:** Survival curves of intact blastocysts in culture comparing *Gfp*-KO (control) and *Tet1/2/3* TKO.

**Figure 24:** Survival curves of intact blastocysts in culture comparing *Gfp*-KO (control), *Tet1/2* DKO and wild-type. n, number of embryos used in each experiment.

**Figure 25:** In vivo diapause efficiency of retransferred control or *Tet1/2* DKO blastocysts.

**Figure 26:** Survival curves of intact blastocysts in culture comparing DMSO treated (control) and Bobcat339 treated embryos.

**Figure 27:** Survival curves of intact blastocysts in culture supplemented with the TET cofactor  $\alpha$ -ketoglutarate or vitamin C.

**Figure 28:** Bright field images of representative embryos captured on indicated days of pausing.

**Figure 29:** Experimental workflow to profile transcriptional and chromatin features of ESCs entering mTORi-induced dormancy.

**Figure 30:** Principal components analysis (based on 5000 most variable genes between 0h and 144h wild-type) of all RNA-seq samples.

**Figure 31:** Spike-in normalized bulk RNA-seq heatmap showing expression of all genes over time in wild-type vs *Tet1/2* DKO ESCs treated with mTORi.

**Figure 32:** Differentially expressed genes in *Tet1/2* DKO vs. wild-type at 72h of mTORi treatment.

**Figure 33:** Correlation of pathway expression in wild-type and *Tet1/2* DKO ESCs at 24h and 72h of mTORi treatment.

**Figure 34:** DNA methylation levels in wild-type vs *Tet1/2* DKO ESCs as mapped by WGBS.

**Figure 35:** DNA methylation levels of different genomic features in wild-type vs *Tet1/2* DKO ESCs.

**Figure 36:** Accessibility of regulatory elements in wild-type vs *Tet1/2* DKO ESCs as mapped by ATAC-seq.

**Figure 37:** Identification of TET-dormancy-targets.

**Figure 38:** Pie charts showing the distribution of different genomic features within TET-dormancy-targets.

**Figure 39:** Heatmap showing mean levels of TET occupancy, DNA methylation, and chromatin accessibility at TET-dormancy-targets in wild-type vs *Tet1/2* DKO ESCs over time during mTORi treatment.

**Figure 40:** Quantification of data shown in Figure 34 vs all TET peaks.

**Figure 41:** Genome browser view of an example TET-dormancy-target active enhancer and a neighbouring non-target primed enhancer.

**Figure 42:** Transcription factor motif enrichment analysis at TET-dormancy-targets.

**Figure 43:** TF footprinting analysis of predicted TET-activity-coupled TFs vs classical pluripotency TFs.

**Figure 44:** Levels of TFE3 binding at TET-dormancy-targets vs controls, mapped by CUT&Tag.

**Figure 45:** Quantification of data shown in (c) vs canonical TFE3 targets (as identified by peak calling at t=0h).

**Figure 46:** Genome browser view of a TET-dormancy-L1Md repeat showing TET and TFE3 occupancy, DNA methylation, and genome accessibility.

**Figure 47:** Proteins co-precipitated with TET1, as identified by IP-mass spectrometry.

**Figure 48:** Inducible TFE3 knockdown (*Tfe3* iKD) and mTORi treatment.

**Figure 49:** Expression levels of top genes that contact TET-target active enhancers (ABC-score > 0.02) as determined by analysis of published HiC and H3K27ac datasets.

**Figure 50:** Expression levels of genes in putative contact with L1Md promoters.

**Figure 51:** Levels of the indicated histone marks at TET-target active enhancers and L1Mds as well as control regions in wild-type and *Tet1/2* DKO cells over a 144h time course of mTORi-mediated pausing and release.

**Figure 52:** Levels of the indicated histone marks at TET-target primed enhancers, the Other category, and at all TET-bound peaks in wild-type and *Tet1/2* DKO cells over 144h time course of mTORi-mediated pausing and release.

**Figure 53:** Levels of shown enhancer marks in all active ESC enhancers excluding TET-dormancy-targets.

**Figure 54:** Quantifications of the shown enhancer marks in all vs TET-target active enhancers.

**Figure 55:** Genome browser view of chromatin dynamics at the same active ESC enhancer shown in Figure 35.

**Figure 56:** Levels of the indicated histone marks at the shown regions during longer-term pausing.

**Figure 57:** Flow cytometry analysis of the pluripotency marker SSEA1 during pausing and after release in wild-type and *Tet1/2* DKO cells.

**Figure 58:** Expression levels of repetitive elements in wild-type and *Tet1/2* DKO ESCs at indicated time points of mTORi treatment.

**Figure 59:** Evolutionary age of LINE1 repeats that are upregulated vs downregulated at 24h of mTORi in wild-type cells.

**Figure 60:** Schematics of FLASH cloning strategy and Western blot of successfully tagged genes.

**Figure 61:** Schematics of the FLASH experiment to map TET-bound RNAs.

**Figure 62:** Volcano plot showing RNAs that are differentially bound to TET1/2 at 72h compared to 0h of mTORi vs 0h. Both TET1 and TET2 bind L1Md repeats.

**Figure 63:** Differential binding levels of TET1 to repeat RNAs at 24h and 144h compared to 0h.

**Figure 64:** Binding of L1Md and IAPLTR repeat RNAs to TET1/2 at all time points.

**Figure 65:** Hi-C distance decay map of wild-type and dormant ESCs.

**Figure 66:** Future experiments to test the impact of L1Md repeats on dormancy.

## List of Abbreviations

µm	micrometer
5caC	5-carboxy cytosine
5fC	5-formyl cytosine
5hmC	5-hydroxy methylcytosine
5mC	5-methylcytosine
ABC	activity-by-contact
AP1	alkaline phosphatase 1
ATAC	Assay for Transposase-Accessible Chromatin
CGI	CpG island
CpG	cytosine followed by guanine base
CRE	cis-regulatory element
CUT&Tag	cleavage under target & tagmentation
DKO	double knockout
DMSO	dimethyl sulfoxide
E4.5	embryonic day 4.5
EDG	equivalent to day of gastrulation
ESC	embryonic stem cell
FACS	Flow assisted cell sorting
GFP	green fluorescent protein
Hi-C	high throughput chromosome confirmation capture
ICM	inner cell mass
KO	knockout
LIF	leukemia inhibitory factor
LINE	long interspersed nuclear element
LTR	long transposable repeat
MAGRI	Mapping RNA–chromatin interaction
mTOR	mammalian target of rapamycin
nm	nano meter
qPCR	quantitative polymerase chain reaction
SAM	S-Adenosyl methionine
SINE	short interspersed nuclear element

TDG	Thymine DNA glycosylase
TE	trophectoderm
TET	ten eleven trasnlocation DNA demthylase
TKO	triple knock out
tracrRNA	trans-activating crispr RNA
UV	ultra violet
WGBS	whole genome bisulfite sequencing

# Abstract

Dormancy represents a vital biological mechanism facilitating the continuity of various life forms across generations and in response to challenging environmental conditions. In the early stages of mammalian development, embryos can enter a state of dormancy known as diapause. In diapause they can remain viable within the uterus for extended periods, lasting from weeks to months. This dormancy state can be mimicked in vitro by inhibiting the central cellular growth pathway, mTOR. However, the cellular mechanisms that maintain the original cell identity amidst the transcriptionally silent landscape of dormancy remain elusive. This thesis demonstrates the significance of safeguarding cis-regulatory elements from transcriptional silencing to preserve pluripotency during dormancy. Further, this thesis elucidates a TET-transcription factor (TF) axis, wherein TET-mediated DNA demethylation and the recruitment of methylation-sensitive TFs orchestrate chromatin modifications essential for transitioning into dormancy. Disruption of TET activity compromises both pluripotency and the viability of dormant embryos, whereas its augmentation enhances survival rates. These findings uncover a critical mechanism governing the preservation of cellular identity during dormancy, with implications for regenerative medicine and understanding disease processes.

# Zusammenfassung

Die Ruhephase ist ein wesentlicher biologischer Prozess für die Fortpflanzung vieler Lebensformen über Generationen unter Stressbedingungen. Frühe Embryonen vieler Säugetiere können in der Gebärmutter wochen- bis monatelang in einem Ruhezustand, der so genannten Diapause, konserviert werden, die in vitro durch mTOR-Inhibition ausgelöst werden kann. Zelluläre Strategien, die die ursprüngliche Zellidentität in der stillgelegten genomischen Landschaft des Ruhezustands schützen, sind nicht bekannt. Wir zeigen hier, dass der Schutz von cis-regulatorischen Elementen vor dem Silencing der Schlüssel zum Erhalt der Pluripotenz im Ruhezustand ist. Diese Arbeit zeigt eine TET-Transkriptionsfaktor (TF)-Achse, bei der die TET-vermittelte DNA-Demethylierung und die Rekrutierung von methylierungssensitiven TFs die transkriptionell inerten Chromatinanpassungen während des Übergangs in den Ruhezustand vorantreiben. Eine Störung der TET-Aktivität beeinträchtigt die Pluripotenz und das Überleben von Embryonen im Ruhezustand, während eine Verstärkung der TET-Aktivität die Überlebensraten verbessert. Unsere Ergebnisse zeigen

einen wesentlichen Mechanismus für die Konservierung der zellulären Identität ruhender Zellen auf, der Auswirkungen auf die regenerative Medizin sowie das Verständnis von Krankheiten hat.



# 1. Introduction

## 1.1 Early embryonic development in the mouse

While transitioning through totipotency in the first three days after fertilization, the early embryo separates into the trophectoderm and the inner cell mass (ICM) at day 3. At this stage, the blastocyst stage, the ICM exhibits pluripotency, meaning its cells can give rise to all three germ layers: the endoderm, mesoderm, and ectoderm (Smith 2017). At the late blastocyst stage, the ICM separates further into the epiblast and the extraembryonic ectoderm. Then, gastrulation will give rise to the three germ layers upon implantation, making naïve pluripotency a transient state between the blastocyst formation and implantation. Upon further development, pluripotency transitions into primed pluripotency and is lost upon lineage differentiation (Boroviak et al. 2014) (Figure 1).

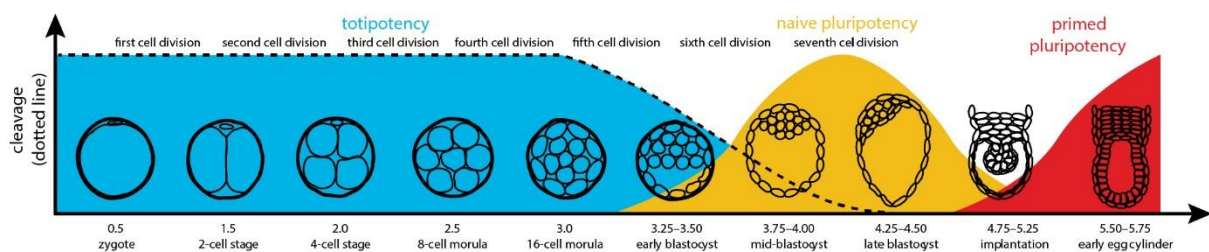


**Figure 1:** Early embryonic development and pluripotency. Cells of the early mouse embryo exhibit totipotency until the morula stage. The early blastocyst comprises of the ICM and the TE, the ICM cells are pluripotent. Upon implantation the former ICM cells, now epiblast, acquire the state of primed pluripotency. Upon further development, pluripotency is quickly lost. From Boroviak et al. 2014.

When ICM cells are grown in vitro, however, pluripotency can be maintained for many generations if the culture conditions are supportive (Schlesinger and Meshorer 2019).

At the late blastocyst stage, the embryo comprises three tissues: The epiblast, the primitive endoderm (layered on top of the epiblast), and the trophectoderm (surrounding both, the epiblast and the primitive endoderm). In vitro models can be derived from all the tissues of the late blastocyst given the right media composition (Figure 2) (Rossant 2015). Extraembryonic endoderm (XEN) cells are derived from the primitive endoderm using serum containing medium that was preconditioned using mouse embryonic fibroblasts and contains FGF4. Trophectoderm stem cells (TSCs) are derived from the trophectoderm and maintained using a combination of FGF4, heparin and activin/nodal (Figure 2) (Rossant 2015).

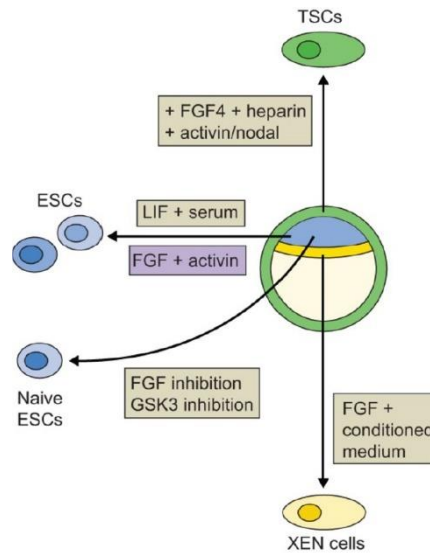


**Figure 2:** Derivation of ESCs, TSCs, and XEN cells from the epiblast, trophectoderm, and primitive endoderm, respectively. Modified from Rossant 2015.

Two common culture conditions are used for ESCs: i) serum/LIF or ii) 2i, corresponding to the early implantation formative pluripotent state or the naive ground state pluripotency, respectively (Leitch et al. 2013; Blaschke et al. 2013). Cells grown in serum/LIF conditions proliferate faster than cells grown in 2i, similar to the increase in proliferation that epiblast cells show after implantation (Kolodziejczyk et al. 2015; Snow 1977). Accordingly with this increase in proliferation, ESCs prevail in a hypertranscriptional state. They further show increased levels of global and nascent transcription compared to their more differentiated counterparts (Efroni et al. 2008).

## 1.2 Transcription factors and signalling pathways of pluripotency

Embryonic stem cells grown in serum, containing many undefined molecules that generally provide growth factors for cell proliferation. Leukaemia inhibitory factor, prevents ESCs from spontaneous differentiation (Gonzales et al. 2015). A majority of the transcription factor and signaling networks that maintain ESCs in the dual capacity to self-renew and differentiate are described (Schlesinger and Meshorer 2019). As described above, pluripotency, and the ability to self-renew indefinitely in culture, is maintained by extrinsic signals (i.e., LIF) and a hierarchical gene-regulatory network (M. Li and Belmonte 2017). The transcription factors OCT4, KLF4, SOX2, MYC, and NANOG lie at the base of this pluripotency gene-regulatory network (Ng and Surani 2011; Nichols et al. 1998; Masui et al. 2007; Mitsui et al. 2003). However, amongst the pluripotency factors, the three prominent transcription factors, OCT4, SOX2, and NANOG, act as central nodes within the core

pluripotency network. They interact with enhancer regions of their target genes, influencing the expression levels of genes associated with gene ontology terms related to differentiation and self-renewal, among other functions (Shanak and Helms 2020). Most compelling evidence of the importance of OCT4, KLF4, SOX2, and MYC has been brought by Yamanaka and colleagues. In 2006, they showed that enforced expression of these factors is sufficient to reinstate pluripotency in terminally differentiated cells (Takahashi and Yamanaka 2006). The core pluripotency transcription factors act cooperatively. If balanced, they maintain pluripotency; however, when the function of any is compromised, differentiation sets in (Loh et al. 2006; Shu et al. 2013). The regulation of their genomic targets by the pluripotency transcription factors is highly complex. For example, are OCT4 and SOX2 required for reprogramming. They form heterodimers that regulate genomic targets, each other included. When their interaction is compromised, i.e., by a mutation of the protein-protein interaction site, reprogramming is less efficient, highlighting the complexity of the pluripotent state (Chew et al. 2005). Nanog is not essential for reprogramming; however, when constitutively overexpressed in pluripotent cells substitutes the extrinsic signalling by LIF (Chambers et al. 2003).

### **1.3 The chromatin state and epigenetics of pluripotency**

Chromatin and epigenetics have become apparent to play a significant role in maintaining this dual capacity. Additionally, chromatin structure and dynamics were distinct in pluripotent cells compared to their differentiated counterparts (Gaspar-Maia et al. 2011). Regarding their genome organization, serum/LIF-grown ESCs exhibit established chromosome territories and low chromosome mingling. Frequent chromosome mingling is typical for differentiated cells (Maharana et al. 2016). Further, it was found that ESCs show a defined higher-order chromatin structure with topological-associated domains confirmed by Hi-C (Dixon et al. 2012; 2015). Polycomb-mediated interactions are among the strongest in ESCs when integrating higher-order genome organization with epigenetic profiles. Upon differentiation into neural progenitor cells, ESCs show changes in all levels of genome organization. The most substantial changes are found in transcription factor networks and polycomb-mediated interactions. Although higher-order organization remains similar between ESCs and differentiated cells, ESCs preferably rely on higher-level organization mediated by polycomb proteins (Bonev et al. 2017).

In hand with their hypertranscriptional state, ESCs depend upon a specially permissive chromatin landscape (Gaspar-Maia et al. 2011; Meshorer et al. 2006). Key mediators of this transcriptionally permissive chromatin landscape are Chd1 and the Myc transcription factor family in ESCs (Gaspar-Maia et al. 2011; Guzman-Ayala et al. 2015; Marks et al. 2012; Ying et al. 2008). Further correlated with the transcriptionally permissive state, ESCs show a globally higher accessibility by micrococcal nuclease (MNase) and DNase I (Morozumi et al. 2016).

In conclusion, ESCs share many characteristics, such as pluripotency, fast proliferation, and transcriptional activity with the peri-implantation epiblast. Pluripotency is a transient state and relies on higher-order genome organization, epigenetic regulation, and a transcriptionally permissive and accessible chromatin environment (Percharde, Bulut-Karslioglu, and Ramalho-Santos 2017; Bulut-Karslioglu et al. 2018).

#### **1.4 DNA methylation**

DNA methylation is an epigenetic mechanism involving the chemical modification of cytosine base with a methyl group at the fifth carbon atom (5-methylcytosine). DNA methylation is catalysed by a family of enzymes called DNA methyltransferases (DNMTs) (Figure 3). These enzymes transfer a methyl group from S-adenyl methionine (SAM) to a cytosine residue. DNMT1 is the maintenance methyltransferase and methylates the newly synthesized DNA strand in cooperation with the protein UHRF1. DNMT3a and DNMT3b are de-novo methyltransferases and can methylate DNA that previously had not been methylated (Moore, Le, and Fan 2013).

Mammalian DNA methylation occurs on cytosines that precede guanines (CpG). Interestingly, CpG sites are depleted from mammalian genomes, which may result from the mutagenic potential of 5mC, which can deaminate to thymine (Coulondre et al. 1978; A. P. Bird 1980). CpG sites are spread across the genome; however, CpG islands usually stay unmethylated (A. Bird et al. 1985). Both mouse and human methylomes have shown hypomethylation of active enhancers potentially being a cause or consequence of protein-DNA interactions at these cis-regulatory elements (Meissner et al. 2008; Lister et al. 2009). In the last decade, DNA methylation has established itself as highly dynamic. With the advance of high-resolution techniques such as whole-genome bisulfite sequencing (WGBS), lowly methylated CpGs appeared in higher abundance in non-CGI regions. 4% of all CpGs

are concentrated in these short regions enriched for transcription factor motifs and exhibit methylation levels between 10 and 50% (Hodges et al. 2011; Stadler et al. 2011). The transcription factor motifs enriched in these regions vary with cell types (Stadler et al. 2011; Kim 2003). Studies reported that transcription factor binding is directly affected by DNA methylation (Watt and Molloy 1988; Becker, Ruppert, and Schütz 1987; Kim 2003). Nevertheless, DNA methylation is also known to modify DNA accessibility and chromatin structure, i.e., via its interplay with histone lysine transferases (Piunti and Shilatifard 2016). Further, a joint profiling effort of DNA methylation, DNA accessibility, and transcription revealed a dynamic coupling between these three layers of regulation (Clark et al. 2019).

A high throughput screen by Yin et al. 2017 showed that about 90% of transcription factors with a CpG in their motif exhibit sensitivity to DNA methylation, while *in vivo* evidence is limited. Kreibich et al. described in 2023 that many transcription factors, among them, are the MYC-MAX bHLH family of transcription factors and CTCF, negatively associate with their motif when it is methylated. Intriguingly, the electrostatic effect of DNA methylation on the shape of DNA might affect the accessibility of a given methylated stretch of DNA for transcription factors (Rao et al. 2018). In fact, according to their systematic predictions, methylation outside of a transcription factor binding site affects the binding of a given transcription factor to DNA. Pioneer transcription factors are also known to reduce DNA methylation in a targeted manner. DNA demethylases do this via processes of active demethylation (Donaghey et al. 2018; Stadler et al. 2011). Adding to the dynamic nature of DNA methylation, a sensitivity of CTCF to the methylation status of its binding sites has been hypothesized. This hints toward the involvement of DNA methylation in 3D chromatin architecture (Monteagudo-Sánchez et al. 2023).

The extent of the sensitivity of transcription factor binding to methylated DNA and whether transcription factor binding is the cause or consequence of local demethylation will likely be answered context- and factor-dependent.

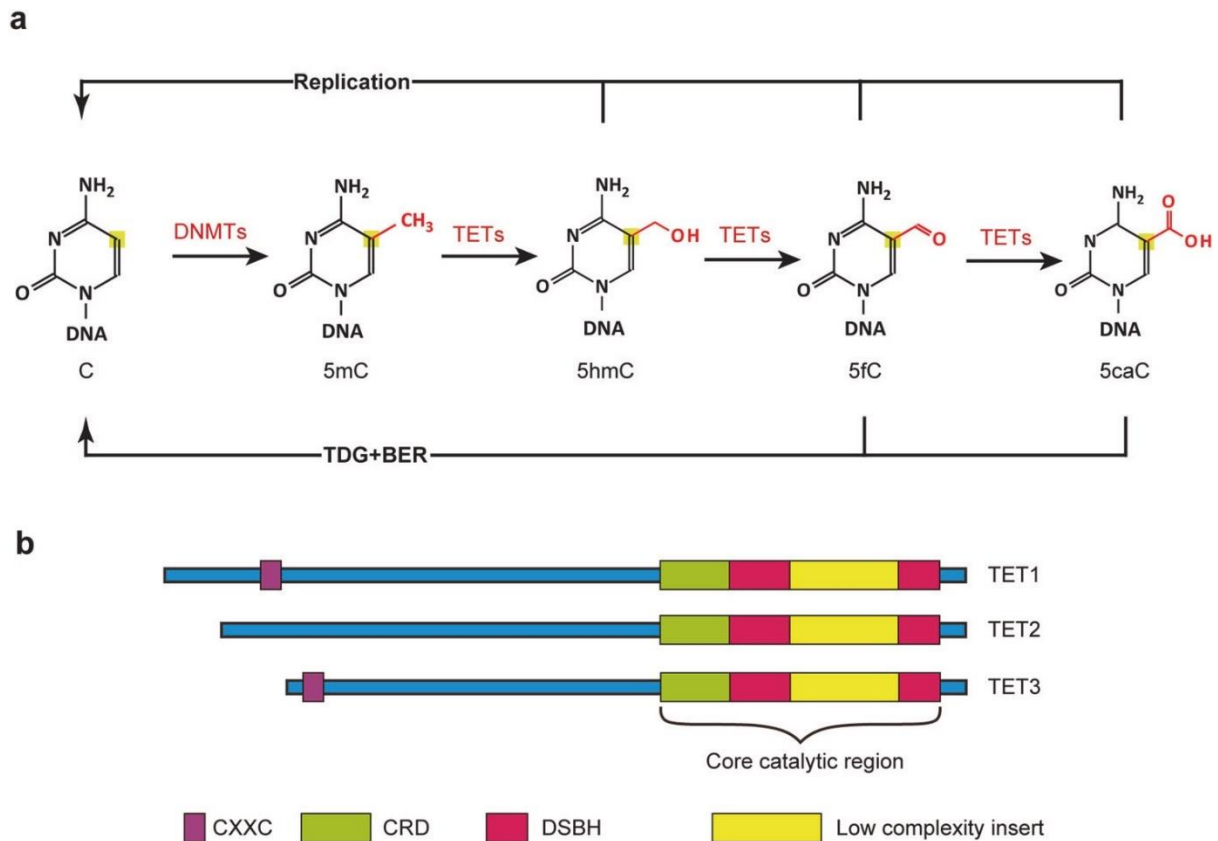


**Figure 3:** DNA methylation and TETs. **a.** DNA methylation is deposited by DNMTs at the 5<sup>th</sup> base of a cytosine. This modification is stepwise oxidised by TETs leading to the derivatives 5-hydroxymethylcytosine, 5-formylmethylcytosine, and 5-carboxymethylcytosine. The latter two can be excised by base-excision-repair and thymidine-DNA-glycosylases to restore an unmodified cytosine. **b.** Schematic protein domain structure of TET1, TET2 and TET3. The core catalytic domain consists of a cysteine-rich domain (CRD), and two double-stranded  $\beta$ -helix (DSBH) regions interspaced by a large low-complexity insert. TET1 and TET3 contain a CpG binding domain (CXXC). TET2 separately associates with a CXXC domain containing protein. From Zhang et al. 2023.

### 1.5 TET DNA demethylases and DNA hydroxymethylation

Ten-eleven translocation (TET) methylcytosine dioxygenases catalyse the demethylation of 5-methylcytosine (5mC) on DNA. TET1 was the first member of this group of enzymes to be identified as a fusion partner of the MLL gene in acute myeloid leukaemia patients with a t(10;11)(q22;q23) translocation. TET2 and TET3 were identified subsequently due to their sequence similarity (Ono et al. 2002; Lorsch et al. 2003). TET1, TET2, and TET3 share a common core catalytic site, a double-stranded beta-helix, at their C-termini (Figure 3) (Iyer et al. 2009; Tahiliani et al. 2009). All three members of the *Tet* gene family come in various isoforms (Zhang et al. 2023; Iyer et al. 2009). Furthermore, all TET enzymes catalyse the oxidation of 5mC to 5-hydroxymethylcytosine (5hmC) to 5-formylmethylcytosine (5fC) to 5-

carboxylcytosine (5caC) (Figure 3) (Ito et al. 2010). The oxidized forms 5fC and 5caC are subsequently removed by thymine DNA glyoxalases (TDG) and the base excision repair (BER) to restore unmethylated cytosine (Maiti and Drohat 2011). The fact that reader proteins for all oxidized forms of 5mC exist suggests a role in gene regulation of each oxidized form (Spruijt et al. 2013).

Recently, TET2 was identified as a naive pluripotency marker, which interacts and co-localizes with Nanog at enhancers (Pantier et al. 2019). OCT4, another pluripotency factor, directly upregulates the expression of *Tet2* (Koh et al. 2011). The *Tet1* gene is a direct target of the main pluripotency factors OCT4, MYC, and NANOG. In turn, TET1 binding to the *Nanog* promoter prevents it from hypermethylation (Neri et al. 2015). The expression of *Tet2* alone is sufficient to reprogram cells from primed to naïve pluripotency (Fidalgo et al. 2016). Further, TET1 supports the pluripotency via its interaction with Sin3a (part of a histone-deacetylase complex). The TET1-SIN3A complex activates the expression of the *Nodal* antagonist *Lefty1* by targeted demethylation of the *Lefty1* promoter (Zhu et al. 2018). Generally, TETs are found at CGI promoters and are positively correlated with the histone modification H3K4me3 (Xu et al. 2011).

Upon knock-out of all three TETs and subsequent whole genome bisulfite sequencing, studies found that 15-25% of enhancers and DNaseI-sensitive sites accumulate DNA methylation. CGI promoters, however, remain unchanged (Hon et al. 2014; Lu et al. 2014). Interestingly, embryonic stem cells and mouse embryos are not compromised upon a knock-out of all *Tet* genes until differentiation or gastrulation, respectively (Cheng et al. 2022).

TET activity can be increased in cell culture systems by adding vitamin C to the cell culture medium, which acts as a cofactor to TETs (Blaschke et al. 2013). Alpha-ketoglutarate is another cofactor of TET enzymes, and alpha-ketoglutarate-based molecules can be used as TET inhibitors. Since alpha-ketoglutarate is a cofactor for all cellular dioxygenases, alpha-ketoglutarate-based inhibitors have pleiotropic effects (Tran, Dillingham, and Sridharan 2019).

In summary, TET enzymes are promiscuously interacting proteins. They are deeply interwoven into the network of pluripotency transcription factors and the pluripotent state of embryonic stem cells and early embryos (Figure 4).

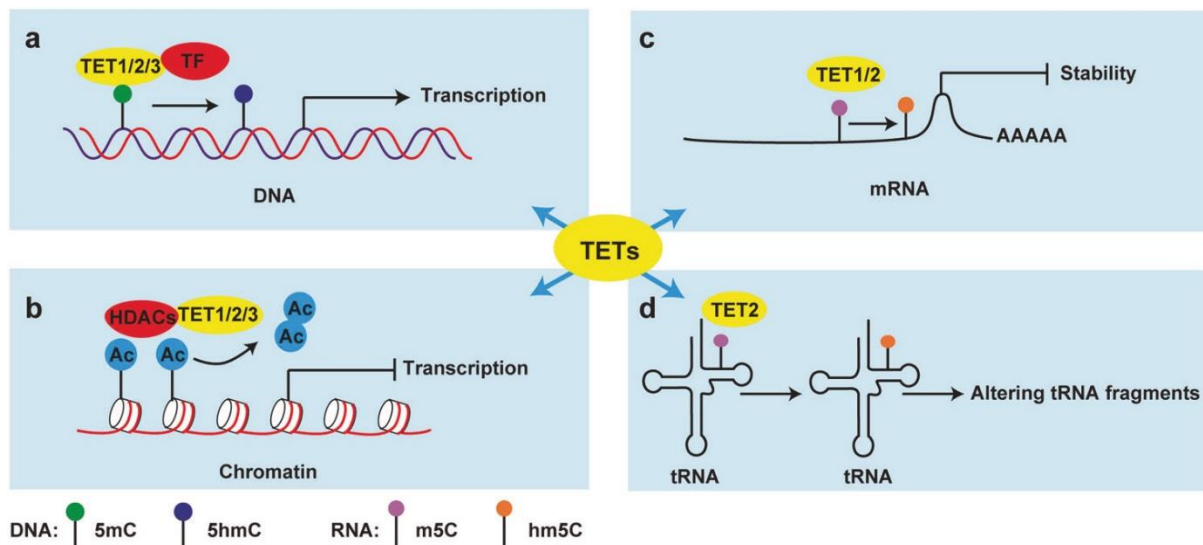


**Figure 4:** Schematic overview of TETs and their promiscuous functions. a. TETs interacting with transcription factors at enhancer and promoters facilitating transcription. b. TETs interacting with HDACs (i.e. SIN3A) repressing transcription. c. TET1 and TET2 hydroxymethylating mRNAs decreasing the half-life of transcripts. d. TET2 hydroxymethylating tRNAs. From Zhang et al. 2023.

## 1.6 Cis-regulatory elements

Cis-regulatory elements (CREs), like promoters and enhancers, are the functional regulators and at the essence of the transcriptional network in cells. Specifically, enhancers are short stretches of DNA; they are bound by transcription factors and contain certain chemical modifications. They act independently of their sequence orientation (Heinz et al. 2015). CREs are cell type specific and usually nucleosome depleted, resulting in a DNaseI-sensitivity (Buenrostro et al. 2013). Additionally enhancers are cell type specifically bound by transcription factors, accompanied by the binding of p300, Cbp and the Mediator complex (Visel, Rubin, and Pennacchio 2009; Kagey et al. 2010). Active enhancers are enriched for H3K27ac which is deposited by p300 and Cbp. H3K4 methylation is deposited by a family of MLL complexes that can mono or trimethylate, respectively. H3K4me3 correlates more with promoters while H3K4me1 correlates more with enhancers. The two marks can be used in combination with H3K27ac to distinguish enhancer and promoter loci (Heintzman et al. 2007). Once an active enhancer landscape is established, the Mediator complex mediates communication between the enhancer element and the promoter, ultimately facilitating efficient transcription (Field and Adelman 2020). Transcription factors mediate the maintenance of an enhancer activity and its specificity (Field and Adelman 2020). The 3D chromatin structure appears to increase the probability of an enhancer contacting a promoter. This is mediated by CTCF, Cohesin, and the transcription factor YY1 that is often found at



enhancer-promoter contacts (Phillips and Corces 2009; Weintraub et al. 2017). Expression levels of transcription factors, repressive complexes, or DNA methylation can significantly impact enhancer elements' function (Kreibich et al. 2023).

### **1.5 Embryonic diapause**

Evolutionary success depends on effectively passing genetic material to the next generation. Animals have developed various reproductive strategies to ensure this propagation. Mammals, for instance, bear live offspring that are relatively well-developed and often undergo extended nursing periods (Cabej 2019). This investment in gestation and lactation, compared to oviparous species, demands significant energy and relies on favourable environmental conditions for success. However, challenges such as nutrient scarcity, suckling of preceding generations of offspring or harsh winters can hinder successful development. To cope with such environmental stresses, certain mammalian species have evolved embryonic diapause as a developmental strategy. Embryonic diapause is the suspension of development in response to adverse conditions, equipping organisms with remarkable resilience (Renfree and Shaw 2000). This phenomenon, first described by Bischoff in 1865, involves delayed implantation occurring at the blastocyst stage (Renfree and Shaw 2000; Bischoff 1865). It is observed in 70 Eutherian and 30 Marsupial species. In some species, i.e., the European roe deer, embryonic diapause became a part of the reproductive cycle (obligatory diapause). In contrast, other species exhibit diapause in response to the environment (facultative diapause) (Renfree and Shaw 2000).

### **1.6 Embryonic diapause in *Mus musculus***

Embryonic diapause in mice is naturally induced via i) starvation, ii) lactation, and iii) experimentally by surgically removing the ovaries and a sustained injection of estrogen antagonists (McCormack and Greenwald 1974; Hunter and Evans 1999). The mouse reproductive cycle allows for pregnancy while the female still nurses its offspring. An emergent pregnancy would ultimately result in a competition for nutrients between the current and the subsequent generation of offspring, and therefore, diapause is induced (Van Der Weijden and Bulut-Karslioglu 2021). During diapause, the embryo remains near the uterine tissue in so-called crypts. The mural part of the trophoctoderm (TE) is oriented toward the uterine wall (Kamemizu and Fujimori 2019). Interestingly, diapause termination is initiated by a decrease in lactation-induced prolactin and a subsequent increase in estrogen (van Der Weijden and Bulut-Karslioglu 2021). Experimentally, a single injection of estrogen

is sufficient to terminate diapause in mice (Yoshinaga and Adams 1966). The uterine receptiveness for implantation, downstream of hormonal regulation, is potentially an initiator of diapause (Ptak et al. 2012). Maternal leukaemia inhibitory factor (LIF) knock-outs are not receptive to implantation. The LIF-KO embryos exhibit diapause-like features, genetically supporting the role of uterine receptiveness as a stimulator for diapause (Stewart et al. 1992). The uterine fluid is another influencing factor in the initiation maintenance and reactivation from diapause. It comprises metabolites, glucose, pyruvate, amino acids, and growth factors (Harris et al. 2005). While the absence of growth factors did not induce diapause, they have been shown to influence the reactivation from diapause. The levels of metabolites have been shown to regulate diapause by maintaining it or delaying its reactivation (Naeslund 1979; Fenelon and Murphy 2017).

Metabolically, like other dormant cells, the diapaused embryo exhibits a decreased metabolic rate with distinct use of metabolic pathways (Hussein et al. 2020; Sousa et al. 2020). Comparing the two primary tissues in the blastocyst, the inner cell mass (ICM) seems more inactive than the TE, suggesting specific regulation of each tissue (Houghton 2006). Three main characteristics define the diapaused state: decreased oxidative phosphorylation, structurally altered mitochondria, and increased autophagy (Naeslund 1979; Lee et al. 2011; Hussein et al. 2020; Sousa et al. 2020). Further, the glutamine transporter Slc38a is crucial since its inhibition is detrimental to diapause (Hussein et al. 2020). Real-time metabolic measurements via the Seahorse instrument, for example, are essential in comprehending the full extent of metabolic regulation of diapause. These assays, however, remain challenging due to the large numbers of embryos required for accurate measurements (Van Der Weijden and Bulut-Karslioglu 2021). RNA, protein, and metabolic profiling provide insight into metabolic pathways utilized during diapause. The utilization of lipid reserves is observed in dormant stem cell types and different dormant tissues (Kinder et al. 2010). Recently, it has been shown that diapause embryos show a higher abundance of free fatty acids and phospholipid phosphatidylcholine compared to proliferating embryos, which suggests active lipolysis (Hussein et al. 2020). Removing lipid droplets from zygotes impairs the ability to diapause in mouse embryos, further supporting the utilization of lipids (Arena et al. 2021). Interestingly, in contrast to that, inhibition of fatty acid oxidation increases the fraction of quiescent stem cells from 4 to 17% (Khoa et al. 2020). Recently, FOXO1 has been identified as a critical regulator of the energy balance in dormant embryos that mediates lipid metabolism (Van Der Weijden et al. 2024).

Since diapaused embryos roughly maintain cell numbers during the duration of diapause, alterations to the cell cycle are inevitable. Studies showed a p21-mediated checkpoint control to keep cells in the G0/G1 phase, thereby reducing DNA replication (Hamatani et al. 2004; Kamemizu and Fujimori 2019). A diapause-like state that can be induced in mouse ESCs by mTOR inhibition. In this state, cells continuously progress through the cell cycle phases, albeit at a slower pace (Bulut-Karslioglu et al. 2016). Taken together, embryonic diapause is a multifaceted phenomenon with many aspects to be still elucidated.

### **1.7 Molecular regulation of diapause in vivo and mTOR inhibition-induced model systems**

Diapause can be studied *in vivo*, as described above. However, via partial inhibition of the mammalian target of rapamycin (mTOR), embryos can enter a diapause-like state (Bulut-Karslioglu et al. 2016). Interestingly, other tested inhibitors, i.e., for translation, Myc-family transcription factors, or histone acetyltransferase inhibitors, did not prolong *ex vivo* embryo survival. In contrast, INK128, an mTOR inhibitor, prolonged embryo survival for up to 22 days (EDG25.5) (Bulut-Karslioglu et al. 2016). This observation is remarkable given that mice's gestation period lasts about 19 days. Besides INK128, another mTOR inhibitor, Rapalink (that catalytically inhibits both enzymatic complexes mTORC1 and mTORC2), extends the survival of blastocyst stage embryos *ex vivo* for up to 30 days (Bulut-Karslioglu et al. 2016; Rodrik-Outmezguine et al. 2016).

Generally, the E4.5 embryo and the diapaused embryo show both, differences and commonalities in their molecular regulation (Figure 5). In both instances the epiblast cells are Nanog positive, indicating naïve pluripotency. The epiblast cells of the diapaused embryo polarize and all surrounding primitive endoderm cells become OCT4 positive, while the E4.5 epiblast stays unpolarized and its surrounding primitive endoderm cells show a mosaic pattern of OCT4 positivity. Compared to the E4.5 epiblast the WNT-pathway activity is increased and the demand for LIF-pathway signalling is increased (Figure 5) (Van Der Weijden and Bulut-Karslioglu 2021).

AKT/p-AKT and 4EBP1/p-4EBP1 are kinases downstream of the mTOR pathway and are active when phosphorylated by mTOR (Saxton and Sabatini 2017). Both *in vivo* and *ex vivo* (mTORi) paused embryos show decreased levels of p-AKT and p-4EBP1. This effect is pronounced explicitly in the epiblast, indicating the involvement of the mTOR pathway in

vivo and ex vivo. When in diapause, embryos show an almost complete absence of proliferation. Accordingly, transcription and translation are strongly decreased in paused embryos (Bulut-Karslioglu et al. 2016). Such dramatic changes in the transcriptional and translational profile usually go in hand with changes to the chromatin environment (Tsompana and Buck 2014). H4K16ac is a marker for active genes and enhancers; it does not alter chromatin compaction but indicates chromatin compaction (Taylor et al. 2013). H3K36me2 is another mark strongly correlated with transcription (Lam et al. 2022). Both marks are highly reduced in paused and diapaused blastocysts, respectively. The reduction in both transcription-associated marks indicates a transcriptionally less permissive environment that hints toward further chromatin alterations.

This phenomenon was more closely studied by Bulut-Karslioglu et al. 2016 by including mouse embryonic stem cells (ESC) as a model system. Interestingly, ESCs react to mTOR inhibition with reduced proliferation but no deflation in phenotypical measurements of pluripotency. Additionally, pausing of ESCs was fully reversible. Intriguingly, ESCs did not show significant enrichment in any cell cycle phase when treated with INK128, distinguishing them from paused and diapaused embryos that do not show continuous progression of the cell cycle, but an arrest in G0/G1 (Kamemizu and Fujimori 2019). RNA-sequencing analysis of paused ESCs compared to ESCs cultured in Serum + LIF showed a globally reduced transcriptional landscape in that study. Reduced transcription included housekeeping genes and genes associated with general pluripotency. In summary, ex vivo paused blastocysts and paused embryonic stem cells closely resemble the features of diapaused blastocysts. They appear to be a suitable model system for studying the dormancy mechanism.

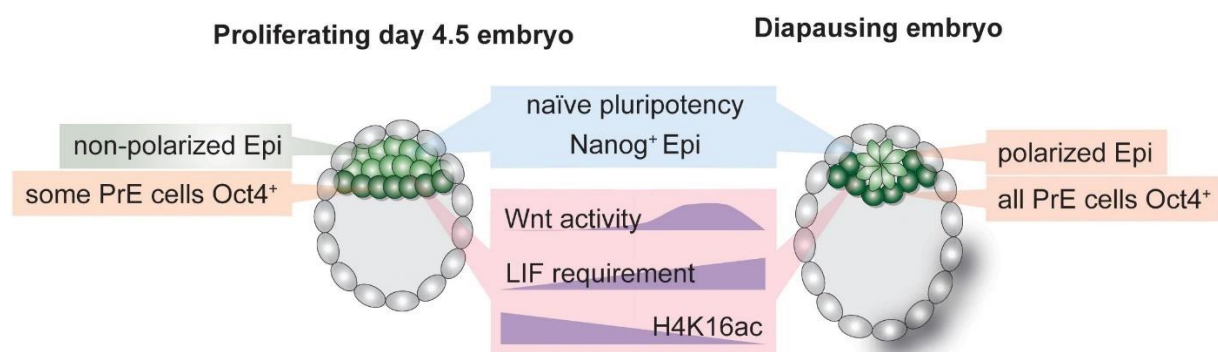


**Figure 5:** Differences and commonalities of the proliferating and diapaused mouse embryo. From Van Der Weijden and Bulut-Karslioglu 2021.

## **Thesis Rationale and Aims**

In this thesis I aimed to understand the role of DNA methylation and TET DNA demethylases in dormancy regulation within the context of embryonic diapause. By generating and phenotyping *Tet1/2* double knockout ESCs, I showed the DNA demethylation activity of TET proteins to be indispensable for embryonic dormancy. I mapped DNA methylation, chromatin accessibility, and binding sites of TET1/2 and employed a computational strategy to identify regions that are specifically targeted by TETs and protected from DNA methylation under dormancy. Overall, I show a TET-TF axis that acts as a bookmarking mechanism and appears as crucial for the successful propagation of pluripotency through embryonic dormancy (Stötzel et al, accepted for publication in Nature Structural and Molecular Biology, 2024).

## 2. Results

### 2.1 Increased methylation is a feature of in vivo diapaused embryos, ex-vivo diapaused embryos, and mouse embryonic stem cells

#### 2.1.1 Dormant ESCs and embryos show increased methylation

Since a detailed assessment of the epigenetic regulation of the dormant state remains elusive, profiling of the epigenome of dormant cells was performed. This included immunofluorescence stainings (IF) of DNA methylation (5-methylcytosine; 5mC) and DNA hydroxymethylation (5-hydroxy methylcytosine; 5hmC). E14 mouse embryonic stem cells (ESCs) were paused using the mTOR inhibitor INK128 for 144h (Figure 6a). Dormant ESCs exhibit significantly increased levels of 5mC and 5hmC compared to their proliferating counterparts (Figure 6b).

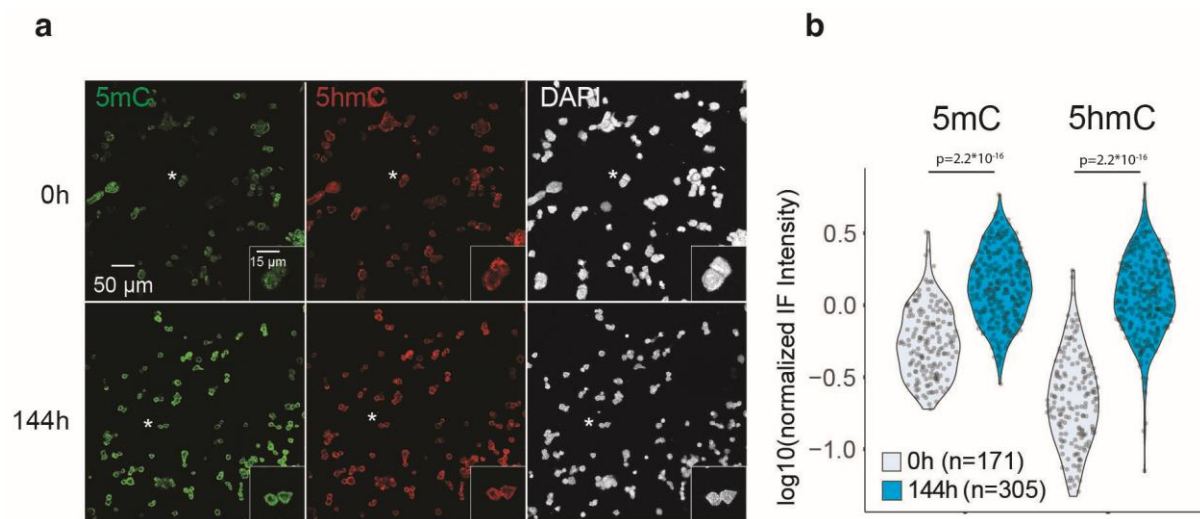


**Figure 6:** **a.** Immunofluorescence staining against 5mC and 5hmC in proliferating (0h) and mTORi treated (144h) paused mESCs. **b.** Single-nucleus quantifications of 5mC and 5hmC intensities normalized to DAPI. n, number of cells. A statistical test is a two-tailed t-test. Each dot represents a quantified nucleus that was segregated using the DAPI signal.

To verify that increased DNA methylation levels are a feature of the dormant state and not an artifact of cultured stem cells, IF was also performed on embryos. Ex vivo-diapaused (144h, using 200 nM Rapalink) and in vivo-diapaused (96h, through ovariectomy) embryos were used (Figure 7a). Both in-vivo diapaused and ex-vivo diapaused embryos exhibit increased methylation (5mC) levels compared to E4.5 blastocysts. This phenotype contrasts the

established knowledge that the blastocyst stage poses a blank sheet of methylation in mouse development (Greenberg and Bourc'his 2019).

We reasoned that the pre-implantation increased methylation levels possibly represent a dormancy-specific and limited feature, since methylation increases post implantation in continuous development. In vivo diapaused embryos (96h) were reactivated in an M2 medium for 48h (Figure 7a) to test this hypothesis. The reactivated embryos show low methylation levels, like those of E4.5 embryos. This suggests that i) increased methylation is a dormancy-specific feature and ii) methylation levels need to revert to the original pre-implantation level before continuation of development.

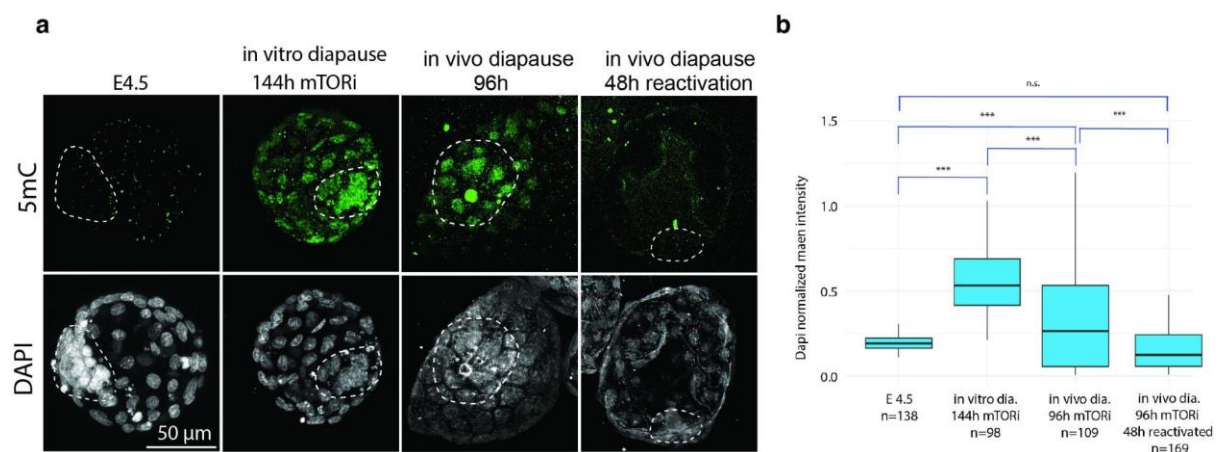


**Figure 7: a.** Immunofluorescence of E4.5, ex-vivo paused, in vivo diapaused, and reactivated (48h post in vivo diapaused) mouse blastocysts for 5mC methylation. Dashed lines mark the ICM. **b** Single-nucleus quantifications of 5mC intensity normalized to DAPI. The horizontal line shows the median, the box spans the IQR, and the whiskers span 1.5 IQR. n, number of cells. A statistical test is a one-way ANOVA with Tukey's multiple comparison test.

The IF signal was quantified based on segregated nuclei. Figure 7b supports the hypothesis that methylation levels revert to the E4.5 preimplantation blastocyst level. Statistically, E4.5 (most left) and the reactivated embryos (most right) show no difference in their methylation levels.

### 2.1.2 Activity of TETs is crucial to successfully establish a dormant state

The naive pluripotent state is classically associated with low levels of methylation, except for the diapaused state (Figure 7). To further interrogate the phenomenon of increased methylation in the dormant state the proliferation and phenotype of two knock-out cell lines under mTORi were accessed: i) a double knock-out of the genes of the de-novo methylating

enzymes Dnmt3a and Dnmt3b (Dnmt3a/b DKO) and ii) a triple knock-out of the genes of the demethylating enzymes *Tet1*, *Tet2* and *Tet3* (*Tet1/2/3* TKO). Both knockouts were compared to their enzyme-carrying parental cell lines (Dnmt3a/b DKO to KH2 mESCs and *Tet1/2/3* TKO to iPSCs). When subjected to mTOR inhibition, the Dnmt3a/b DKO and wild-type Kh2 cells established dormancy, respectively (Figure 8a). In contrast, *Tet1/2/3* TKO cells did not establish dormancy when subjected to mTOR inhibition, while the parental counterpart did (Figure 8b). *Tet1/2/3* TKO cells showed significantly reduced proliferation. Further, their colonies lost classic phenotypic pluripotency markers, such as roundness, shininess, and a dome-like shape. These findings indicate that the dormant state relies on the demethylating activity of TETs but not on the de-novo DNA methylation activity of the DNMT3a/b enzymes.

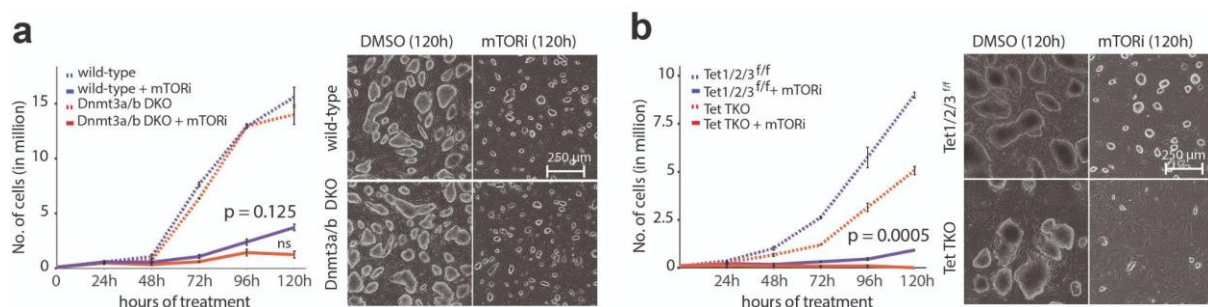


**Figure 8:** *Tet1/2/3* TKO does not sustain a pluripotent culture under mTORi conditions. **a.** Proliferation curves and bright field images of wild-type and Dnmt3a/b DKO ESCs (devoid of de novo methyltransferase activity) treated with the mTOR inhibitor INK128 for 120h. Data are from two biological replicates. The statistical test is a two-tailed Wilcoxon matched-pairs signed rank test and compares wild-type and Dnmt3a/b DKO ESC proliferation rates in mTORi condition. **b.** Same as in (a) for *Tet1/2/3*<sup>flox/flox</sup> vs. *Tet1/2/3* TKO iPSCs28. *Tet* TKO cells lose pluripotent colony morphology over time under dormancy conditions.

Next, the *Tet1/2/3* TKO cells were used to ectopically express either *Tet1* or *Tet2* using random integration of pCAGGs plasmids containing the *Tet1* or *Tet2* gene, respectively (Figure 9). The expression of *Tet1* or *Tet2* in the *Tet1/2/3* TKO background rescued the phenotype and allowed cells to establish dormancy, respectively.



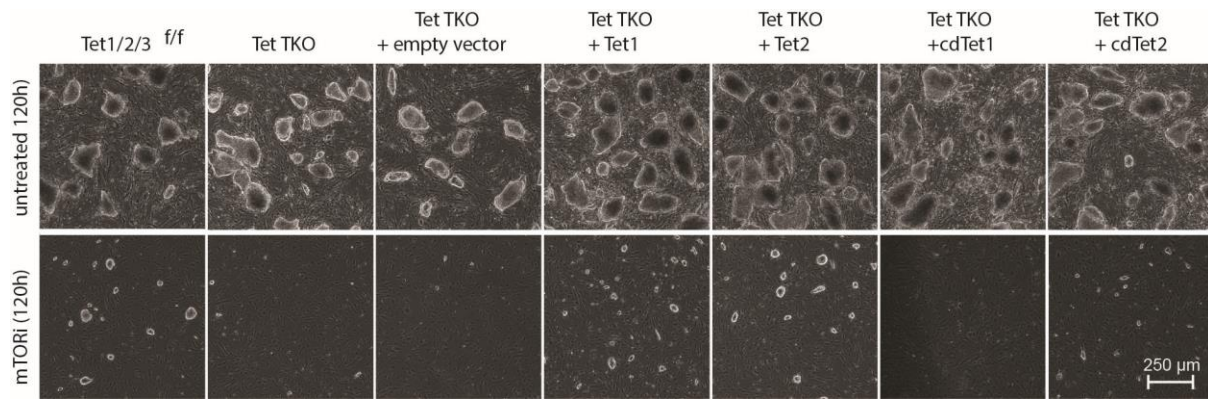


**Figure 9:** Rescue of *Tet* TKO dormancy defect via overexpression of wild-type, but not catalytic dead (cd), *Tet1* or *Tet2*. The catalytic-dead mutations can be found in the Methods and Figure 10.

Ectopic expression of the catalytic dead version of the enzymes (Figure 10) did not rescue the phenotype in the case of TET1. It partially rescued the phenotype in the case of TET2 (Figure 9, most right two panels). This indicates that establishment of the dormant state relies on TETs and their demethylating activity.



**Figure 10:** **a.** The mutation of H1651Y and D1653R lead to a catalytic dead version of TET1. **b.** The mutation of H1651Y and D1653R lead to a catalytic dead version of TET2.

To get further insight into the importance of the demethylating activity during dormancy, whether TET activity is needed when there is no increase in methylation, was tested. A *Dnmt1/3a/3b* TKO cell line (kindly provided by the Meissner lab) was used, lacking all methylating enzymes. The *Dnmt1/3a/3b* TKO cells and Kh2 wild-type cells were treated with a combination of mTOR inhibition and inhibition of TETs using 200 nM Ink128 and 100  $\mu$ M Bobcat339, respectively (Figure 11). Although the proliferation difference was statistically insignificant, the Kh2 cells performed visibly worse when treated with mTORi and TETi than *Dnmt1/3a/3b* TKO cells. *Dnmt1/3a/3b* TKO cells treated with both TETi and mTORi behaved not different from *Dnmt1/3a/3b* TKO cells or Kh2 cells only treated with mTORi. This result indicates that in the absence of DNA methylases, the demethylating activity of TETs is dispensable.

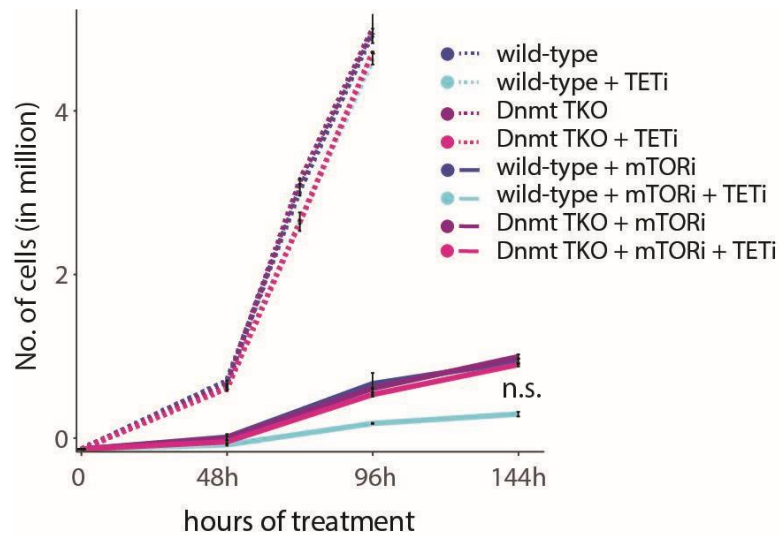


**Figure 11:** Rescue of *Tet* TKO dormancy defect in the absence of DNA methyltransferase activity. Wild-type or *Dnmt* TKO ESCs were treated with the TET inhibitor (TETi) Bobcat339 with or without mTORi. TETi-treated cells are depleted specifically under mTORi treatment in wild-type but not *Dnmt* TKO ESCs.  $p = 0.5614$ .

### 2.1.3 Generation of a feeder-free system using E14 mESCs

E14 cells are established as a model system to study dormancy (Bulut-Karslioglu et al. 2016). An E14 feeder-independent *Tet1/2* DKO ESC line was generated using Cas9-assisted deletion of the entire coding region of the genes (Figure 12).

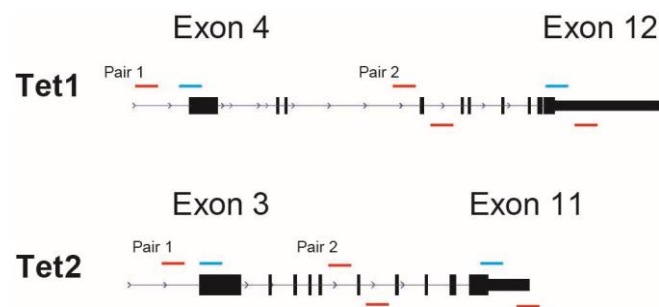


**Figure 12:** Schematic visualization of the *tet1* and *tet2* knock-out strategy. For both genes, all coding exons were removed using CRISPR-Cas9. Guide RNA binding sites are indicated in blue. Genotyping primer binding sites are indicated in red. Exact sequences can be found in the Methods section.

Only Tet1 and Tet2 are expressed in ESCs, therefore a *Tet1/2* DKO instead of a *Tet1/2/3* TKO was generated. Successful removal of the coding region of both genes was confirmed by PCR and gel-electrophoresis using the primers indicated in Figure 12 (Figure 13).

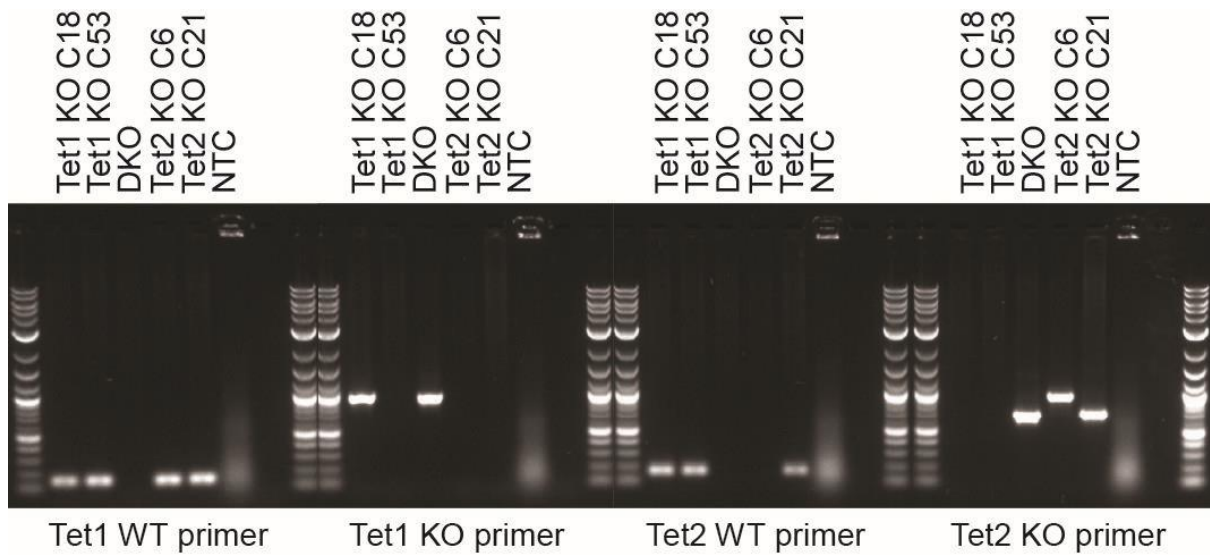


**Figure 13:** PCR followed by gel-electrophoresis indicates successful deletion of *tet1* and *tet2*, respectively.

Neither Tet1 nor Tet2 protein was detectable via Western blot in the *Tet1/2* DKO cells (Figure 14).

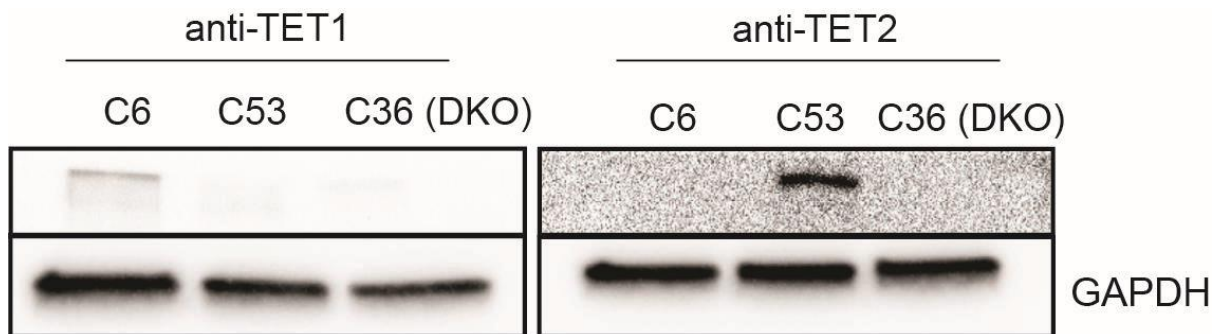


**Figure 14:** Western blot against Tet1 (left) and Tet2 (right) and Gapdh as a housekeeping control. Clone 6 is a Tet2 KO line (C6), clone 53 a Tet1 KO line (C53) and clone 36 a *Tet1/2* DKO (C36).

As before, when subjected to mTORi, *Tet1/2* DKO cells failed to establish a dormant pluripotent state (Figure 15).

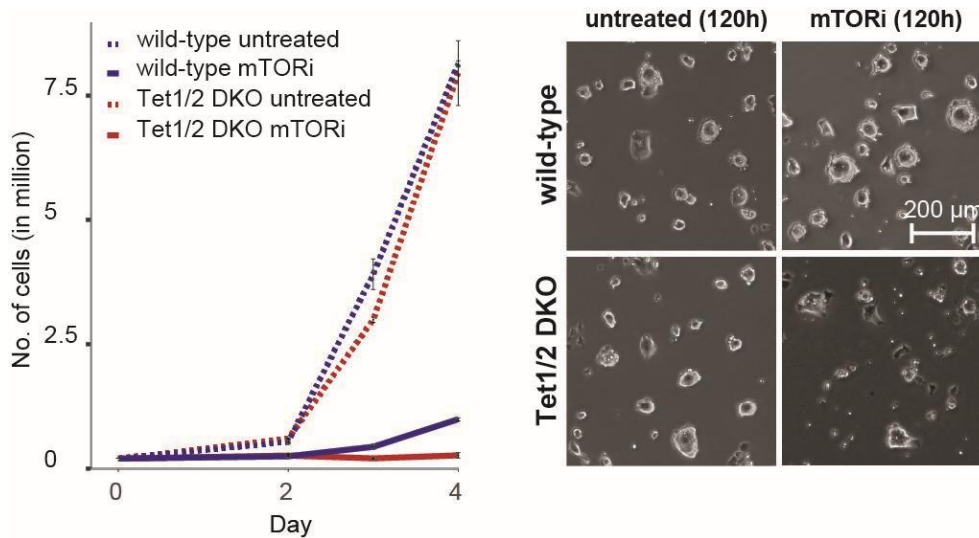


**Figure 15:** Bright field images and survival curves of wild-type and *Tet1/2* DKO ESCs (E14 cells, feeder-independent) treated with the mTOR inhibitor INK128.

The feeder-free cell culture system allows in-detail observation of the decay of *Tet1/2* DKO cells i.e. when stained for alkaline phosphatase 1 activity (Figure 16). Until 72h of mTORi, *Tet1/2* DKO cells are morphologically similar to wild-type cells. At 96h of mTORi, however, the *Tet1/2* DKO cells show signs of differentiation such as asymmetrically-shaped colonies and a loss of AP1 signal. Furthermore, *Tet1/2* DKO cells are depleted from the culture plate over time (Figure 15).

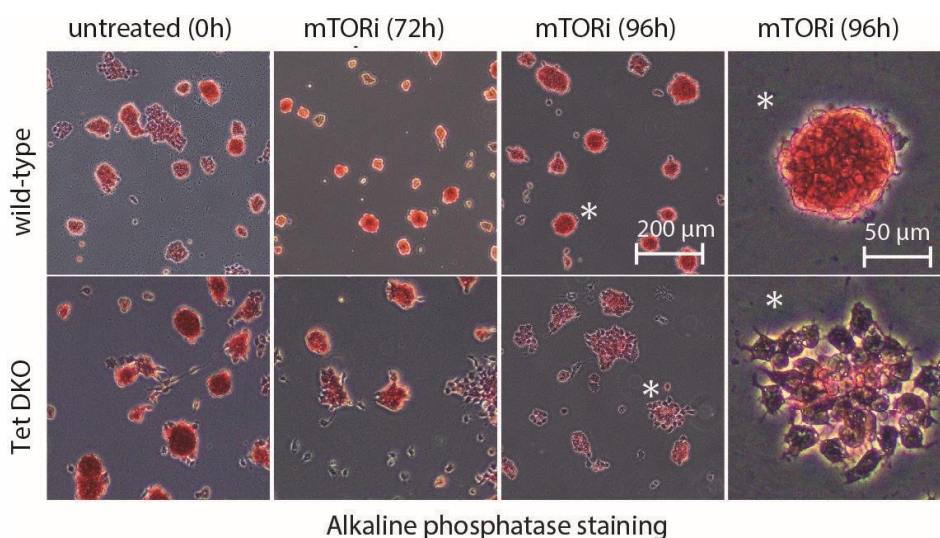


**Figure 16:** Alkaline phosphatase staining of an independently generated, feeder-independent *Tet1/2* DKO ESC line in normal and mTORi conditions. *Tet1/2* DKO ESCs lose pluripotent colony morphology and marker (alkaline phosphatase) expression during mTORi treatment.



To further investigate this deterioration of the *Tet1/2* DKO cells under mTORi compared to their wild-type counterpart two flow-assisted cell sorting (FACS) assays were performed: i) a staining for the cell surface pluripotency marker SSEA1 and ii) a staining for the cell surface apoptosis marker Annexin V in combination with an intracellular live/dead marker (Figure 17 and 18). To quantify the SSEA1 FACS analysis results, unlabelled cells were used to gate the negative fraction (orange fraction). The remaining cells were divided into half, SSEA1 low (light blue) and SSEA1 high (blue) (based on 0h wild-type). In the FACS plots and adjacent quantifications it is visible that wild-type cells continuously increase the fraction of SSEA1 high cells, reaching 70% at 96h (Figure 17). In contrast to that, the *Tet1/2* DKO cells show an initial increase of the SSEA1 high fraction (48h), however, do not manage to progress on that trajectory (25% SSEA1 high at 96h). This data highlights that the divergent response to mTORi manifest between 48h and 72h.

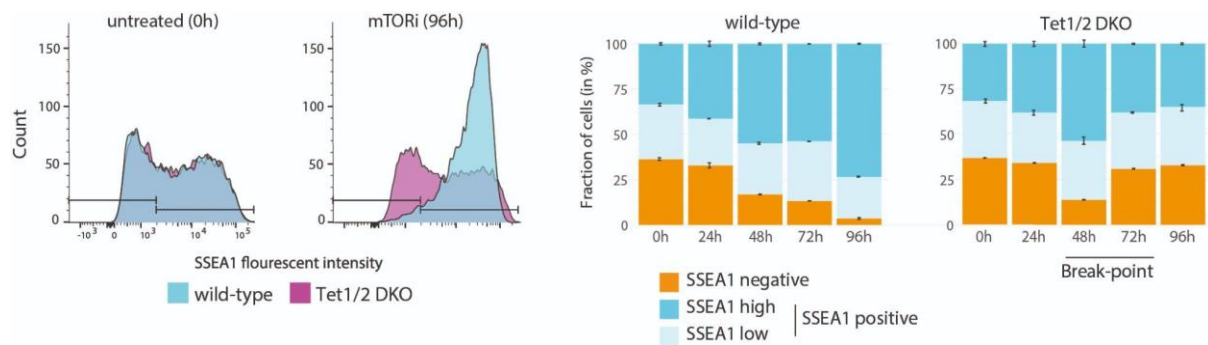


**Figure 17:** Flow cytometry analysis of SSEA1 expression levels (a pluripotency marker) in wild-type and *Tet1/2* DKO cells in normal and mTORi conditions. Overlays of SSEA1 expression at 0h vs 96h in wild-type or *Tet1/2* DKO cells. The stacked bar plots on the right shows quantification of SSEA1 expression levels at all quantified time points.

Apoptosis levels increased slightly in *Tet1/2* DKO cells compared to the wild-type (Figure 18). The increased levels of apoptosis, a potential stress response and the differentiating phenotype poses an explanation for the vanishing of *Tet1/2* DKO cells from the culture dishes when subjected to mTORi.

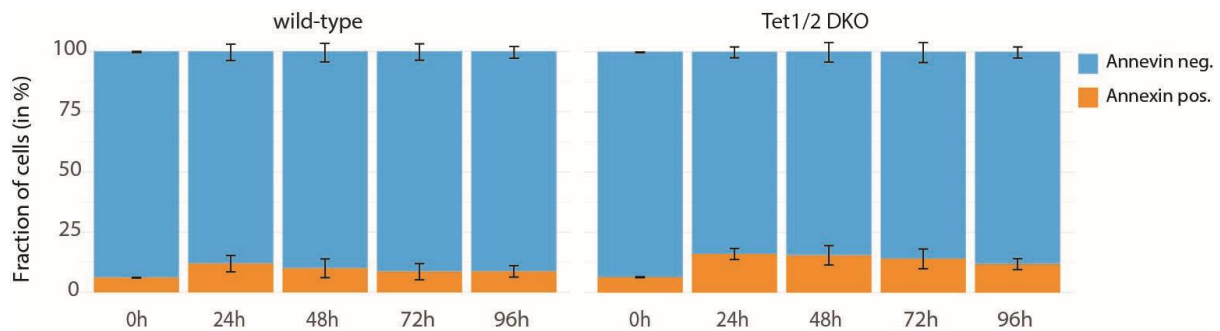


**Figure 18:** Flow cytometry analysis of apoptosis levels in wild-type and Tet1/2 DKO cells in normal and mTORi conditions. Annexin V was used as an apoptosis marker. Quantification of Annexin V-positive and -negative cells are represented as stacked bar plots.

In summary, the assessment DNA methylation and knock-out cell lines of writers and erasers of DNA methylation showed an increase of methylation in the dormant state. We hypothesised the need to counteract this trend by TET DNA demethylases. *Tet1/2* DKO cells show a divergent response to mTORi from 72h onwards compared to wild-type cells.

## 2.2 TETs are required for ex vivo- and in vivo-diapause

### 2.2.1 Validation of the *Tet1/2* DKO dormancy phenotype in vivo

The experiments using *Tet1/2* DKO cells indicate a dependency of dormancy on the presence of Tet1 and Tet2. We validated this finding using mouse blastocysts for an in-depth understanding of dormancy regulation. Figure 19 provides an overview of the different efforts that were taken to provide a solid validation of the phenotype. Zygotic knock-outs of Tets (a), the TET-specific inhibitor Bobcat339 (b,c), and zygotic knock-out embryos were used for reimplantation and in-vivo diapause induction (d).

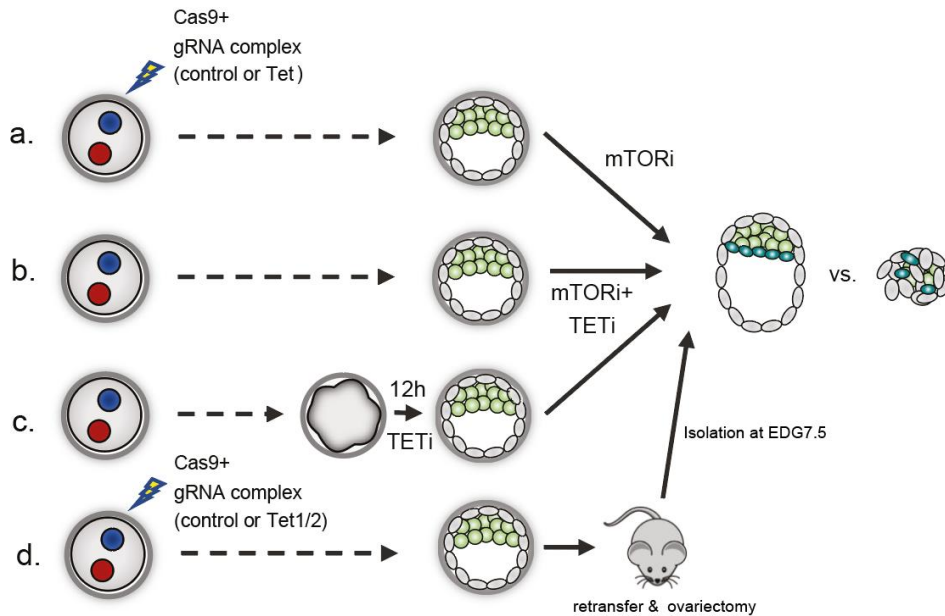


**Figure 19:** Overview of genetic and pharmacological TET loss-of-function experiments.

For the zygotic knock-out experiments, three guide RNAs were designed against each *Tet* gene (Figure 20). Single embryo qPCR and genotyping at the blastocyst stage were attempted without success.

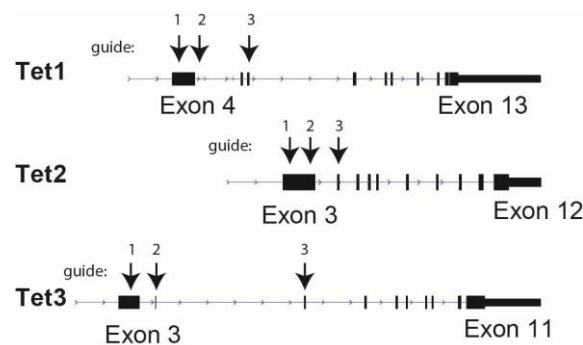


**Figure 20:** Schematics of Cas9-assisted Tet deletions via zygotic electroporation. Guides were designed in collaboration with Abishek Sampath-Kumar.

Since deficiency of all three TET enzymes is known to not be viable past the gastrulation stage (Cheng et al. 2022), we performed zygotic knock-outs and reimplanted the embryos back into surrogate females. We then accessed embryo development at E8.5 morphologically and via qPCR. In Figure 21, it is visible that embryos with a guide RNA for a zygotic KO of *Gfp* (control) developed normally (head, heart sack, and tail visible). Contrarily, the *Tet1/2/3* TKO embryos showed mostly empty deciduae and malformed embryos.

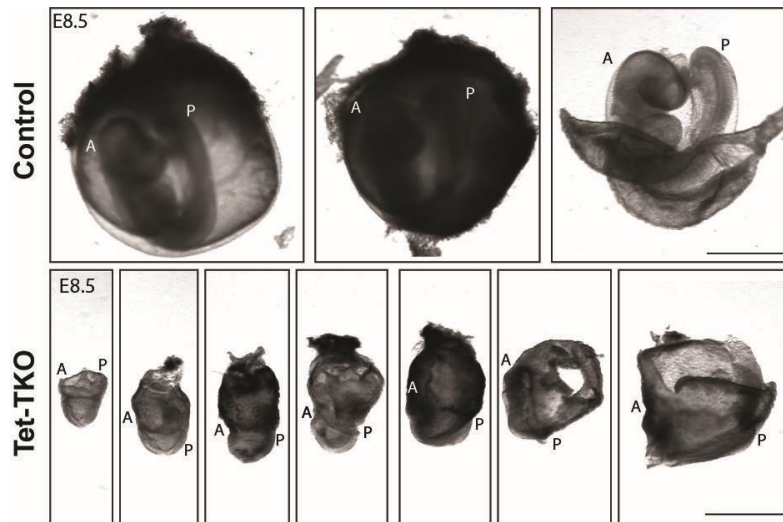


**Figure 21:** Phenotype of *Tet* TKO vs control embryos collected at E8.5 after retransfer. Scale bar = 500  $\mu$ m. Phenotypical assessment was done in collaboration with Abishek Sampath-Kumar.

qPCR of these isolates confirmed substantially reduced expression or complete absence of *Tet* mRNA from the TKO embryos (Figure 22).

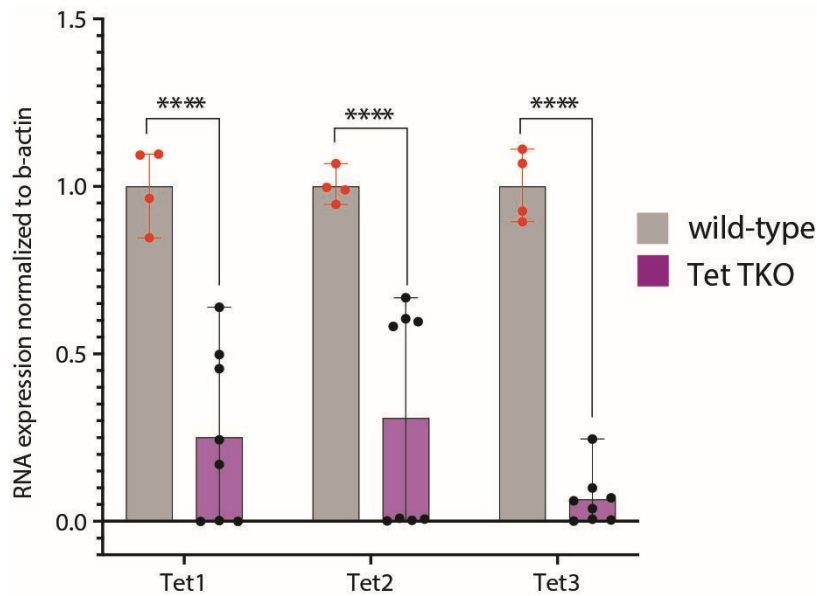


**Figure 22:** RT-qPCR showing expression levels of *Tet1/2/3* RNAs in control vs. targeted embryos. Each data point represents an embryo. 3 out of 8 embryos carry homozygous KO for all *Tet* genes.

We used the zygotic knock-out system and subjected *Tet1/2/3* TKO and *Gfp* KO E3.5 blastocysts to mTORi using 200 nM Rapalink, which resulted in a significantly decreased survival of the TKO embryos (Figure 23).



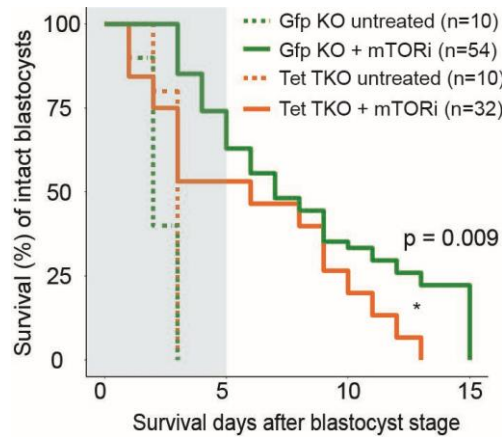


**Figure 23:** Survival curves of intact blastocysts in culture comparing *Gfp*-KO (control) and *Tet1/2/3* TKO. *n* is the number of embryos used in each experiment. The statistical test is a log-rank test (R package survdiff) comparing KO and control. The time window in which wild-type and *Tet* loss-of-function embryos show the most divergent response is highlighted. Zygotic knockouts were performed by the transgenic unit of the MPI for molecular genetics.

To corroborate the finding from the *Tet1/2* DKO ESCs, we further performed *Tet1/2* zygotic DKO. When subjecting these embryos to mTORi the *Tet1/2* DKO embryos showed significantly decreased survival compared to the *Gfp* KO control (Figure 24).

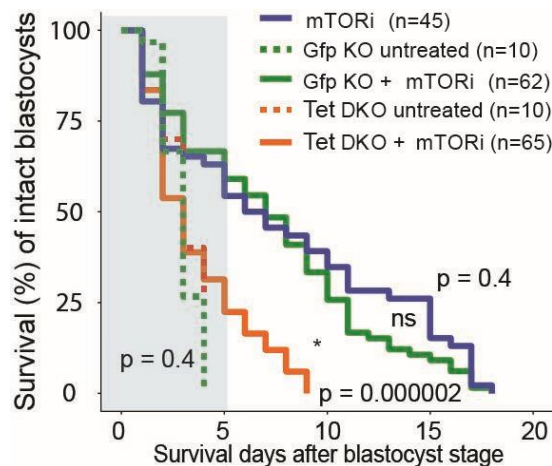


**Figure 24:** Survival curves of intact blastocysts in culture comparing *Gfp*-KO (control), *Tet1/2* DKO and wild-type. *n*, number of embryos used in each experiment. Statistical test is log-rank test (R package survdiff) comparing each KO to mTORi-only pausing. The time window in which wild-type and *Tet* loss-of-function embryos show the most divergent response is highlighted. Zygotic knockouts were performed by the transgenic unit of the MPI for molecular genetics.

Notably, the *Tet1/2* DKO embryos performed worse than the *Tet1/2/3* TKO embryos when subjected to mTORi. An increased knock-out efficiency with fewer genes targeted most

likely explains the discrepancy in the survival of these two knockouts. Additionally, zygotic knock-out efficiencies are prone to various sources of error, including time after fertilization, voltage, temperature, and experience of the experimenter. Unfortunately, genotyping of, i.e., embryos that died in a survival experiment remains challenging, potentially due to the necrotic or apoptotic nature of the dead cells. To overcome uncertainties, we used many embryos and redundant systems i.e. knock-out followed by ex-vivo pausing, knock-out followed by in-vivo diapause and knock-out followed TETi (using 100 $\mu$ M Bobcat339).

To complete the phenotypic characterization of the lack of TET enzymes and the associated inability to acquire a dormant state, we performed *Tet1/2* zygotic knockouts. We reimplanted these embryos together with *Gfp* knock-out control embryos into surrogate females and induced diapause (ovariectomy and daily injections of 30mg progesterone). After 96h of diapause, we assessed the quantity and quality of embryos that entered diapause (Figure 25). In the control knock-out, 30.8% of reimplanted embryos successfully entered diapause. In contrast, 9.4% of embryos successfully entered dormancy in the case of the *Tet1/2* DKO.

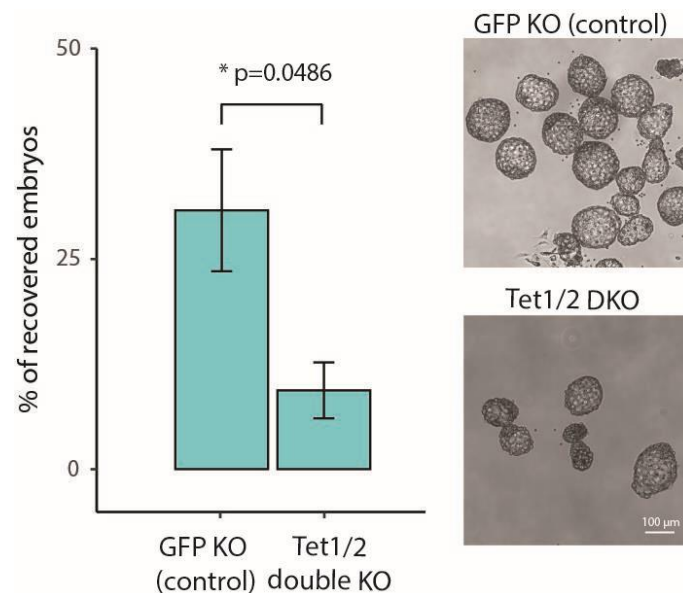


**Figure 25:** In vivo diapause efficiency of retransferred control or *Tet1/2* DKO blastocysts. TET deficiency significantly reduces the recovery rate after in vivo diapause. Right, representative bright field images. Zygotic knockouts were performed by the transgenic unit of the MPI for molecular genetics.

### 2.2.2 Pharmacological modulation of TET activity in ex vivo diapause

The cytosine-based TET inhibitor Bobcat339 provides a pharmacologic means to inhibit TET activity in a mid-micromolar range (Chua et al. 2019). Treatment with the inhibitor at 100

$\mu\text{M}$  in combination with Rapalink significantly decreased the survival of embryos compared to those treated with DMSO and Rapalink (vehicle control) (Figure 26a). The effect was even more pronounced when treating the embryos for 12h before reaching the E3.5 blastocyst stage (Figure 26b). The pharmacokinetics of Bobcat339 might explain this effect. Notably, most Bobcat339- and Rapalink-treated embryos did not enter a dormant state at all and collapsed before the control embryos. The treatment of Bobcat339 did not affect the control embryos.

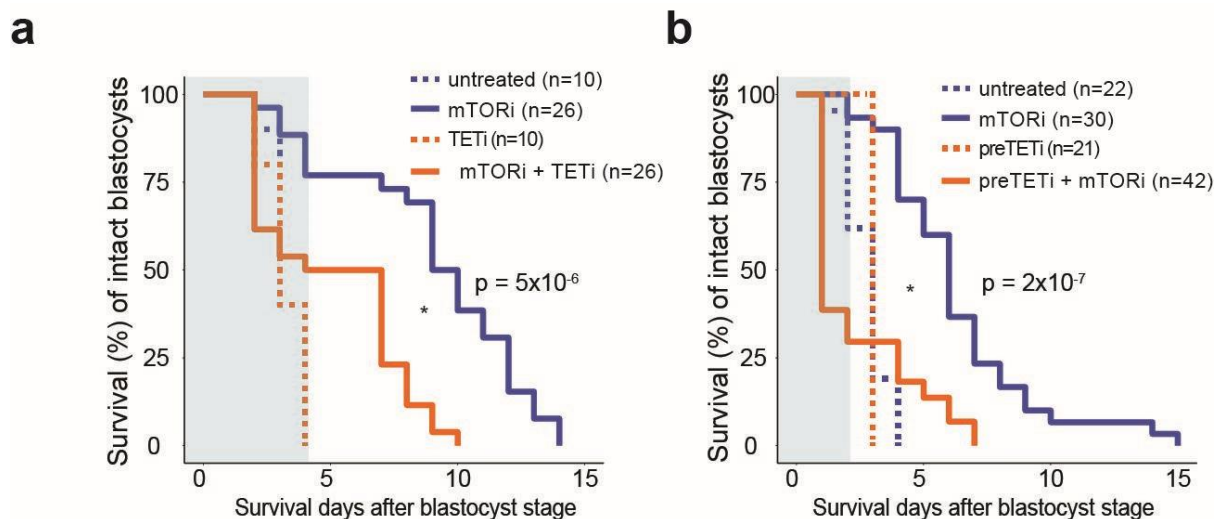


**Figure 26:** Survival curves of intact blastocysts in culture comparing DMSO treated (control) and Bobcat339 treated embryos. n is the number of embryos used in each experiment. The statistical test is a log-rank test (R package survdiff). The time window in which DMSO and Bobcat339 treated embryos show the most divergent response is highlighted. Zygotic knockouts were performed by the transgenic unit of the MPI for molecular genetics.

Lastly, we tested the effect of supplementing embryos with the TET enzyme co-factors vitamin C and alpha-ketoglutarate. Both cofactors seemed to promote the survival of the embryos in the first 5 days of mTOR. However, there was no effect on the maximum survival of these embryos (Figure 27).

These experiments provide a consistent phenotype and show that TETs are crucial for the dormant state in ESCs and embryos. Figure 28 provides an overview of how knock-out and Tet inhibitor-treated embryos look compared to their control knock-out and vehicle-treated counterparts.

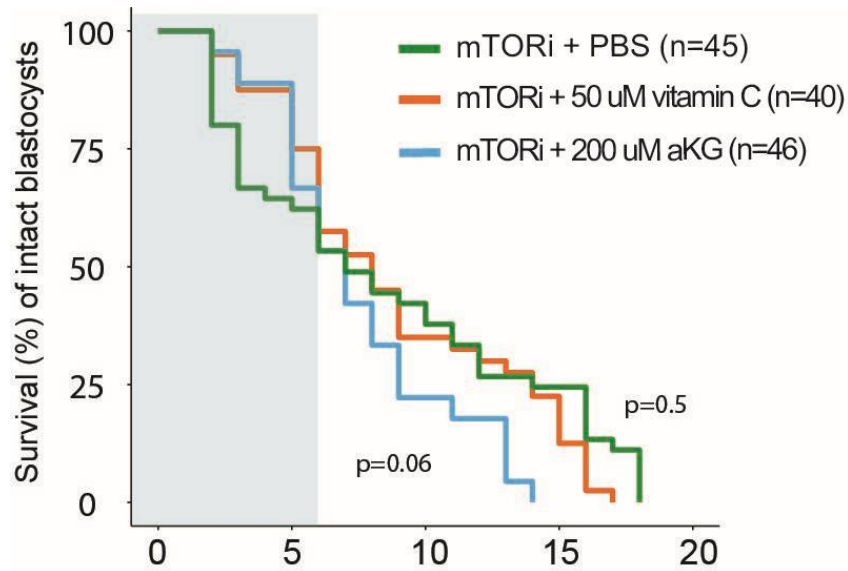


**Figure 27:** Survival curves of intact blastocysts in culture supplemented with the TET cofactor a-ketoglutarate or vitamin C. n, number of embryos used in each experiment. A statistical test is a log-rank test (R package survdiff) comparing each condition to mTORi-only pausing. The effectivity window is highlighted. Zygotic knockouts were performed by the transgenic unit of the MPI for molecular genetics.

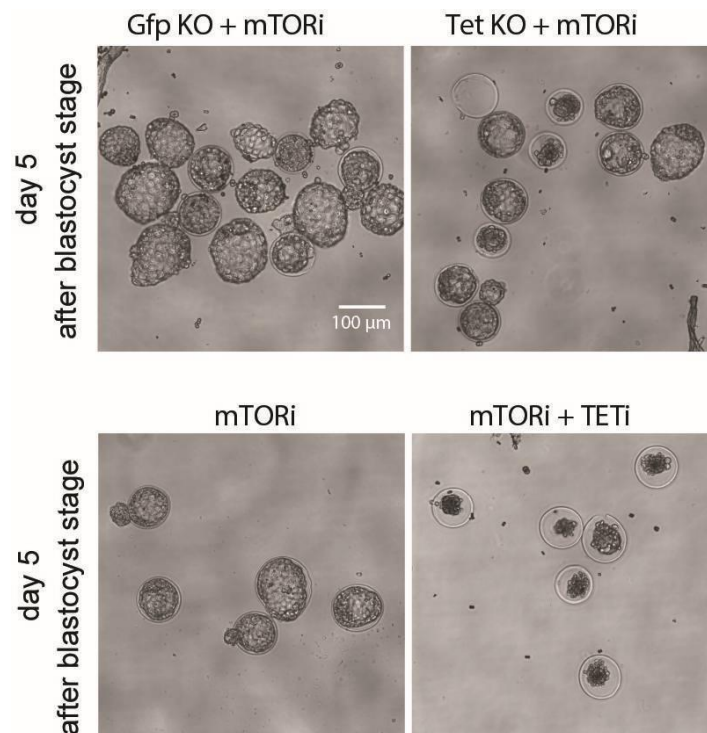


**Figure 28:** Bright field images of representative embryos captured on indicated days of pausing.

## 2.3 Epigenetic profiling of wild-type and *Tet1/2* double knock-out mESCs

### 2.3.1 *Tet1/2* DKO ESCs show global defects in DNA accessibility and transcription but not DNA methylation

The inability to acquire a dormant pluripotent state in absence of TETs appears as a reproducible phenotype in both ESCs and embryos. Due to a limited number of ESCs and animal ethical reasons, it was decided to epigenetically profile the dormant state and the regulation of the dormant state with respect to TETs in ESCs. Dormant embryos and ESCs exhibit increased methylation and we found TETs to play a crucial role in dormancy. To get further insight, WGBS was performed, and CUT&Tag was performed for TET1 and TET2. We further hypothesized that increasing methylation in hand with the global suppression of transcription would impact the chromatin landscape. Therefore, we performed the Assay for Transposase-Accessible Chromatin using sequencing (ATAC-seq). All experiments were performed in wild-type and *Tet1/2* DKO ESCs and in a time-resolved manner (Figure 29).

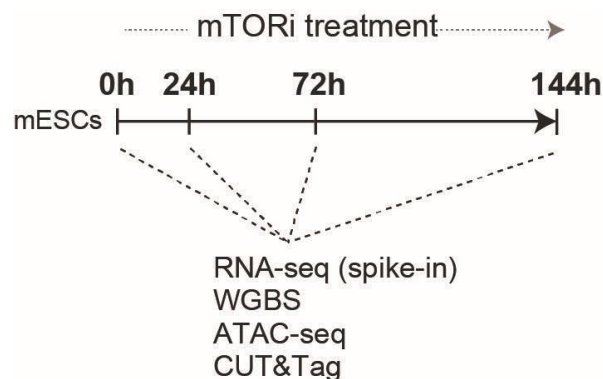


**Figure 29:** Experimental workflow to profile transcriptional and chromatin features of ESCs entering mTORi-induced dormancy. Two replicates were performed for all experiments.

Besides untreated ESCs, an early time point (24h), an intermediate time point (72h), and a time point that represents the established dormant state (144h) were chosen to profile the ESCs. The goal was to capture the dynamic regulation of the dormant state. Notably, we profiled the *Tet1/2* DKO ESCs only until 72h. This is based on the phenotypical observations and pluripotency assays performed in Figures 16 and 17. The lack of TET1 and TET2 seems incompatible with dormancy from 72h onwards. This incompatibility manifests in a decrease of SSEA1-positive ESCs at 72h (Figure 17).

A full disintegration and absence of alkaline phosphatase is observed at 96h (Figure 17). A principal component analysis of the RNA-seq data revealed that the *Tet1/2* DKO ESCs initially follow the trajectory into the dormant state (Figure 30, compare 0h and 24h of wild-type and DKO, respectively). This goes in hand with the SSEA1 assay which showed the breakpoint between wild-type and DKO to be between 48h and 72h and indicates that initially TET activity might be overwritten by other cues of the mTORi. In Figure 30 it is visible that wild-type ESCs progress into a dormant state (72h and 144h) but the 72h *Tet1/2* DKO samples revert towards their starting point on principal component one and two, respectively.

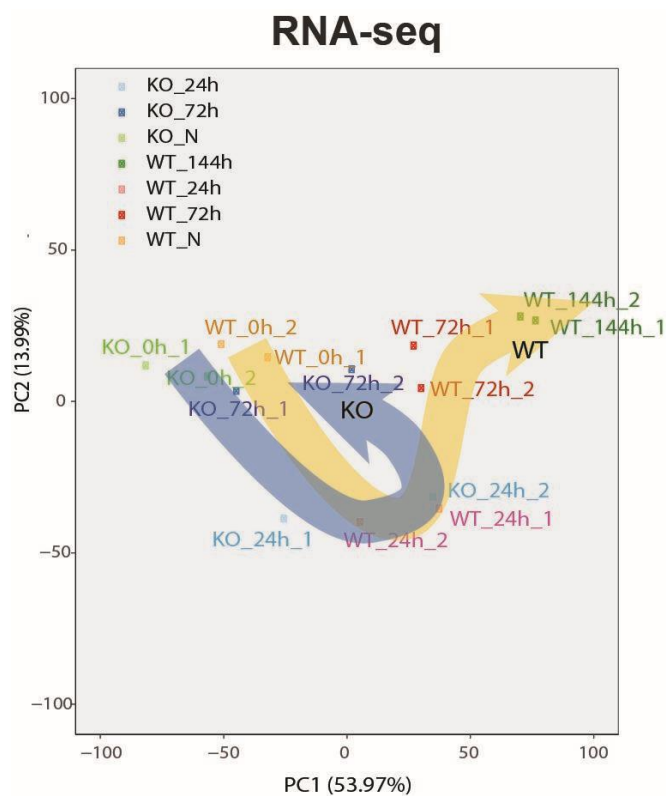


**Figure 30:** Principal components analysis (based on 5000 most variable genes between 0h and 144h wild-type) of all RNA-seq samples. *Tet1/2* DKO ESCs were collected until 72h before differentiation of colonies. *Tet1/2* DKO ESCs initiate the dormancy program however fail to fully establish it.

This is further observable when plotting the total of the expressed genes in a heatmap (Figure 31). The wild-type shows a stepwise downregulation of the transcriptome over time. The *Tet1/2* DKO ESCs seem to follow this trend only until 24h and fail to further suppress transcription at 72h.

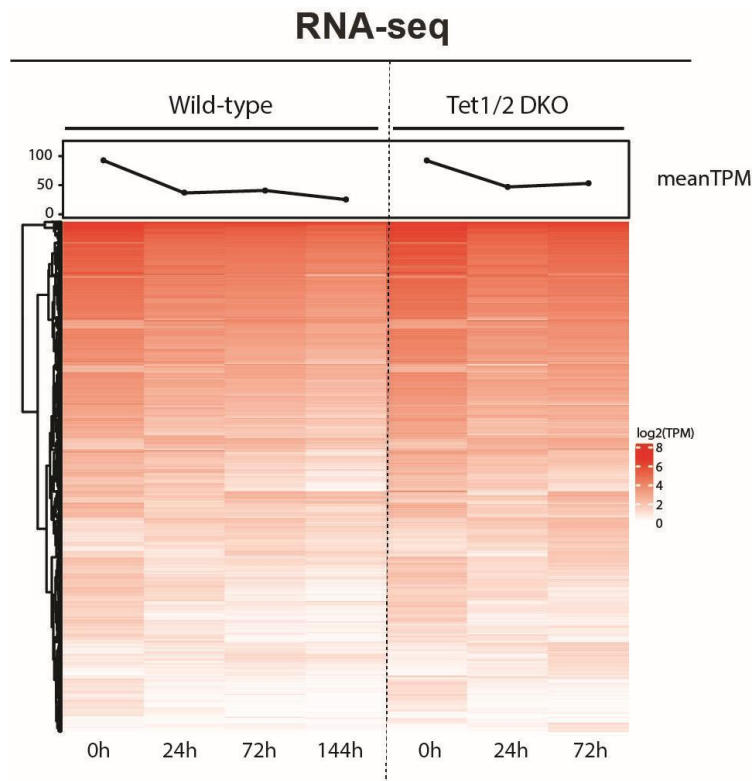


**Figure 31:** Spike-in normalized bulk RNA-seq heatmap showing expression of all genes over time in wild-type vs *Tet1/2* DKO ESCs treated with mTORi. Line plot on top shows mean TPM at each time point. RNA-seq analysis was advised by Helene Kretzmer.

A differential expression analysis at 72h comparing the *Tet1/2* DKO ESCs vs. wild-type revealed the upregulation of stress and apoptosis related proteins such as FXYD5, RTKN, RCSD1, CDK18, AQP3, and AQP6 (Figure 32).

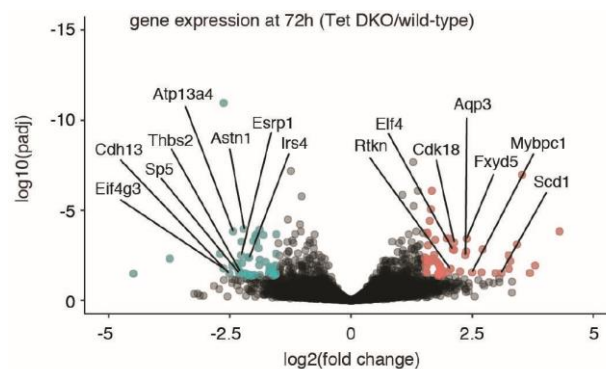


**Figure 32:** Differentially expressed genes in *Tet1/2* DKO vs. wild-type at 72h of mTORi treatment.

Using the RNA sequencing data, the expressed pathways per time point were accessed and their change in expression compared to 0h was quantified. The same pathways and their respective change in expression compared to 0h was subsequently quantified in the *Tet1/2* DKO ESCs. The relative expression of each pathway compared to 0h was then plotted as a



correlation plot between wild-type and *Tet1/2* DKO at 24h and 72h (Figure 33). This analysis supports the previous data showing that the relative pathway expression correlates significantly at 24h ( $R=0.56$ ,  $p < 2.2 \times 10^{-16}$ ) but is not correlated at 72h ( $R=-0.012$ ,  $p=0.83$ ).

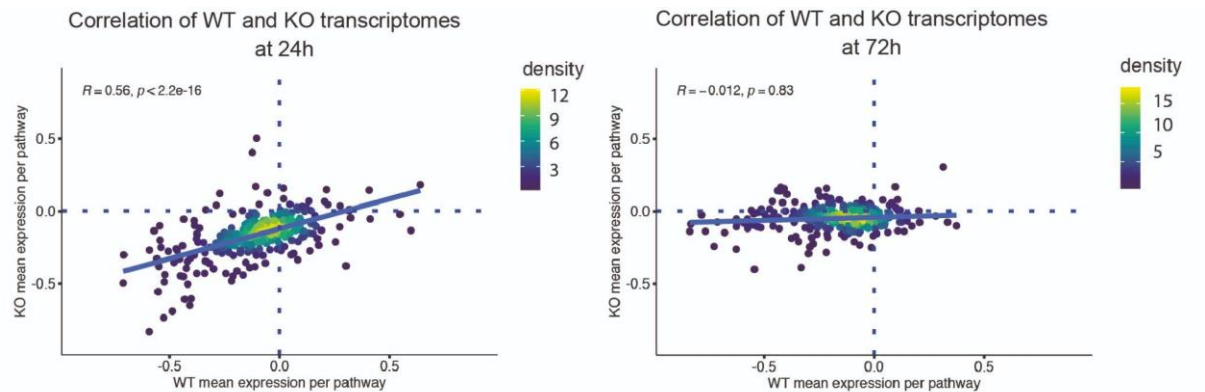


**Figure 33:** Correlation of pathway expression in wild-type and *Tet1/2* DKO ESCs at 24h and 72h of mTORi treatment. In collaboration with Vera van der Weijden.

The undirected upregulation of the transcriptome and the upregulation of stress factors, as mentioned earlier, indicate a general deregulation due to an incompatibility of dormancy with a lack of Tet enzymes. Taken together the RNA-seq results show a stepwise suppression of the transcriptome in dormant ESCs and support the finding that the knock-out of *Tet1* and *Tet2* is incompatible with the dormant state.

Plotting the average methylation per 1kb tile from the WGBS data showed that dormant ESCs exhibit increased methylation and supported the results from the initial IF experiments (Figure 34). Both wild-type and *Tet1/2* DKO ESCs show the onset of increased methylation at 72h when looking at average methylation per 1kb tile of the genome. This increase peaks at 144h in the wild-type. Notably the increased methylation is not observable in CpG island containing promoters (Figure 34).



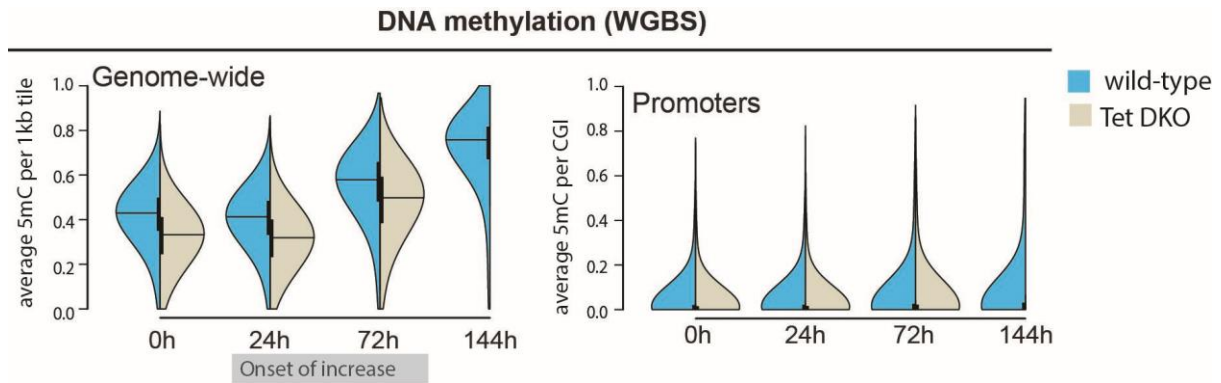


**Figure 34:** DNA methylation levels in wild-type vs *Tet1/2* DKO ESCs as mapped by WGBS. Average DNA methylation levels of the entire genome in 1kb tiles (top) or CpG islands (bottom) are shown. Horizontal lines show the median; box plot within violin plots show interquartile range (IQR) and the whiskers show 1.5 IQR. In collaboration with Helene Kretzmer.

Other genomic features such as CGI shelves, CGI shores, LINES, SINES and LTRs were analysed for their methylation state and increased methylation over time was observed, respectively (Figure 35). Repetitive DNA features such as LINES, SINES and LTRs showed the same trend of increased methylation at 72h and 144h as the genome wide analysis (Figure 35).

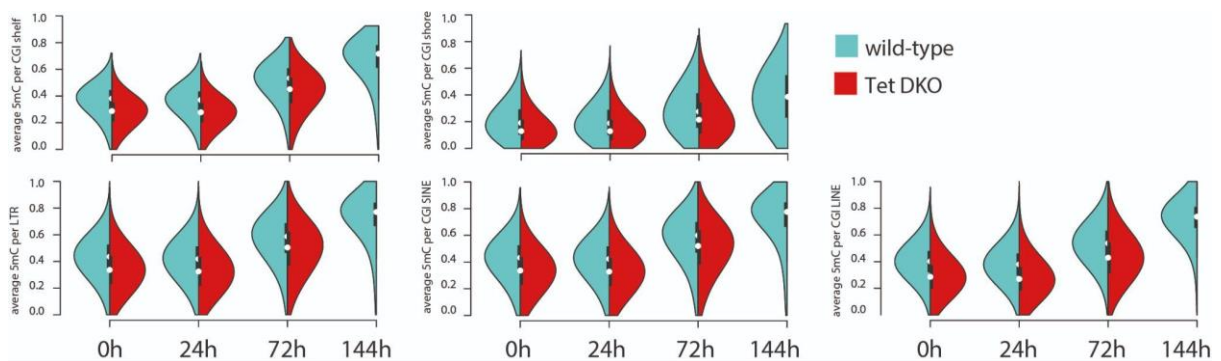


**Figure 35:** DNA methylation levels of different genomic features in wild-type vs *Tet1/2* DKO ESCs. In collaboration with Helene Kretzmer.

In summary, we observed a genome-wide increase in methylation levels that did not affect the CGI-containing promoter regions. Changes in methylation were consistent between the wild-type and the *Tet1/2* DKO at 0h, 24h, and 72h.

Previous studies show that the dormant state in embryos is accompanied by a decrease of H4K16ac, a histone mark positively correlated with chromatin accessibility. To analyse the chromatin accessibility, peak calling was performed in all four wild-type samples (time

points) of ATAC-seq. data and this set was used as a reference set of peaks. Further, deeptools was used to divide the reference peaks set into three clusters based on their accessibility at 0h in the wild-type. After this, these clusters were used to plot chromatin accessibility globally for all wild-type and *Tet1/2* DKO time points, respectively (Figure 36).

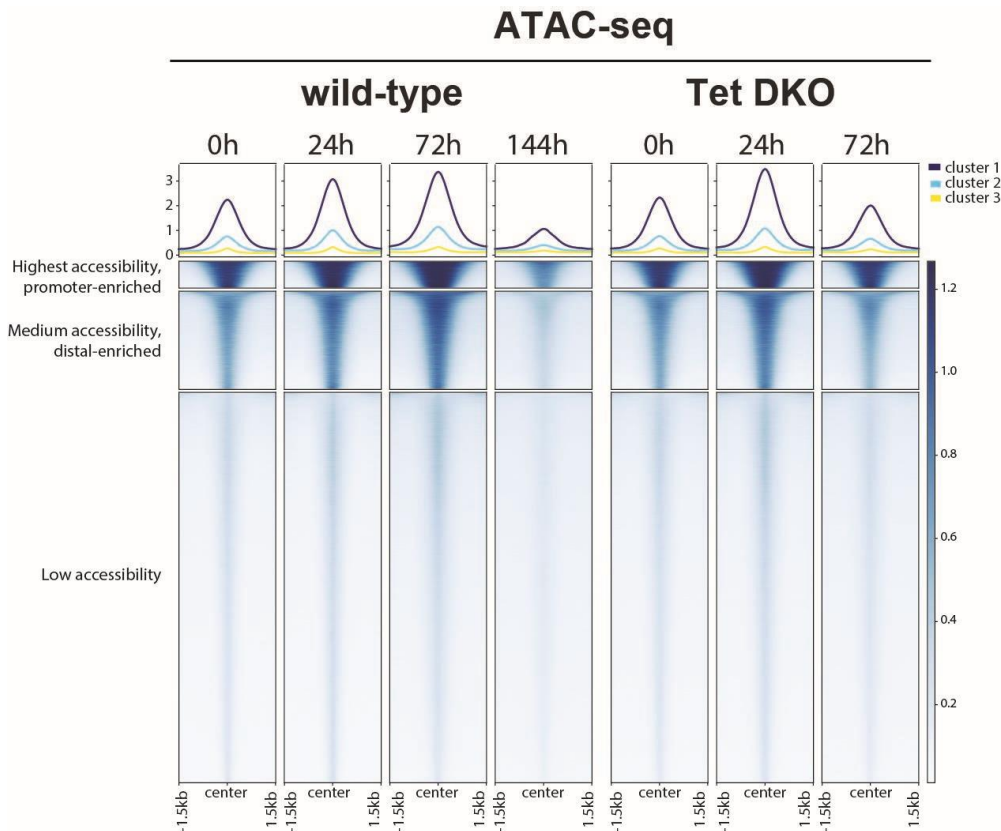


**Figure 36:** Accessibility of regulatory elements in wild-type vs. *Tet1/2* DKO ESCs as mapped by ATAC-seq. All accessible regions, as determined by peak calling, were clustered into three groups showing high, medium, and low accessibility.

Surprisingly, chromatin accessibility followed neither the trajectories of the RNA-seq data nor that of the WGBS data. Global accessibility showed an initial increase in both wild-type and DKO ESCs. The established dormant state in the wild-type showed reduced accessibility compared to 0h. Interestingly, wild-type and *Tet1/2* DKO diverge in the patterns of accessibility. While accessibility peaks at 72h in wild-type ESCs, it peaks at 24h in *Tet1/2* DKO ESCs.

In summary, the phenotypical divergence in response to dormancy observed earlier is recapitulated by the RNA-seq and the accessibility data. Methylation was consistent in both cell lines, further hinting towards a TET-driven remodelling of the chromatin landscape.

Therefore, despite undertaking the initial phases of dormancy transition, *Tet1/2* DKO ESCs deviate from the dormancy pathway and decrease the expression of pluripotency markers following an elevation in DNA methylation levels.

## 2.4 TET dormancy targets

### 2.4.1 TETs demethylate enhancers and LINE elements in dormancy

Previous studies have shown that the knock-out of TET enzymes is compatible with the ESC state and that there is limited aberrant methylation (Cheng et al., 2022). Wild-type and *Tet1/2* DKO ESCs showed increased global methylation levels at 72h. Further, it was established that TETs are crucial to successfully enter the dormant state. We hypothesized that there are regions in the genome that are dormancy-specific Tet regulated in the wild-type. The dysregulation of these regions in the *Tet1/2* DKO limits its capacity to enter dormancy. Since the canonical function of TETs is to demethylate and both wild-type and *Tet1/2* DKO ESCs show increased methylation at 72h, we hypothesized that their absence should cause aberrant methylation in the *Tet1/2* DKO ESCs at 72h. To test this hypothesis, peak calling for TET1 and TET2 in the TET CUT&Tag data sets was performed. All peaks identified in the wild-type conditions were summarized as a reference set (107461 and 12486 peaks for TET1 and TET2, respectively). Methylation levels of these peaks between the wild-type and the *Tet1/2* DKO were compared and filtered for a difference in methylation (*Tet1/2* DKO > wild-type) of more than 10% (Figure 37).

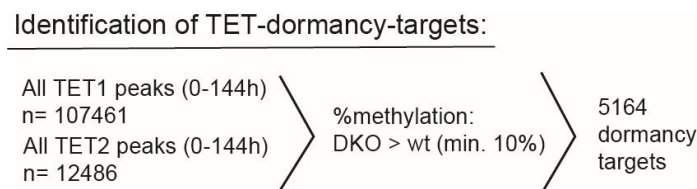


**Figure 37:** Identification of TET-dormancy-targets. Sites bound by TET1 and/or TET2 and kept demethylated by TET activity (i.e., methylation is increased only in the *Tet1/2* DKO at 72h) are specified as targets.

Of the 119947 total TET peaks, 5164 showed increased methylation, specifically in the *Tet1/2* DKO ESCs at 72h. The analysis indicates that TETs actively target the underlying regions during dormancy, and these regions were named Tet dormancy targets. The identified peaks were annotated, and 23% appeared to be ESC enhancers (10% active enhancers and 13% primed enhancers) (Figure 38). Most dormancy targets were annotated as repetitive

elements, of which L1Md LINE repeats stood out as a group with 33% (Figure 38). Taken together, the computational strategy employed identified a subset of genomic targets regulated by TET1 and TET2.

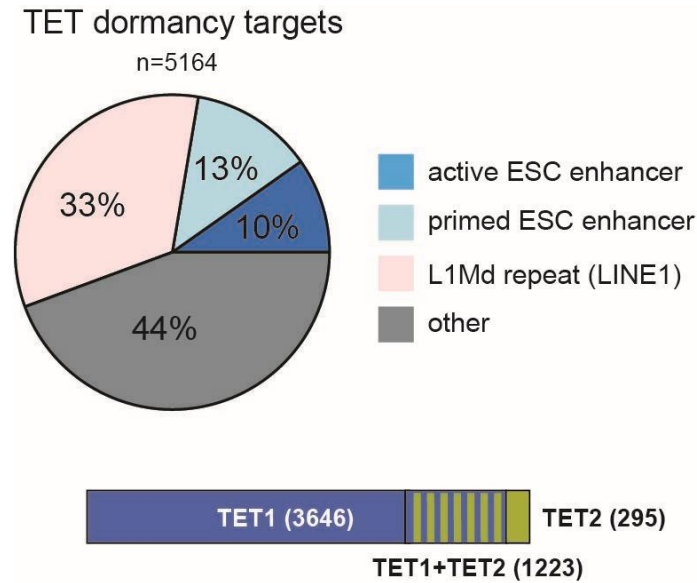


**Figure 38:** Pie charts showing the distribution of different genomic features within TET-dormancy-targets. The bar plot shows TET1- and/or TET2-bound targets as determined by CUT&Tag.

#### 2.4.2 TET dormancy targets are characterized by low methylation and enrichment of transcription factor motifs

To further characterize the regulatory elements targeted by TETs during dormancy, their levels of TET occupancy, DNA methylation, and DNA accessibility were analysed. The results are shown as a heatmap (Figure 39). Signal quantifications over a set of genomic features displayed as boxplots and violin plots (Figure 40). The two ways of visualization, enable the discrimination of modes of regulation between the TET dormancy targets versus the remaining genome. To keep this analysis comprehensive, the 72h hours timepoint was chosen for visualization since the trajectories into dormancy between wild-type and *Tet1/2* DKO diverge at that point (Figure 39).

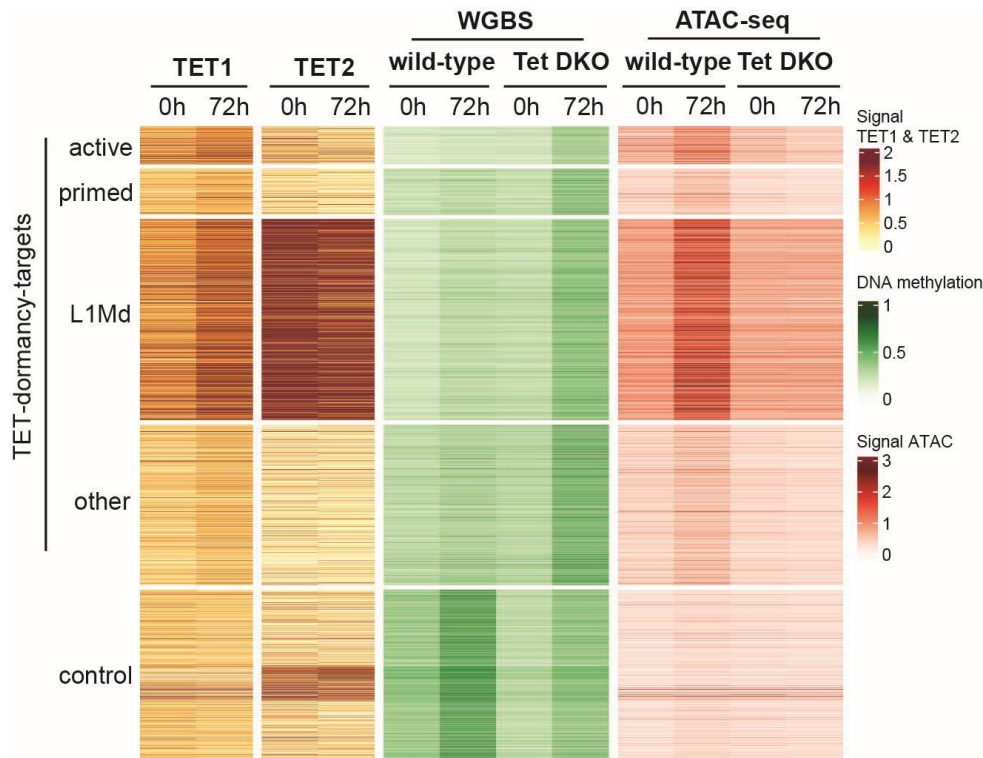


**Figure 39:** Heatmap showing mean levels of TET occupancy, DNA methylation, and chromatin accessibility at TET-dormancy-targets in wild-type vs *Tet1/2* DKO ESCs over time during mTORi treatment. Control: 2000 random sites with increased DNA methylation in wild-type ESCs at 72h compared to 0h.

The identified TET dormancy targets share the specific feature of staying devoid of methylation in the wild-type ESCs while gaining methylation in the *Tet1/2* DKO ESCs. As a control, randomly sampled TET peaks show increased methylation at 72h of dormancy in wild-type and KO ESCs. Comparing the violin plots in Figure 40 (top lane), it is visible that all TET peaks (all peaks) show low methylation levels at 0h and increased methylation levels at 72h in wild-type and *Tet1/2* DKO ESCs. The “active enhancer” cluster shows the low starting methylation level at 0h in both cell lines. At 72h only the *Tet1/2* DKO ESCs show increased methylation at the active enhancer cluster while it stays devoid of methylation in the wild-type (Figure 39 & Figure 40). The same trend can be seen for the other TET dormancy target clusters. Interestingly, staying devoid of methylation correlates with increased accessibility for the dormancy target regions in the wild-type.

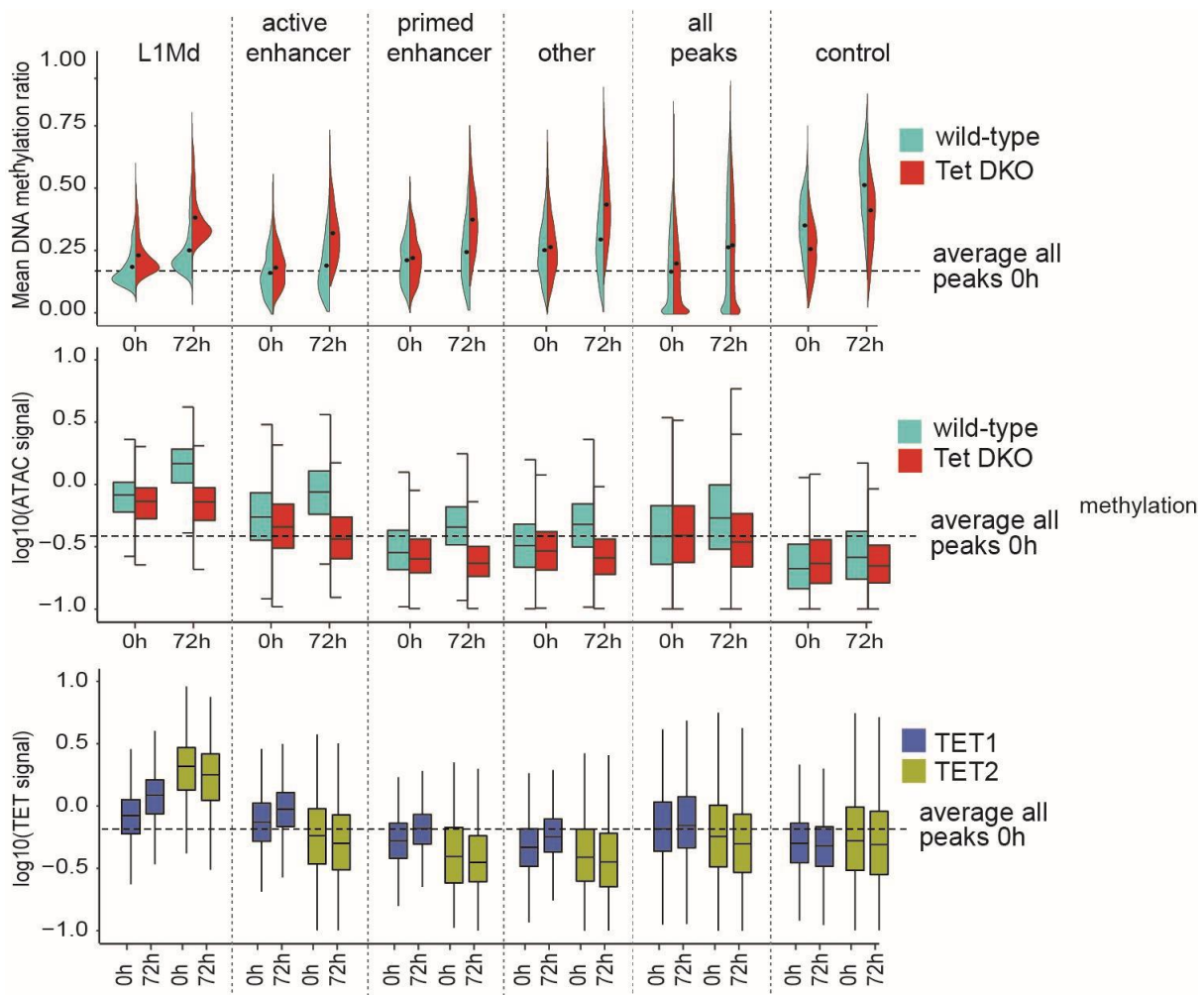


**Figure 40:** Quantification of data shown in Figure 39 vs all TET peaks. Dashed lines show the median signal at all TET peaks in wild-type ESCs at 0h. Horizontal lines show the median; box plots within violin plots show interquartile range (IQR), and the whiskers show 1.5 IQR.

The protection from increasing methylation and increased accessibility is specific to the TET dormancy targets. Although all TET peaks show increased DNA accessibility, the amplitude and discrepancy of this increase are more pronounced in the TET dormancy targets. Lastly, the TET dormancy targets seem to be unique in their level of TET occupancy and a dormancy-specific increase in the level of TET occupancy. Figure 41 highlights these results by zooming in on an example region of a TET dormancy target provided as a scaled genome viewer snapshot.



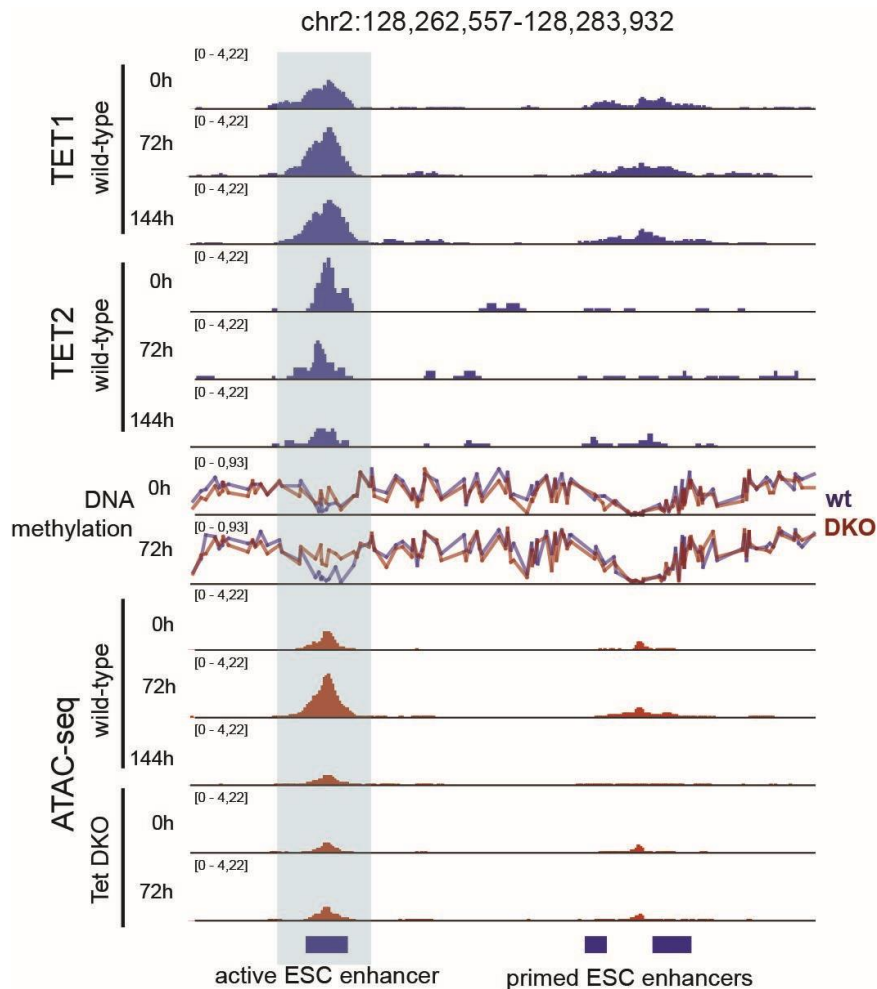








**Figure 41:** Genome browser view of an example TET-dormancy-target active enhancer and a neighboring non-target primed enhancer.

## 2.5 TET activity facilitates the enrichment of transcription factors at dormancy targets

### 2.5.1 Dormancy targets show enrichment of the transcription factors KLF4, YY1, TFE3, ZFP57, SMAD3 and MYOD1.

To gain insight into a potential commonality of the dormancy target regions, a motif enrichment analysis against the background genome using “homer” was performed (Figure 42). This analysis yielded several transcription factor motifs found in more than 20% of the dormancy target regions but had only little occurrence in the remaining genome. Most of the enriched transcription factor motifs contain a CpG. Further KLF4, TFE3, and YY1 have been shown to exhibit sensitivity to methylation (Kreibich et al. 2023; Kim 2003).

Logo	TF	% of TET targets	% of background
	KLF4	28.66	1.77
	SMAD3	27.72	1.00
	TFE3	24.36	0.58
	MYOD1	32.11	2.30
	YY1	33.50	1.96
	ZFP57	39.07	3.05

**Figure 42:** Transcription factor motif enrichment analysis at TET-dormancy-targets. The presented motifs are all significant with p-value < 0.0001.

Subsequently, a transcription factor footprinting analysis was performed with the dormancy enriched TFs and the classical pluripotency TFs (c-MYC, NANOG, OCT4, and SOX2) (Figure 43). The footprinting algorithm TOBIAS uses ATAC-seq data and statistically analyses the read distribution over a transcription factor motif (Bentsen et al. 2020). If a transcription factor motif shows statistically less reads at the site of the motif, the algorithm infers that the motif was occupied by the corresponding transcription factor. This is then reflected as a positive binding activity level (Figure 43). Binding activity is increased for the dormancy target transcription factors at 72h 144h, respectively, compared to 0h. Generally, it can be observed that the dormancy target transcription factors show increased binding activity levels while the classical pluripotency TFs show decreased binding activity levels over time. The pluripotency TFs NANOG, OCT4, and SOX2 increase their binding activity level at 24h. This correlates with the globally increased DNA accessibility at 24h in the wild-type and *Tet1/2* DKO, respectively. It indicates that increased DNA accessibility potentially provides a window where TF binding is facilitated globally. At the 72h and 144h time points, however, the binding activity level of all tested pluripotency TFs is decreased. This raises the question of how specificity for the dormancy TFs is achieved opposed to general pluripotency TFs.



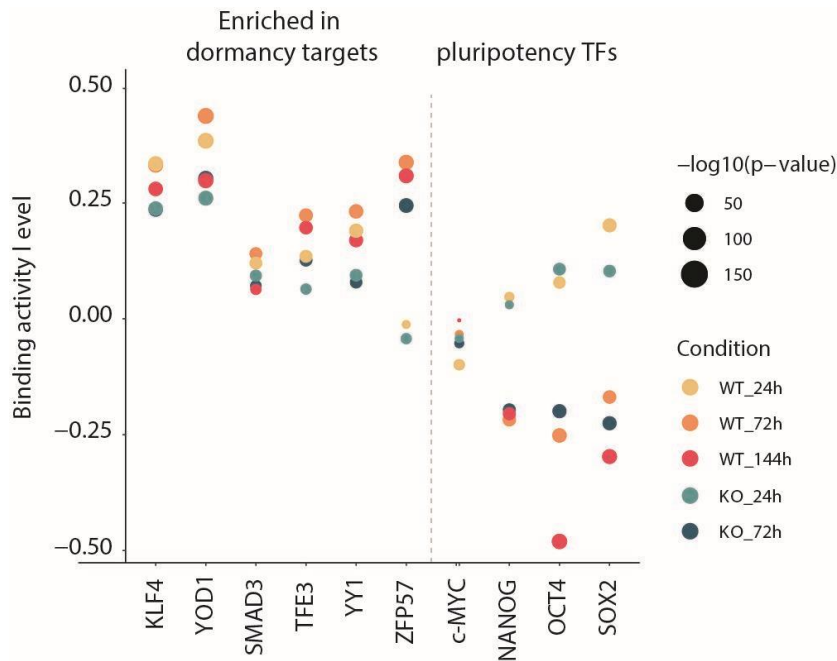


**Figure 43:** TF footprinting analysis of predicted TET-activity-coupled TFs vs classical pluripotency TFs. ATAC-seq signal from wild-type and *Tet1/2* DKO ESCs was used. TFE3, YY1, and ZFP57 footprints are elevated at 144h in wild-type ESCs compared to *Tet1/2* DKO ESCs. In contrast, footprints of pluripotency-associated TFs are reduced. In collaboration with Yufei Zhang.

### 2.5.2 TFE3 accumulation is TET-dependent and dormancy specific

To get further insight into the nature of the dormancy targets and their regulation by the TFs, TFE3 was profiled using CUT&Tag. When plotting the TFE3 signal over the dormancy targets, the active enhancer and L1Md cluster showed the strongest enrichment over time in the wild-type ESCs. The control cluster, the ‘other’ cluster, and the primed enhancer cluster showed rather constant binding levels (Figure 44). The DKO ESCs did not show enrichment of TFE3 at dormancy targets at 72h, except for the L1Md cluster. This result suggests i) active enhancers and L1Md repeats predominantly recruit TFE3, ii) TFE3 is not recruited to active enhancers in the absence of TETs, and iii) there are likely TET-independent recruitment mechanisms for TFE3 in L1Md repeats.

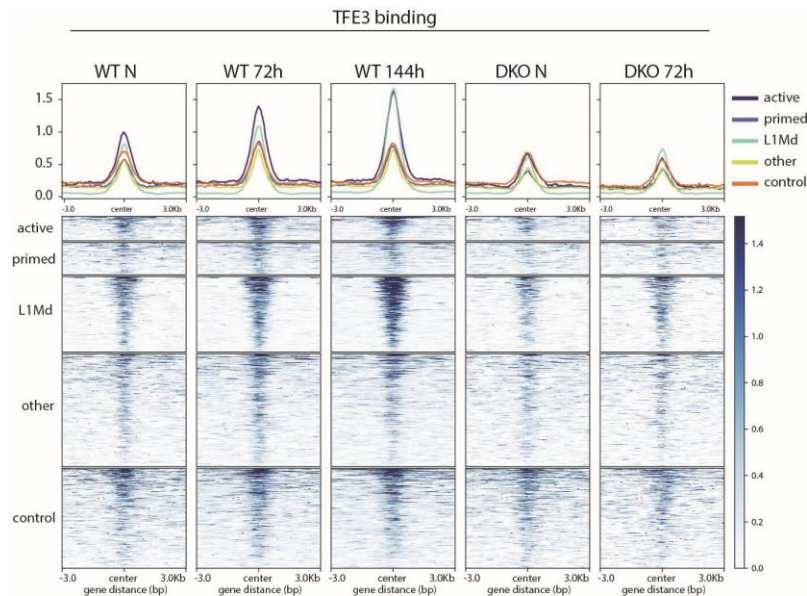


**Figure 44:** Levels of TFE3 binding at TET-dormancy-targets vs. controls, mapped by CUT&Tag. TFE3 occupancy increases over time, specifically at sites kept demethylated by TETs, particularly at LIMd repeats and active enhancers. In collaboration with Joy Cheng.

To get further insight into the specificity of TFE3 accumulation, its signal was compared between the TET dormancy targets and canonical TFE3 binding sites (defined by MACS2 peak-calling at 0h in the wild-type) (Figure 45).

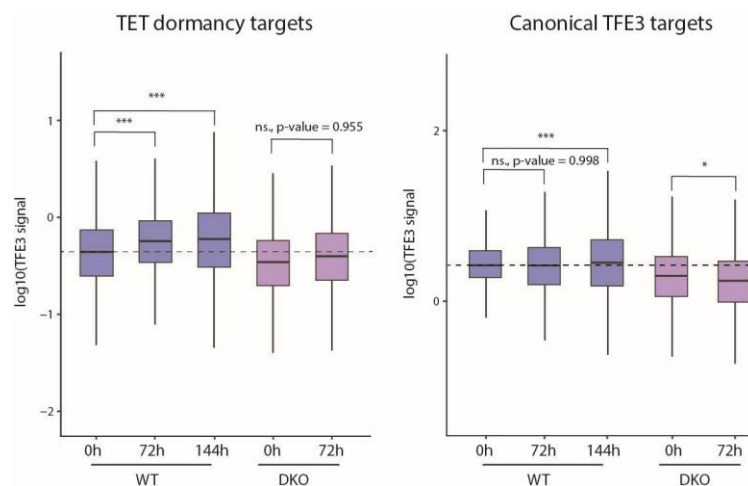


**Figure 45:** Quantification of data shown in (c) vs canonical TFE3 targets (as identified by peak calling at  $t=0h$ ). Dashed lines show the median TFE3 signal in wild-type ESCs at 0h. A statistical test is a one-way ANOVA with Tukey's multiple comparison test.

This shows an enrichment of TFE3 over time in the dormancy targets but not the canonical TFE3 binding sites. The same comparison in the *Tet1/2* DKO ESCs shows less binding of TFE3 in the absence of TETs. Canonical TFE3 binding sites show decreased binding of

TFE3 at 72h in the absence of TETs. This supports previous findings that increased methylation decreases the probability of bHLH transcription factors like TFE3 (Kreibich et al. 2023). The genome viewer snapshot in Figure 46 highlights the TET-TFE3 axis at an example L1Md element.

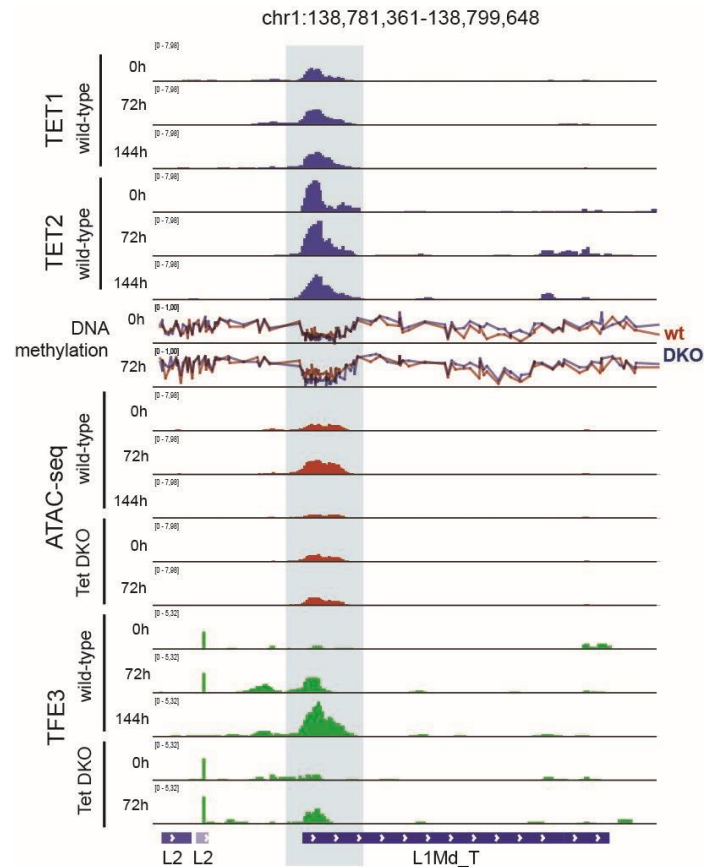


**Figure 46:** Genome browser view of a TET-dormancy-L1Md repeat showing TET and TFE3 occupancy, DNA methylation, and genome accessibility.

### 2.5.3 TFE3 and YY1 co-immunoprecipitate with TET1

As introduced, TETs are promiscuously interacting proteins, and the list of experimentally confirmed interaction partners is growing (Zhang et al. 2023). To corroborate the transcription factor motif enrichment analysis results, a native co-immunoprecipitation of TET1 in proliferating and 144h dormant wild-type ESCs was performed. Figure 47 shows the proteins identified in both conditions as a correlation plot. The approach identified known TET1 interaction partners such as SIN3A, DNMT3b, and KDM2a. Further, this approach identified TFE3 and YY1 as co-immunoprecipitated, supporting potential recruitment or co-binding of these TFs with TETs.

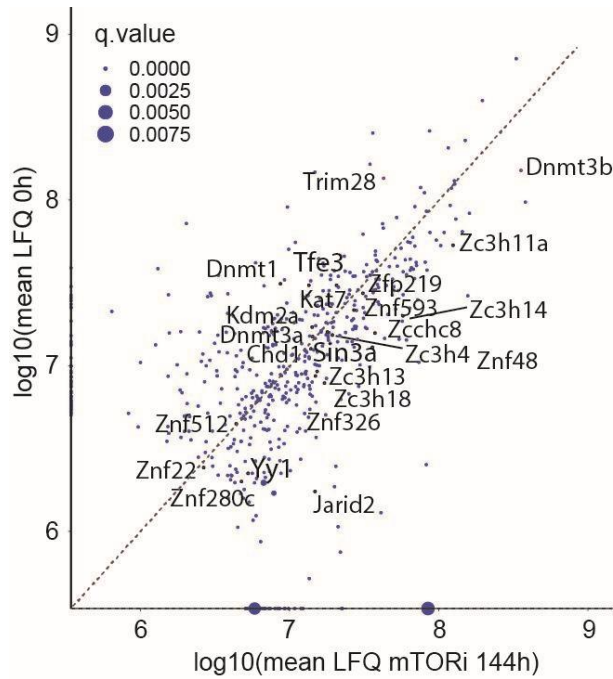


**Figure 47:** Proteins co-precipitated with TET1, as identified by IP-mass spectrometry.

### 2.5.4 Knock-down of TFE3 prevents ESCs from entering a dormant state

To validate the importance of TFE3 in the regulation of dormancy, a doxycycline-inducible shRNA-mediated TFE3 knock-down cell line was created. Using three shRNAs against TFE3, efficient loss of TFE3 signal was observable after 24h of doxycycline induction (Figure 48a). Transduced ESCs were treated for 24h with doxycycline and/or the vehicle control and subsequently subjected to mTOR. While the vehicle control entered the dormant state, the TFE3 KD ESCs failed to acquire a dormant state and showed a similar phenotype as the *Tet1/2* DKO ESCs (Figure 48b). This result supports the importance of properly regulated dormancy targets for ESCs to enter a dormant state.

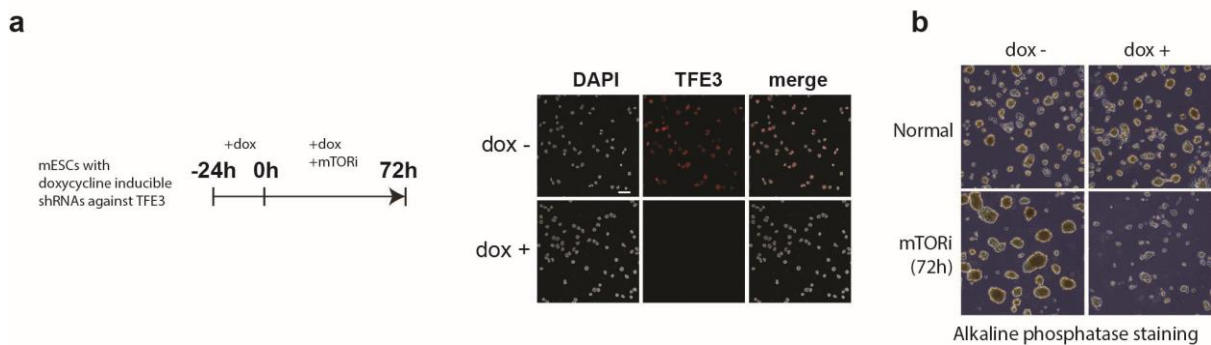


**Figure 48:** a. Experimental outline of inducible TFE3 knockdown (*Tfe3* iKD) and mTORi treatment. Right: Immunofluorescence images showing efficient knockdown of TFE3 expression after 24h of doxycycline

treatment. **b.** Alkaline phosphatase staining of control or *Tfe3* iKD ESCs with or without mTORi treatment. *Tfe3* iKD ESCs lose pluripotent colony morphology and marker expression after 72h of mTORi culture.

## 2.6 TET dormancy targets are bookmarked

### 2.6.1 TET regulation of dormancy targets does not influence transcription of associated genes

In the chapters 2.4 and 2.5, it has been established that a subset of TET peaks that coincide with enhancers and LINE1 repeats. Both are protected from an increase in methylation, show increased binding activity of TFE3, KLF4, YY1, and ZFP57, and accumulate TFE3 in dormancy. Enhancers create an obvious connection to transcription, and LINE1 repeats have also been shown to act as enhancers (Elbarbary, Lucas, and Maquat 2016; Karttunen et al. 2023). To probe possible effects on transcription, the Activity-By-Contact model was used. The model uses H3K27ac, ATAC signal, and Hi-C data to predict the contact of non-promoter accessible DNA to genes was used to predict contacted genes (Fulco et al. 2019). The probability cutoffs for potential contacts were used as recommended by the authors. Genes contacted by active enhancers in wild-type ESCs did not show elevated expression compared to *Tet1/2* DKO ESCs (Figure 49).

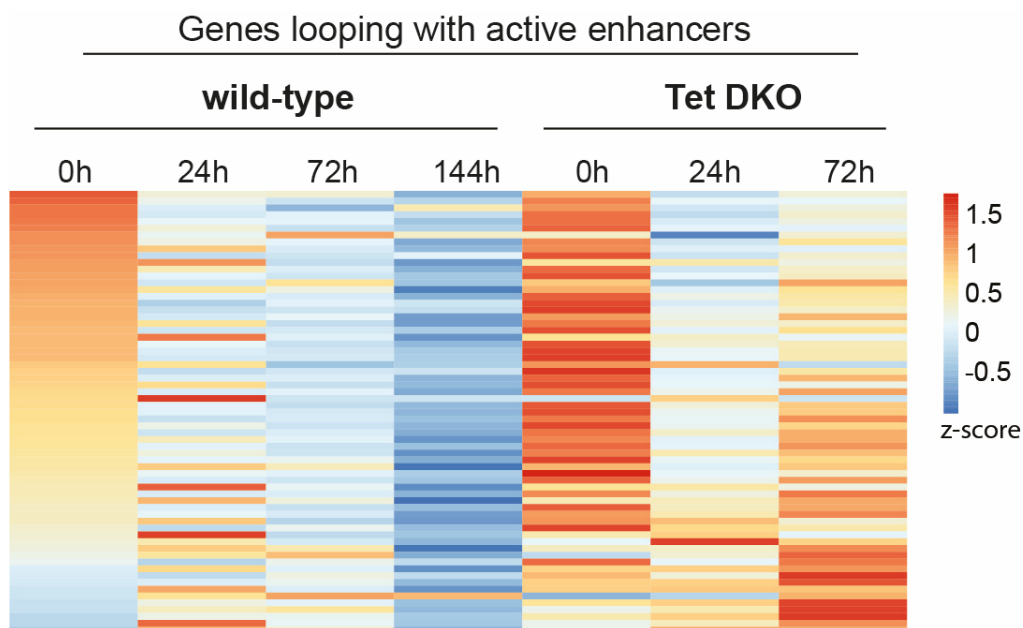


**Figure 49:** Expression levels of top genes that contact TET-target active enhancers (ABC-score > 0.02) as determined by analysis of published HiC and H3K27ac datasets. TET activity at enhancers is largely uncoupled from transcription under dormancy conditions.

Similarly, genes contacted by LINE1 elements did not show different expression levels when comparing wild-type and *Tet1/2* DKO ESCs over time (Figure 50). In conclusion, the unique regulation of dormancy targets did not affect the general transcriptional depression.

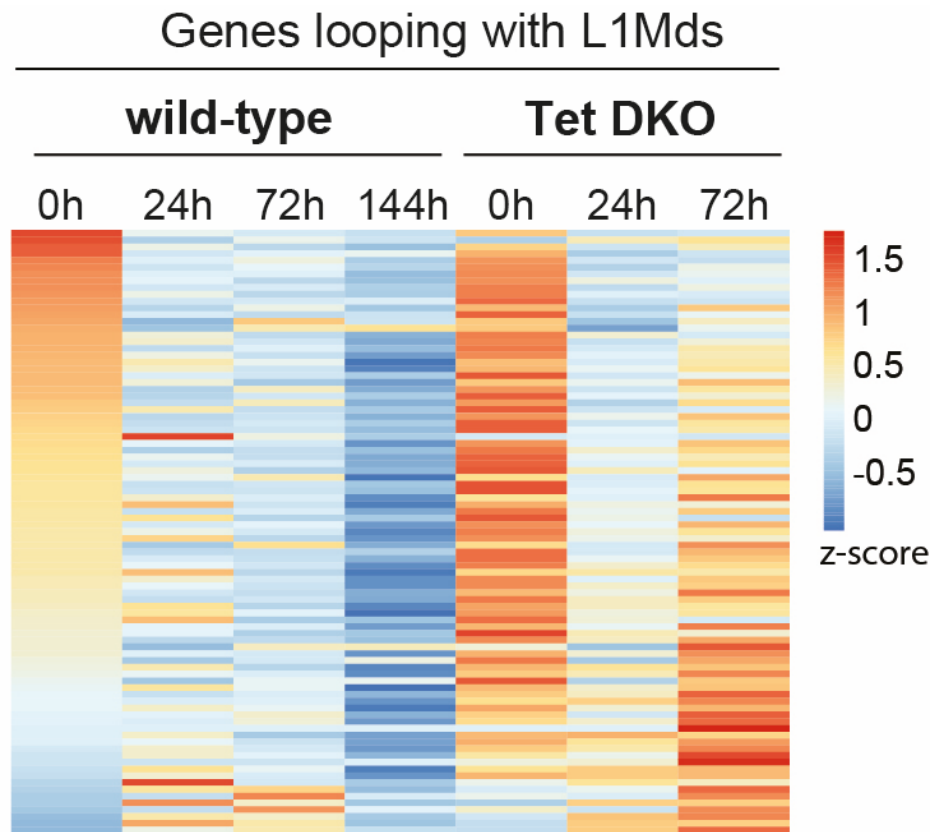


**Figure 50:** Expression levels of genes in putative contact with L1Md promoters. Contact was determined by analysis of published HiC datasets (see Methods, ABC-model) with a contact probability > 15). TET activity at L1Md elements is uncoupled from transcription during dormancy.

### 2.6.2 Bookmarking of CREs and LINE1 repeats in dormancy

We hypothesised that TET-dormancy targets are being bookmarked for reactivation. To test this, time course CUT&Tag profiling of the histone marks H3K27ac, H3K4me3, and H3K4me1 was performed. ESCs were profiled on their trajectory into the paused state (0h, 24h, 72h, 96h, 120h, and 144h) and on their trajectory back to proliferation (6h, 12h, 24h, 48h, 72h, 96h, 120h, and 144h) (Figures 51 and 52).



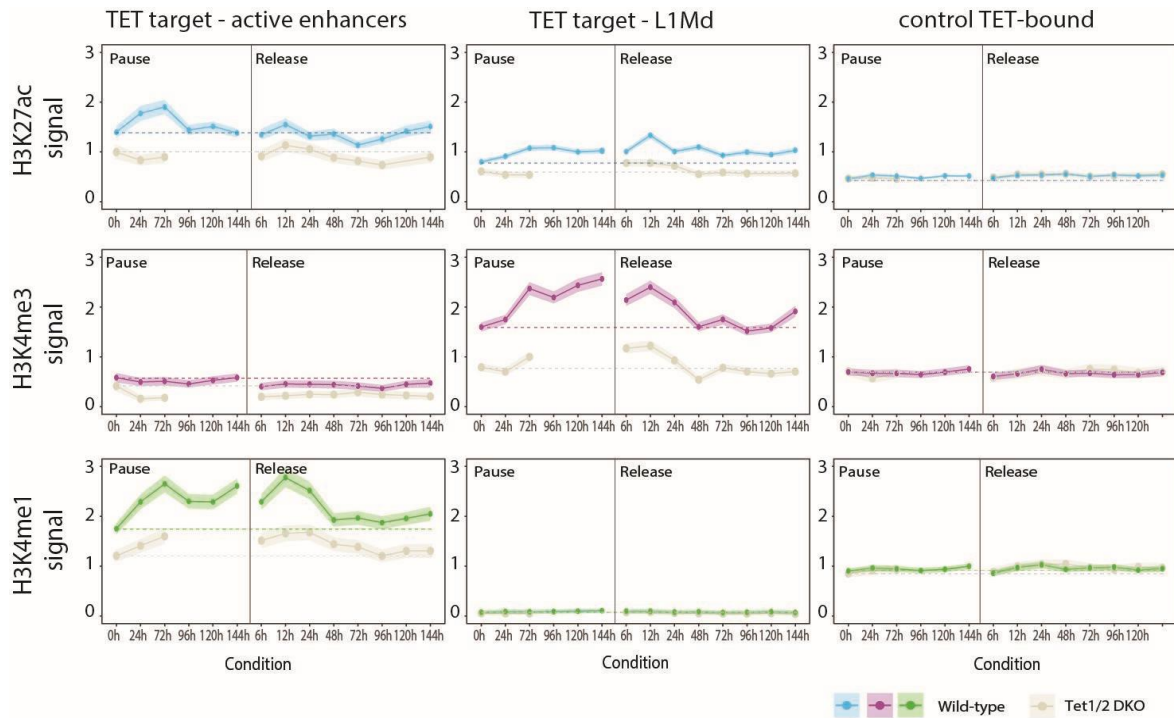


**Figure 51:** Levels of the indicated histone marks at TET-target active enhancers and L1Md regions in wild-type and *Tet1/2* DKO ESCs over a 144h time course of mTORi-mediated pausing and release. *Tet1/2* DKO ESCs were paused for 72h and then released to avoid losing pluripotent colonies. Lines show mean values. The shade shows the confidence interval. Dashed lines denote levels of each mark at 0h in the color-corresponding genetic background.

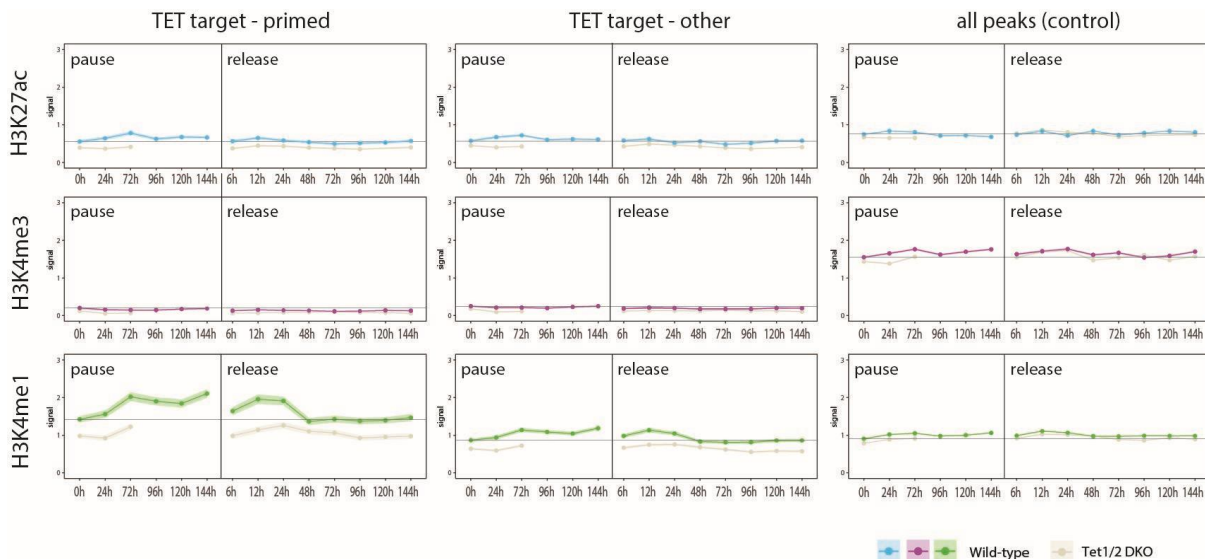


**Figure 52:** Levels of the indicated histone marks at TET-target primed enhancers, the Other category, and at all TET-bound peaks in wild-type and *Tet1/2* DKO ESCs over 144h time course of mTORi-mediated pausing and release. *Tet1/2* DKO ESCs were paused for 72h to avoid losing pluripotent colonies. Lines show mean values. The shade shows the confidence interval. Black lines denote levels of each mark at 0h in each genetic background.

Since the *Tet1/2* DKO ESCs only maintain pluripotency under mTORi conditions until 72h, they were released back to proliferation after 72h. The previously established dormancy targets were used to analyse the mean signal of each histone modification (Figure 51). TET-targeted active enhancers and TET-targeted LIMd elements showed divergent regulation of the histone modifications between wild-type and *Tet1/2* DKO (Figure 51). Dormancy target active enhancers show a spike in H3K27ac and H3K4me1 at 72h. Interestingly, although both marks decrease after their peak at 72h into dormancy, H3K4me1 remains above starting levels throughout dormancy. H3K4me1 shows a second peak at 12h of reactivation, indicating an increased poisedness of dormancy target active enhancers. In the *Tet1/2* DKO ESCs, dormancy target active enhancers did not show a spike in H3K27ac levels at 72h. Similarly, H3K4me1 levels increased to some extent but did not reach wild-type levels. Notably, the starting levels of both marks were lower in the *Tet1/2* DKO ESCs compared to the wild-type. Control TET-bound regions did not show different levels between wild-type and knock-out and remained unchanged over the sampled time course. This indicates a unique targeting of dormancy targets over other TET-bound regions.

Dormancy target LIMd elements showed increased levels of H3K27ac and H3K4me1 from 24h of dormancy onwards. This elevation persists throughout dormancy and normalizes only after 48h of reactivation, potentially resulting in a preferential transcription over other elements once ESCs reactivate. Specifically, at 12h of reactivation, both marks show a spike in wild-type that was not observed in the *Tet1/2* DKO ESCs.

Dormancy target primed enhancers showed an elevation in the H3K4me1 signal but not in H3K27ac and H3K4me3 (Figure 52). TET targeted other regions, and all peaks (control) showed little differences in the profiled histone modifications and behaved similarly to the control TET-bound regions. Differences between wild-type and *Tet1/2* DKO ESCs were minimal for other and all peaks (control), respectively (Figure 52).

A major difference between the H3K27ac and H3K4me1 levels of the TET-targeted active enhancers was observed compared to all active enhancers (excluding the TET dormancy targets) (Figure 53).



all active ESC enhancers (excluding TET dormancy targets)

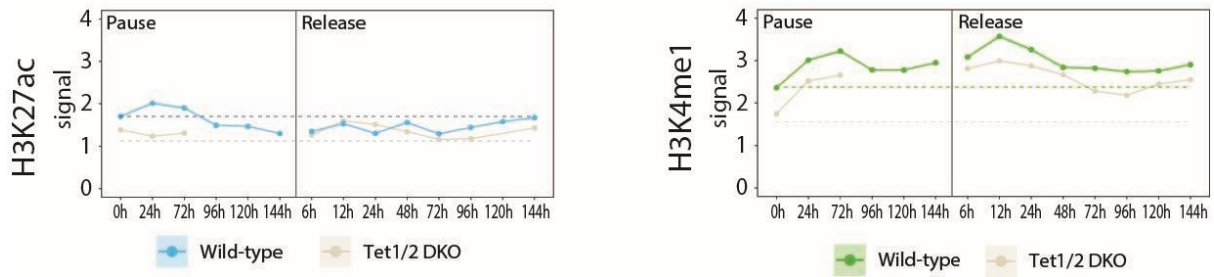


**Figure 53:** Levels of shown enhancer marks in all active ESC enhancers excluding TET-dormancy-targets. H3K27ac levels decline below 0h after 96h and only reach original levels at 120h of release.

At nondormancy target active enhancers, H3K27ac showed an initial increase in the wild-type; however, it dropped below the starting levels (0h) at 96h, 120h, and 144h. Strikingly, although starting with overall lower levels, at 0h, the dormancy-target active enhancers exceed all active enhancers in dormancy (Figure 54). Upon reactivation, all active enhancer H3K27ac levels are only fully recovered after 144h of release from mTORi. During the release, dormancy target enhancers show higher levels than all active enhancers (12h), and their ground state is recovered after 144h. Interestingly, H3K4me1 levels showed a steep increase at TET dormancy target active enhancers and remained high throughout the reactivation. This behaviour was also observed at all active enhancers and in combination with the decreased H3K27ac levels; indicating partially redundant mechanisms to ensure poisedness of the dormant genome.

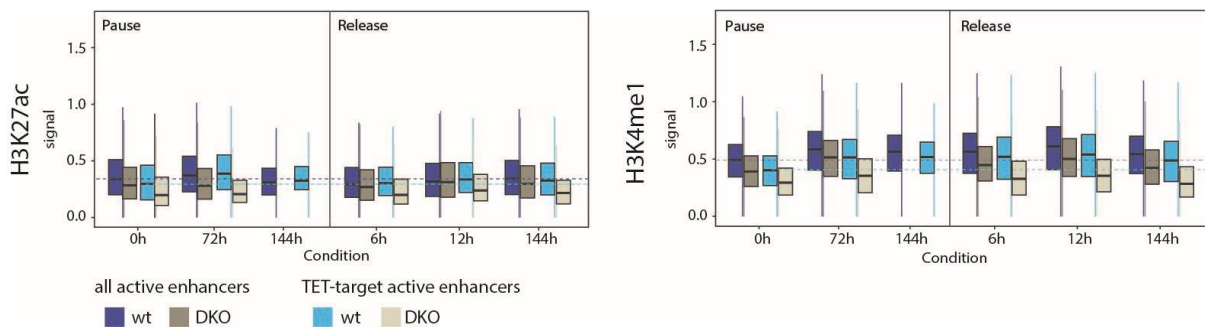


**Figure 54:** Quantifications of the shown enhancer marks in all vs TET-target active enhancers. Dashed lines denote levels of each mark at 0h in the colour-corresponding genetic background. TET-targets acquire acetylation earlier than all enhancers in released wild-type ESCs and show a larger deficit in *Tet1/2* DKO ESCs.

In summary, TET dormancy targets show a specific histone modification signature that is not observed in control TET bound regions or all TET peaks. Figure 55 is a genome browser

snapshot highlighting the dormancy-specific regulation of a TET dormancy target active enhancer (highlighted in grey).

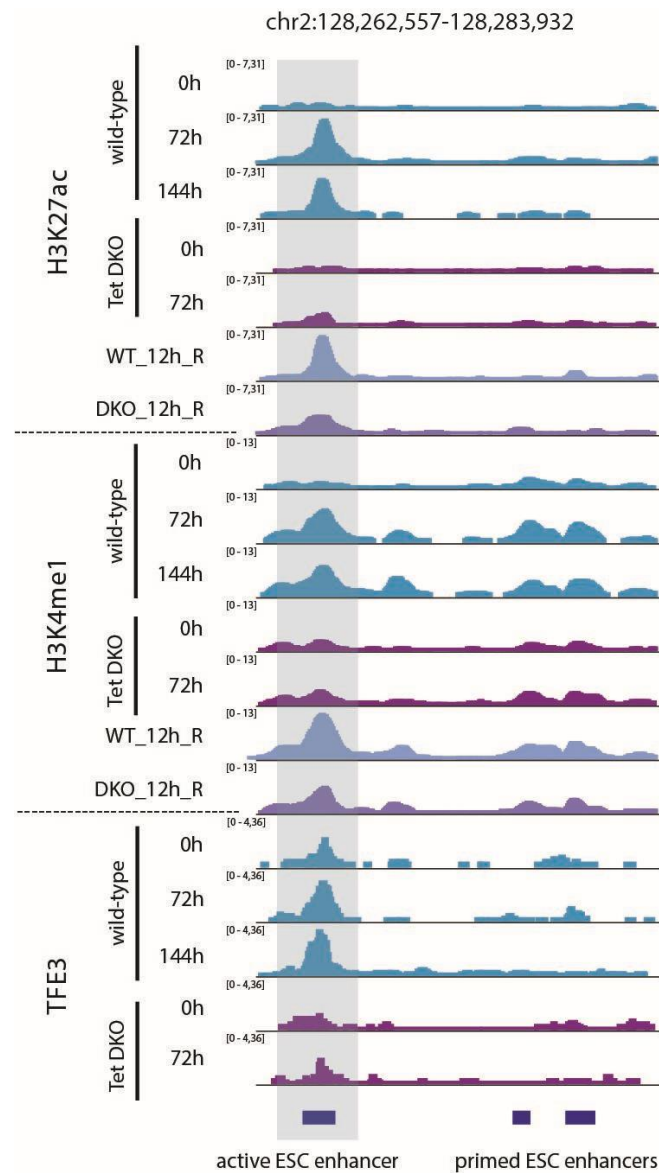


**Figure 55:** Genome browser view of chromatin dynamics at the same active ESC enhancer shown in Figure 41. The enhancer fails to accumulate H3K4me1 and H3K27ac and TFE3 in *Tet1/2* DKO ESCs during pausing and at release.

### 2.6.3 The dormant epigenetic signature is stably propagated

To access the temporal dynamics of regulating the paused state long-term, ESCs were additionally profiled at 12 and 15 days of dormancy (Figure 56). Strikingly, the levels of H3K27ac, H3K4me3, and H3K4me1 maintained a steady state in the profiled regions, respectively. H3K27ac levels that initially spiked and at 144h settled at levels comparable to

the starting level at 0h. However, they remained high at 12d and 15d at TET dormancy target active enhancers. H3K4me1 levels at TET dormancy target active enhancers remained high as they were at 144h. H3K4me1 levels stayed high at dormancy targets at primed enhancers. Further, levels of H3K27ac and H3K4me3 remained high at dormancy target L1Md elements at 12d and 15d of dormancy. The continuous high levels of histone modifications at the TET dormancy target regions indicate a stable propagation of the pausing specific epigenetic signature.

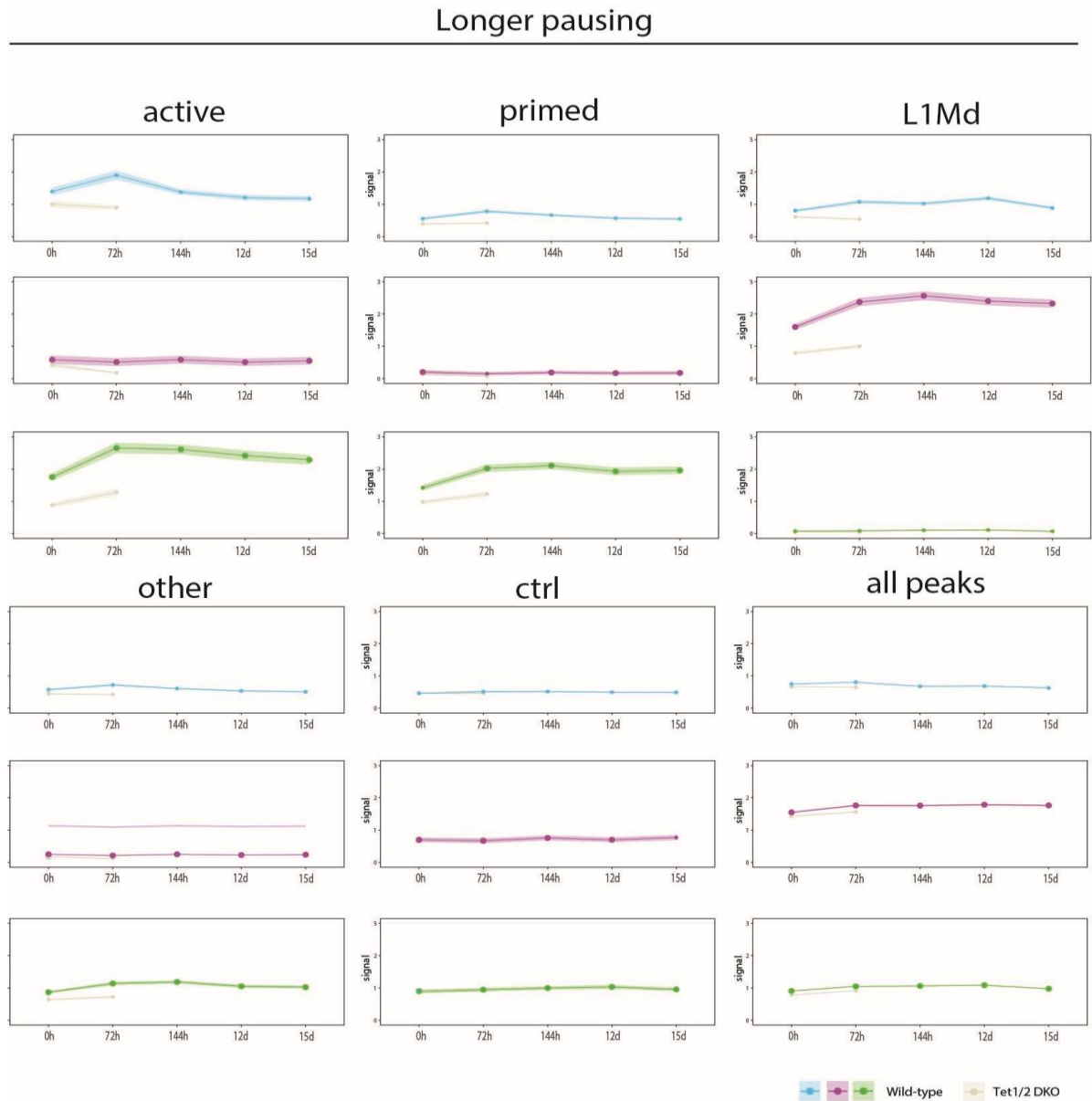


**Figure 56:** Levels of the indicated histone marks at the shown regions during longer-term pausing. Time points up to 15 days were collected in wild-type ESCs.

## 2.6.4 Reactivated wild-type ESCs show a homogeneous pluripotent phenotype

In addition to the histone modification profiling using CUT&Tag, ESCs were monitored for their pluripotency coming out of the dormant state using the surface pluripotency marker SSEA1. ESCs were paused for either 24h, 48h, 72h, or 96h and released for 48h before being analysed using FACS (Figure 57). In a standard ESCs culture, SSEA1 surface staining shows a bimodal distribution (Figure 17). The FACS profile for 24h dormant ESCs following release did not change. A change was observable for ESCs that were paused for 48h following release in wild-type and *Tet1/2* DKO ESCs, respectively. Both wild-type and *Tet1/2* DKO ESCs showed an increase in the SSEA1 high fraction. This trend continued for the wild-type ESCs when paused for 72h or 96h and released, but not for the *Tet1/2* DKO ESCs. After 96h of dormancy and 48h of release, the measured population shifted almost fully into the SSEA1 high fraction. Interestingly, there appears to be a breakpoint between 48h and 72h where ESCs do not further progress into a paused state when lacking TET1 and TET2.

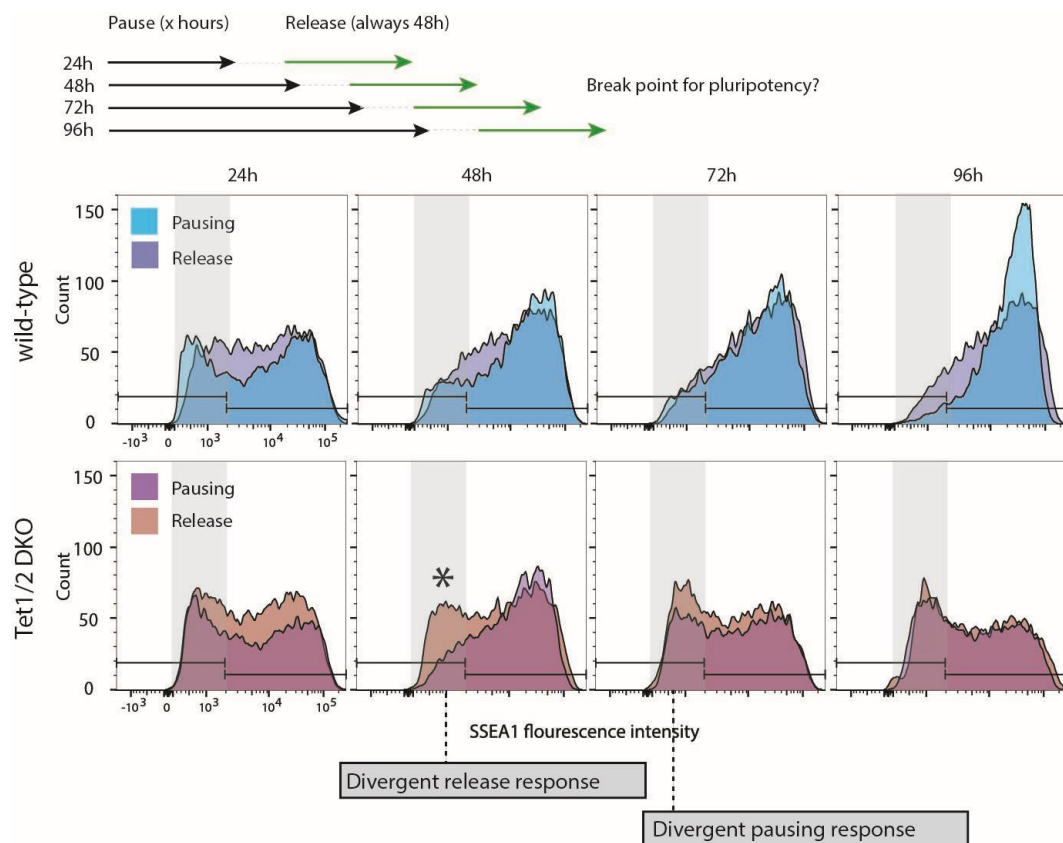


**Figure 57:** Flow cytometry analysis of the pluripotency marker SSEA1 during pausing and after release in wild-type and *Tet1/2* DKO ESCs. At 48h of pausing, *Tet1/2* DKO ESCs appear like wild-type in the SSEA1 expression pattern; however, they already show defective reactivation.

## 2.7 LINEs are transiently upregulated and interact with TETs

### 2.7.1 Evolutionary young L1Md subfamilies are transiently upregulated in dormancy

The expression of LINE1 repeats is correlated with the state of pluripotency in early development (Percharde et al. 2018). TFE3 accumulates at L1Md repeat elements, and a possible effect on the transcription of this group of LINE1 repeats was investigated. Due to their repetitive nature, repeats cannot be mapped to their exact locus of origin in the genome. Expression levels of repetitive elements was accessed by mapping RNA-seq data from wild-type and *Tet1/2* DKO ESCs to the consensus sequence of each repeat using the RepBase database (Jurka et al. 2005) (Figure 58, shown is a selection of L1Md repeats and LTRs).

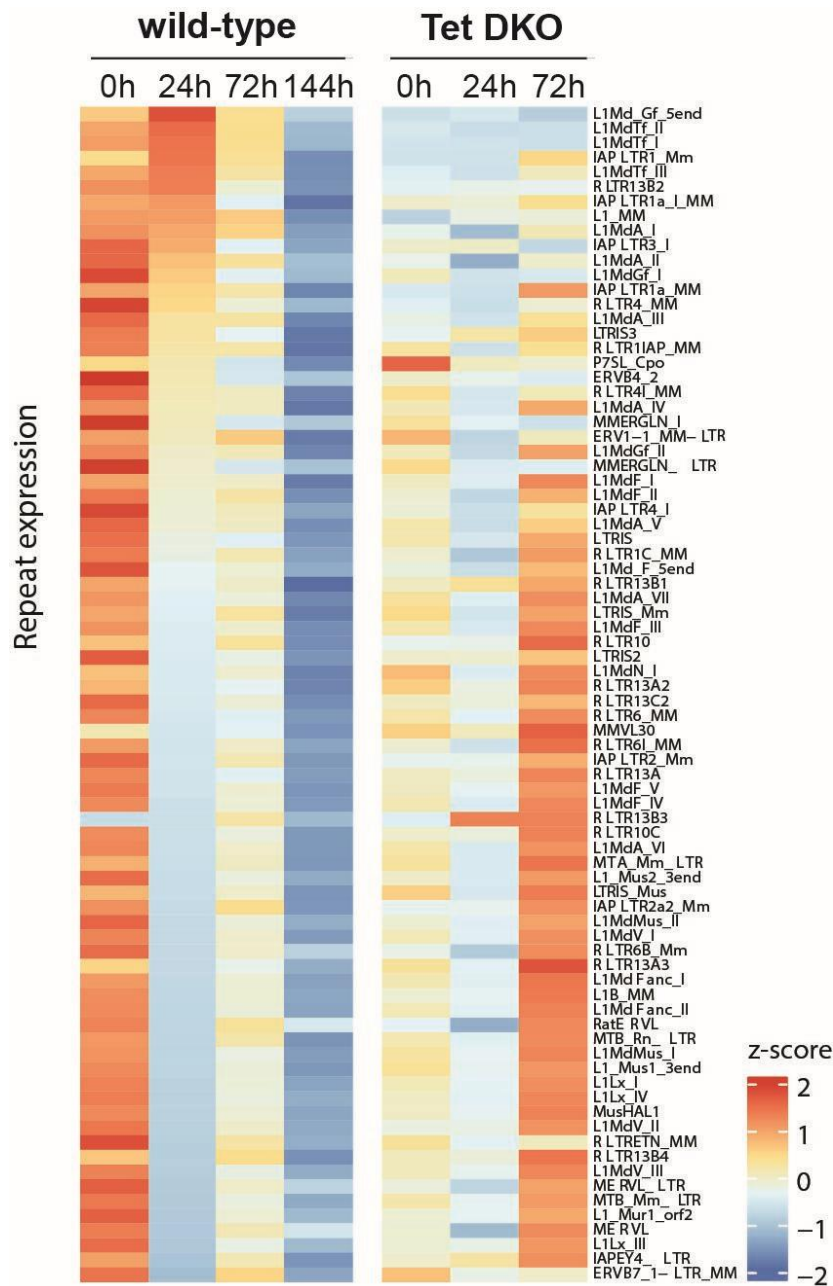


**Figure 58:** Expression levels of repetitive elements in wild-type and *Tet1/2* DKO ESCs at indicated time points of mTORi treatment. Reads were mapped to the consensus sequence of each repeat retrieved from RepBase. L1Md repeats are transiently upregulated at 24h of mTORi treatment.

Expression of L1Md repeats was higher in wild-type ESCs compared to *Tet1/2* DKO at 0h. L1Md\_Tf (I, II, and III), \_Gf\_5end, and \_A\_I repeats were transiently upregulated at 24h of treatment in wild-type ESCs. Most other L1Md elements, as well as other LINES and LTRs, were not (Figure 58). Notably, the upregulated subfamilies of repeats (L1Md\_fI, \_fII, \_f, and Gf) tend to be evolutionary younger compared to non-upregulated ones (Sookdeo et al. 2013) (Figure 59). These evolutionary younger repeats have more intact 5'ends and are more

transcriptionally active (Bulut-Karslioglu et al. 2014). Their transient upregulation is potentially an outcome of early TET-TFE3 activity, supported by the fact that there is no upregulation in the *Tet1/2* DKO at 24h. Contrary to wild-type ESCs, most other repeats are upregulated in *Tet1/2* DKO ESCs at 72h of mTORi, supporting the hypothesis of overall transcriptional deregulation due to a stress response.

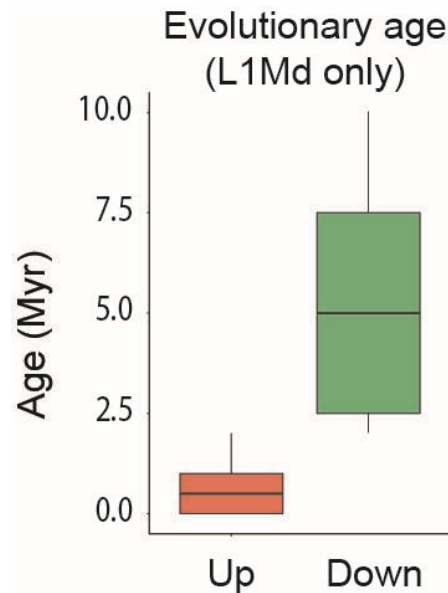


**Figure 59:** Evolutionary age of LINE1 repeats that are upregulated vs downregulated at 24h of mTORi in wild-type ESCs.

### 2.7.2 L1Md repeats directly interact with TET proteins

Previous work has shown that TET-RNA interactions mediate cellular transitions (Lan et al. 2020). Therefore, we explored whether TETs bind L1Md RNAs in ESCs transitioning into dormancy. To capture potential TET-RNA interactions, we tagged the endogenous locus of TET1 and TET2 with a biotin receptor tag (Figure 60).

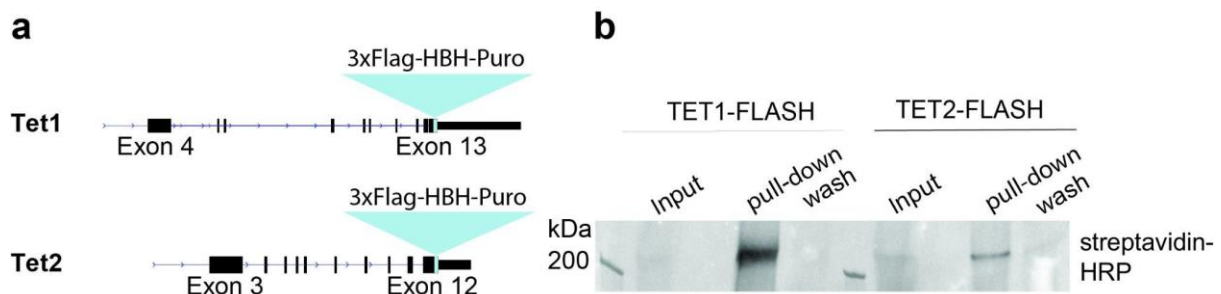


**Figure 60:** **a.** Schematics of FLASH tag insertion into the *Tet1* and *Tet2* loci. **b.** Western blots showing successful pull-down of the tagged TET1 and TET2 proteins.



Using this tag, FLASH (Fast Ligation of RNA after some sort of Affinity Purification for High-throughput Sequencing) was performed as described previously (Ilik et al. 2020) (Figure 61). FLASH relies on UV crosslinking of RNAs to proteins and subsequent affinity purification using streptavidin beads. The streptavidin-biotin interaction is among the strongest biochemical interactions known. The tag allows stringent washes, which decreases the likelihood of false positive interactions. Untagged wild-type ESCs were used as a control.

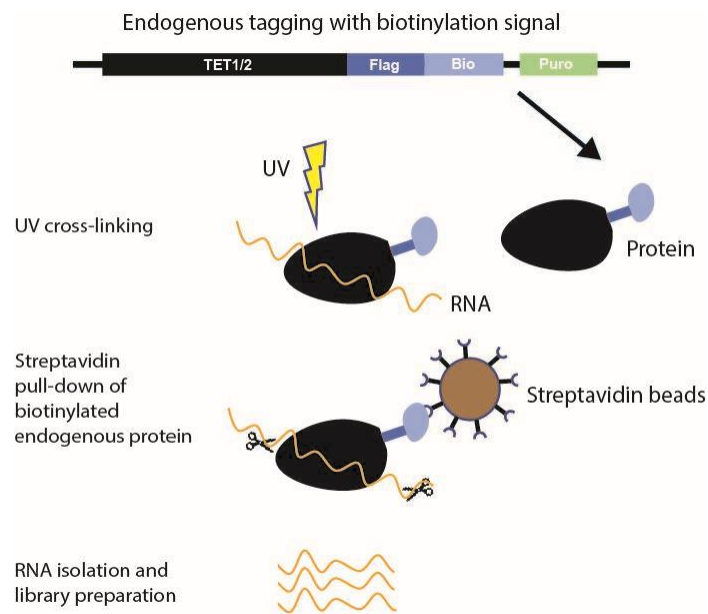


**Figure 61:** Schematics of the FLASH experiment to map TET-bound RNAs. The protocol allows stringent washes due to streptavidin-mediated capture. FLASH was performed in collaboration with Tugce Aktas and Ibrahim Ilik.

We detected increased binding of LIMd repeat RNAs to TET1 and TET2 at 72h and 144h but not at 24h (Figures 62 and 63).



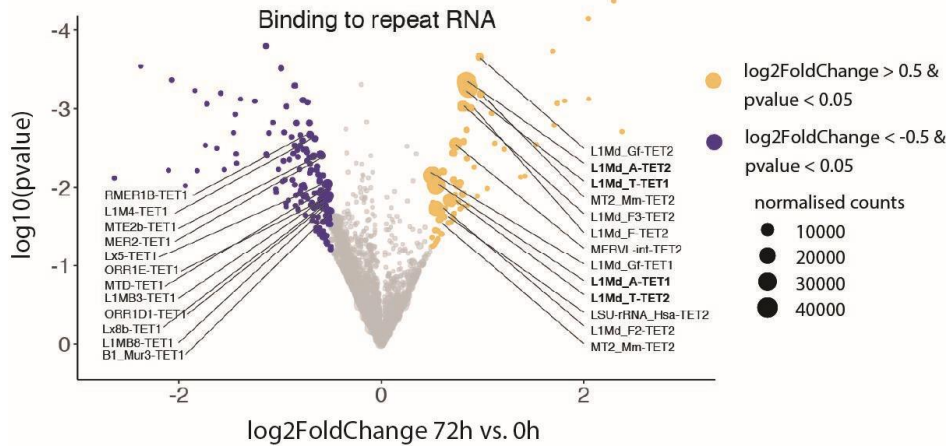


**Figure 62:** Volcano plot showing RNAs that are differentially bound to TET1 and TET2 at 72h compared to 0h of mTORi vs 0h. Both TET1 and TET2 bind L1Md repeats.

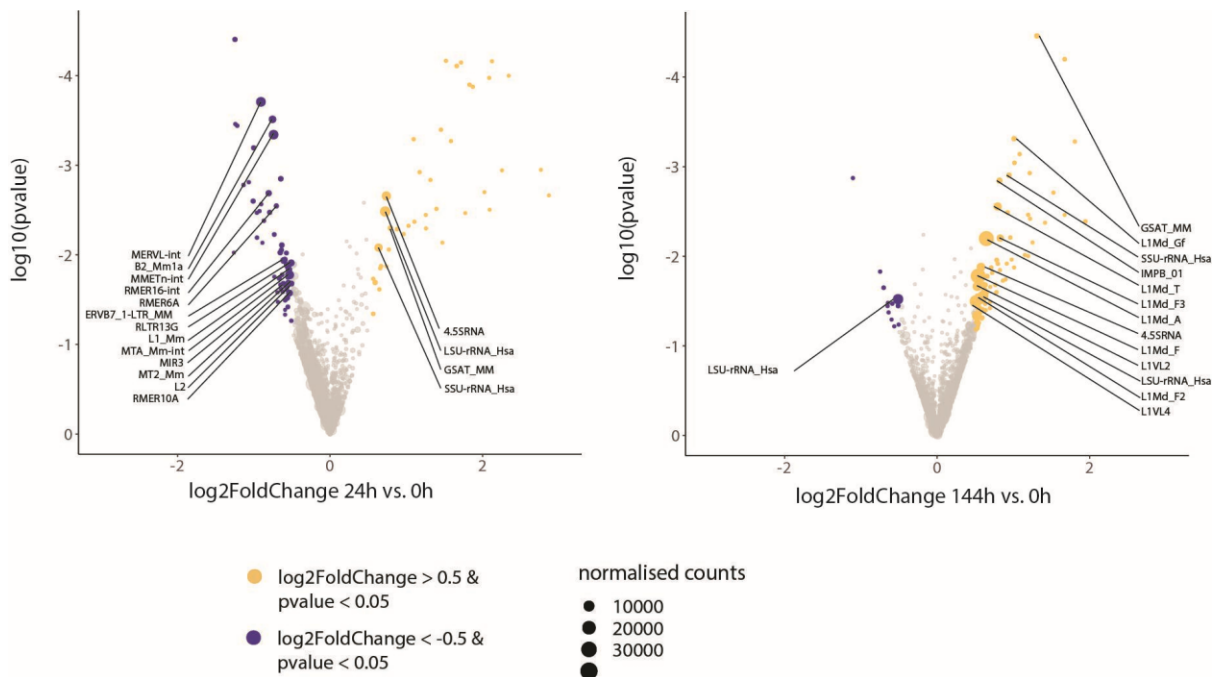


**Figure 63:** Differential binding levels of TET1 and TET2 to repeat RNAs at 24h and 144h compared to 0h. Gray indicates no significant differences between the time points.

The binding of TETs to these repeats is likely not co-transcriptional since they are highly transcribed at 24h but highly bound at 0h, 72h, and 144h (Figure 64).

The binding of TETs to L1Md repeat RNA is specific since other highly transcribed repeat RNAs, such as IAPLTR1a\_Mm, did not show TET binding. Generally, the most abundant TET-bound RNAs belonged to L1Md\_A, \_T, and \_F elements. TET-LINE interactions could promote or stabilize TET occupancy and influence chromatin accessibility at 72h.

In summary, the L1Md family of LINE1 repeats is transiently upregulated at 24h of ESCs entering dormancy. The TET-L1Md interaction predominantly occurs at 72h and 144h of dormancy.

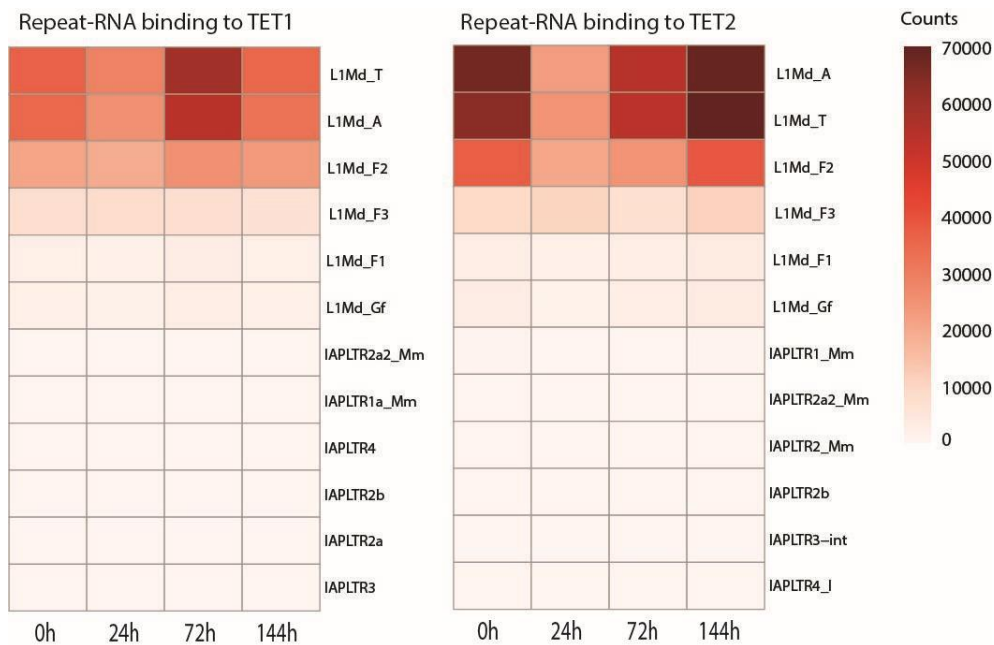


**Figure 64:** Binding of L1Md and IAPLTR repeat RNAs to TET1/2 at all time points. IAPLTRs are also transiently upregulated (shown in a) but do not bind TETs.

## 3. Discussion

### 3.1 Dormancy and Methylation

Diapause was officially described in 1854 by Bischoff, but its exact regulation has remained an enigma ever since. In this work, I laid the ground for the dissection of the chromatin landscape in dormant ESCs and further diapaused embryos. The blastocyst stage is commonly known for its low methylation levels (Greenberg & Bouchquis 2019). The global increase in methylation observed in dormant ESCs paused blastocysts, and diapaused blastocysts presented itself as a striking phenotype. In vivo diapaused and subsequently ex-vivo reactivated embryos showed a loss of methylation after reactivation. The regulation of this transiently increased methylation remains unknown (**Figures 6 and 7**).

Knocking out the writers of DNA methylation did not compromise the cell's efficiency to undergo dormancy. Strikingly knocking out or inhibiting the erasers of DNA methylation, the TET demethylases led to a loss of the ability to undergo dormancy (**Figure 8**). This discrepancy between the two genotypes' ability to undergo dormancy argues that the increase in DNA methylation might occur passively due to strongly reduced or absent proliferation. Although the E4.5 epiblast exhibits particularly low methylation levels, the E6.5 epiblast shows high global methylation close to somatic methylation levels. With previous observations that the diapaused epiblast shows polarization (Fu et al. 2014; Fan et al. 2020), the increase in methylation potentially indicates a progression of the diapaused epiblast towards primed pluripotency. This would allow immediate progression of development once the diapause-inducing stimuli are levitated. This hypothesis, however, needs to be experimentally tested. Different genetic backgrounds, including DNMT1, DNMT3A, DNMT3B, and UHRF1 knockouts, could help to disentangle the nature of this dormancy-specific increase of global methylation. Further time-resolved probing of the methylome between the reactivation and the implantation would help to understand the function of the increase in methylation during this unique period of development. Finally, manipulating demethylase activity after the release from dormancy would answer the question of whether the epiblasts genome would need to undergo active demethylation before the continuation of development.

Monteagudo-Sánchez and colleagues in 2023 hypothesized a relationship between the 3D architecture of the genome and DNA methylation, mediated by CTCF and its sensitivity to DNA methylation. We observe a major decrease of DNA accessibility (**Figure 36**) at 144h of dormancy and globally increased levels of methylation (**Figure 34**). In collaboration with the Mundlos laboratory we started profiling proliferating and dormant ESCs using High throughput chromosome conformation capture (Hi-C) (**Figure 65**). An initial analysis revealed that short range interactions seem to persist while long range interactions seem to increase in dormancy. In **Figure 65**, the lines of the two dormant samples deviate from the two control samples in their interchromosomal contact frequency at distances between  $10^7$  and  $10^8$  base pairs. This finding is in line with the decreased DNA accessibility in this study and previously reported decreased levels of H4K16ac (an indicator of genome compactness) (Bulut-Karslioglu et al. 2016). Increased heterochromatinization has previously been described in the ex vivo diapaused epiblast (Van der Weijden et al. 2024). Specifically, the nuclear lamina seemed to accumulate heterochromatin (accessed by H3K9me2 IF and electron microscopy). In ESCs polycomb-mediated interactions are amongst the strongest (Bonev et al. 2017). Therefore, increased heterochromatinization could be an important player in compacting the dormant genome. DNA methylation, however, could play a buffering role in the compaction since PCR2 and high-density DNA methylation seem to be mutually exclusive in vivo (Yang and Li 2020). To get further insights into the relationship between genome compaction and DNA methylation, experimental data is required.

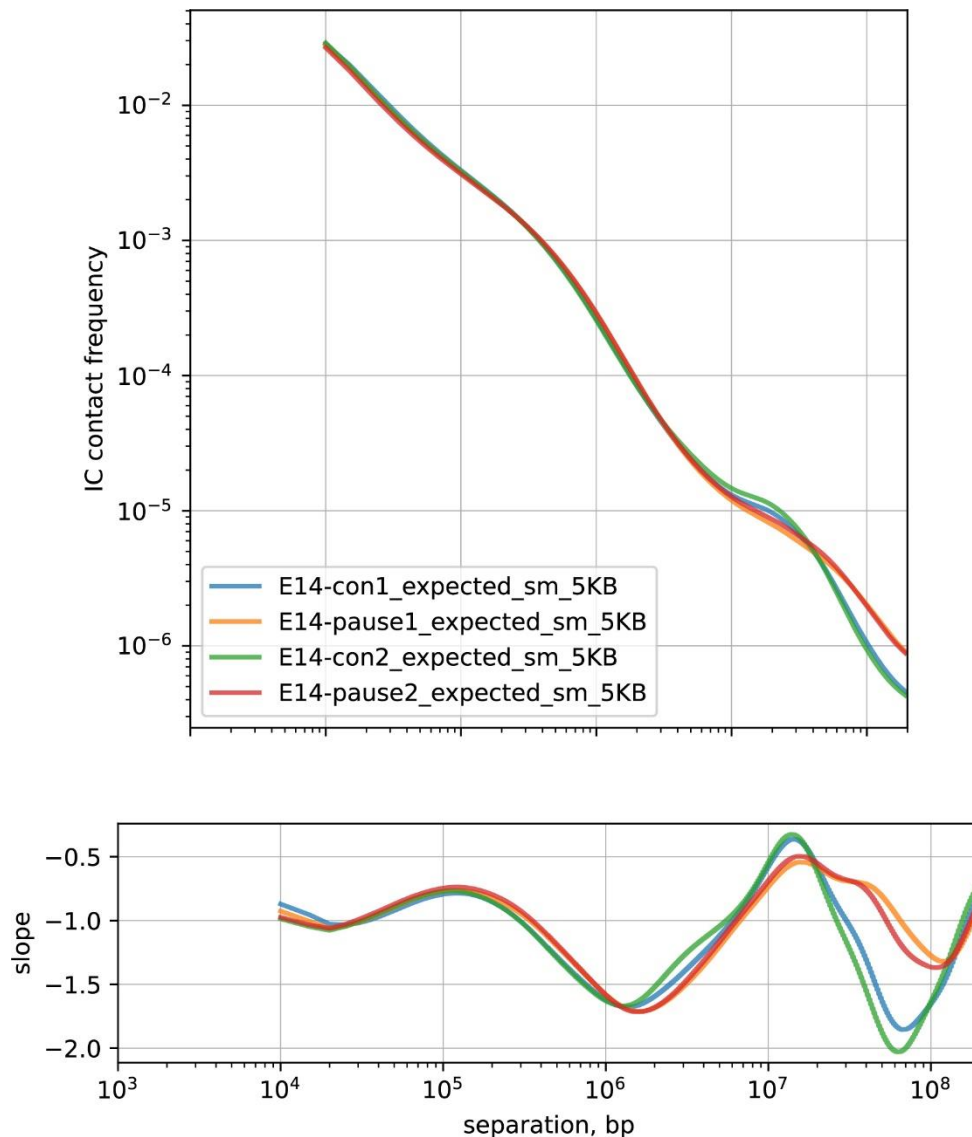


**Figure 65:** Hi-C distance decay map of wild-type and dormant ESCs. Shown is the interchromosomal (IC) contact frequency in relation to separation in base pairs (bp) in the upper plot. The plot below shows the same as the first derivative of the plot above. In collaboration with Mike Robson and Maria Stefanova.

### 3.2 TETs counteract increasing methylation and remodel the chromatin

We observed a detrimental effect on the ability to undergo dormancy in ESCs and embryos lacking the TET DNA demethylases but not in ESCs lacking the DNA methyltransferases (**Figure 8**). Both wild-type and *Tet1/2* DKO ESCs respond with decreased proliferation to mTORi (**Figure 15**). Additionally, both cell lines show increased methylation levels at 72h, but only wild-type ESCs progress into dormancy (**Figures 30 and 34**). This allows us to conclude that at least in ESCs, but potentially in embryos, too, the increase in methylation is connected to the reduction in proliferation. Further, the hypothesis is that the dormant state relies on the ability of TET DNA demethylases to demethylate and counteract the increase in

methylation. This hypothesis is supported by the rescue experiments, which showed that only the expression of wildtype TETs in the TET TKO background rescued the ability to undergo dormancy. The expression of catalytically dead versions of the enzymes did not (**Figure 9**). The corroboration and phenotypical assessment of this phenotype in a feeder-independent E14 ESC background further supported this hypothesis (**Figures 16 and 17**). Alkaline phosphatase staining and surface pluripotency marker SSEA1 staining showed that *Tet1/2* DKO ESCs lose both markers gradually when subjected to dormancy-inducing mTORi conditions. RNA-sequencing showed the increased expression of stress-related and apoptotic genes when the wildtype transcriptome was compared to the *Tet1/2* DKO transcriptome at 72h. Annexin V flow cytometry analysis confirmed increased rates of apoptosis (**Figure 18**). These findings indicated a dysregulation of the cellular program to undergo dormancy, resulting in a loss of pluripotency and increased apoptosis in the absence of TETs.

Notably, *Tet1/2* DKO ESCs exhibited an initial advance towards a dormant cellular state like the wildtype ESCs. This initial advance is visible in the SSEA1 flow cytometry analysis and the principal component analysis of the RNA-seq data at 48h, respectively (**Figures 17 and 30**). In line with that, a global depression of transcription is observable in both wild-type and *Tet1/2* DKO ESCs at 48h. Global depression of transcription continues in the wild-type ESCs. The *Tet1/2* DKO's transcriptome, however, diverges at this point and does not show further depression (**Figures 30, 31, 32, and 33**). Interestingly, the global rise in methylation is first observed at 72h in the WGBS data. Therefore, its onset is likely between 48h and 72h post dormancy induction (**Figure 34**). This concordance of phenotypic divergence at the phenotypical and transcriptomic level together with the onset of the DNA methylation increase supports the idea of TET demethylase activity in the regulation of dormancy. It also indicates that mTORi-mediated dormancy affects different layers of cellular regulation. The initial reduction in transcription and the global rise in methylation is not tolerated past 72h of dormancy without TET-mediated regulation.

### **3.3 A unique state of hypotranscription and globally increased DNA accessibility during the transition into dormancy**

Surprisingly, global DNA accessibility does not follow the trend of depressed transcription with a reduction in accessibility in wild-type ESCs. Usually, transcriptional activity of the genome correlates with its level of accessibility (Gaspar-Maia et al. 2011; Meshorer et al. 2006). On the contrary, accessibility increased and peaked at 72h hours in wildtype ESCs

(**Figure 36**). *Tet1/2* DKO ESCs showed this peak in DNA accessibility at 48h of mTORi treatment. This indicates that the lack of TET activity leads to defects in genomic regulation, preventing *Tet1/2* DKO ESCs from successfully entering dormancy. The decoupling of chromatin accessibility as probed by ATAC-seq and the state of transcription poses another uniqueness of dormancy. The increased expression of L1Md elements at 24h of dormancy might offer an explanation (**Figure 58**). Each L1Md family is represented by several thousand copies in the genome (Sookdeo et al. 2013). This increased state of expression might increase DNA accessibility. Further, several cases of RNA-chromatin interactions have been described (Bonetti et al. 2020). Intriguingly, the TET-L1Md interactions identified in this thesis are likely to occur in a chromatin context. This interaction, if happening in a chromatin context, could help to explain the increased accessibility of DNA (**Figure 36**). Further insight into this type of chromatin regulation by repetitive DNA could be generated using sequencing methods like MAGRI that identify DNA-RNA interactions and manipulating the expression of the L1Md repeats (Wu et al. 2019).

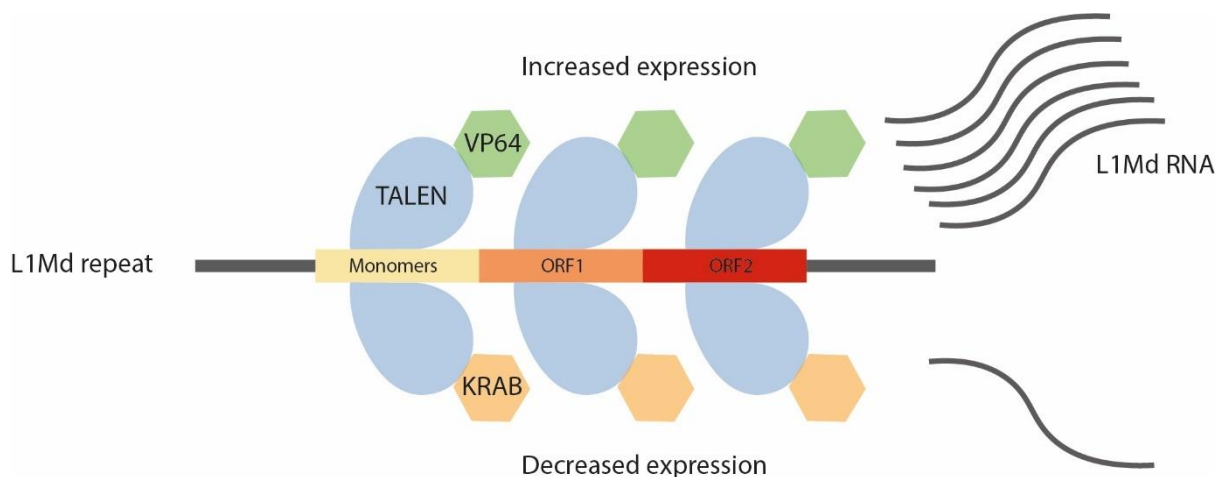


**Figure 66:** Future experiments to test the impact of L1Md repeats on dormancy. Shown is the sequence architecture of an L1Md repeats featuring Monomers, open reading frame (ORF) 1 and ORF2. TALENs targeting each of the three repeat features are fused with a VP64 or KRAB domain, respectively.

We hypothesised that L1Mds impact the dormant chromatin directly or via the interaction with TETs. To test this hypothesis, we initiated experiments to either increase or decrease the expression of L1Md repeats. For this we used TALENs that were designed to target L1Md repeats as depicted in **Figure 66** (TALENs were modified from Jachowicz et al. 2017). We then fused these TALENs with either a transcription activating VP64 domain, or a transcription repressing KRAB domain, respectively. These constructs will be used to create

ESC lines in which the LIMd expression can be modulated. We will then analyse the effects of varied LIMd expression in the context of dormancy using pluripotency assays like SSEA1 staining followed by FACS and ATAC-sequencing.

### **3.4 TETs facilitate transcription factor binding through demethylation**

TET1 and TET2 CUT&Tag data, in combination with the WGBS data, revealed the dormancy-specific demethylation of enhancers and LINE1 repeat elements. Interestingly, using gene enhancer contact predictions, an upregulation of transcription of associated genes to these target regions was not observed (**Figures 49 and 50**). However, these dormancy TET targeted regions showed the enrichment of transcription factors motifs with increased binding activity (**Figure 43**). CUT&Tag subsequently confirmed the enrichment of TFE3 specifically in TET dormancy target regions but not canonical TFE3 target regions. Dormancy TF binding therefore appears TET-dependent in those regions (**Figure 45**). The interaction between transcription factors and DNA in relation to DNA methylation has been under debate for the last decade. A landmark study from 2017 reported that 90% of transcription factors, which motifs contain a CpG, are affected when the DNA is methylated (Yin et al. 2017). A year later, another study relativized the previous finding by showing that the methylation of DNA changes the electrostatic properties. In turn this leads to a change in transcription factor binding, regardless of whether the motif itself or an adjacent CpG is methylated (Rao et al. 2018). Further, research reports that the pioneer activity of transcription factors such as FOXA2 is sufficient to induce local demethylation (Donaghey et al. 2018). In the case of TET dormancy targets, it is evident that local methylation is increased, and accessibility is decreased at 72h in the absence of TETs. Increased binding of TFE3 at these sites occurs only in wild-type ESCs, while only residual binding is observable in the *Tet1/2* DKO ESCs (**Figure 44**). This indicates that in this context, mere pioneering activity, described for TFE3 (Zaret and Carroll 2011), is insufficient to induce demethylation at these sites. Methylation sensitivity and the TET dependence of transcription factors at dormancy targets is supported by a recent publication that shows methylation sensitive binding of bHLH transcription factors such as MYC and MAX at enhancers (Kreibich et al. 2023). TFE3 interestingly belongs to the group of bHLH transcription factors (Hershey and Fisher 2004), while KLF4 and YY1 are zinc finger transcription factors (Katz et al. 2002; J. Li et al. 2012).



### 3.5 TETs as dormancy-specific transcription factor hubs

Apart from their demethylating enzymatic activity, TETs are known for their promiscuous interaction with other transcription factors and chromatin remodelers (Zhang et al. 2023). Therefore, TETs likely function as hubs that recruit transcription factors to target sites in dormancy. This idea is further supported by the dynamic deposition of histone modifications at dormancy targets (**Figure 51**). Dormancy target active enhancers showed elevated levels of H3K27ac and H3K4me1 at 72h of pausing that remained above starting levels normalized only 144h after release. This observation is interesting because of its restriction to dormancy targets and its relation to other active enhancers. While all active enhancers showed an initial increase of H3K27ac levels to dormancy, the level decreased below starting levels at 96h (**Figure 53**). In direct comparison, it becomes evident that dormancy target active enhancer's H3K27ac and H3K4me1 levels surpass that of all active enhancers in dormancy. Further both marks stay high throughout reactivation, and only normalize when ESCs are fully released from pausing at 144h of release (**Figure 54**). This observation allows us to argue for an increased poisedness of dormancy target enhancers. A similar trend can be observed for the dormancy targeted LINE1 elements. The possible functionality of such a regulation is discussed in Chapter 4.5. It remains unknown how the specificity for TETs and the dormancy TFs is created to enrich at and demethylate only dormancy targets.

### 3.6 Bookmarking in the context of dormancy

The dormant state is defined by strongly reduced metabolic activity and proliferation rates, hypotranscription, and hypotranslation (Bulut-Karslioglu et al. 2016). Even ESC-defining markers, such as TBX3, NANOG, SOX2, and OCT4, show a substantially lower abundance of their transcripts (Bulut-Karslioglu et al. 2016). As described in the introduction, ESCs, specifically those cultured in Serum/LIF, prevail in a state of duality. This duality allows the maintenance of the pluripotent state but preserves a readiness for differentiation (Schlesinger and Meshorer 2019). The state of duality, together with hypotranscription and hypotranslation in dormancy, raises the question: How do ESCs and embryos maintain pluripotency once proliferation, transcription and translation kick start upon reactivation from dormancy. Bookmarking poses an intriguing mechanism to ensure a trajectory towards pluripotency upon reactivation. The enrichment of binding motifs of transcription factors involved in pluripotency and a preimplantation metabolism like KLF4 and TFE3 support this idea. With higher levels of H3K27ac, H3K4me1, and binding of TFE3 (and potentially other

transcription factors identified in the motif enrichment analysis), the dormancy targeted enhancers and their associated genes activate first upon reactivation. In turn, this preferential activation of bookmarked genes safeguards pluripotency through the state of dormancy. The same is true for the L1Md elements associated with pluripotency (Percharde et al., 2018).

Pausing with subsequent reactivation and pluripotency analysis via SSEA-1 labelling and flow cytometry supported the idea of a TET-dependent bookmarked dormant genome (**Figure 57**). Wild-type ESCs paused for 48h, 72h, or 96h exhibited a more homogenous pluripotent population when reactivated for 48h, respectively. 24h of pausing did not create this effect. Notably, *Tet1/2* DKO ESCs did not show this effect, arguing that this effect is TET dependent. For example, nascent transcription analysis with a method like TT-Slamseq could generate further supporting evidence for this idea on the transcriptional level. A recent publication by Chervova et al 2024 proposed a similar mechanism for bookmarking mitotic genes that ensures fast reactivation after mitotic silencing in pluripotent ESCs. Bookmarking, even if not called as such, generally seems to protect or preset states and fates in ESCs. An example of this is the default adoption of a neuroectodermal fate of ESCs in the absence of extrinsic inductive signals. ZFP521 appears necessary and sufficient for ESCs to adopt this neuronal fate (Kamiya et al. 2011). ZFP521 is present in ESCs at the pluripotent state, and neuroectodermal genes show higher accessibility than genes involved in the differentiation of other lineages (Meléndez-Ramírez et al. 2021). In summary, bookmarking often occurs in pluripotent ESCs and safeguards pluripotency through dormancy.

### **3.7 Outlook: Dormancy type bookmarking in aging and disease**

Originally, it was hypothesized that a state, like dormancy in ESCs, requires significant chromatin rewiring to be endured. In this thesis, a bookmarking type mechanism was shown for CREs and LINE1 repeat promoters in dormancy that safeguards pluripotency. This mechanism explains how the absence of the hallmarks of ESCs (hyper-transcription, hyper-translation, metabolic activity, and proliferation) may coexist with the duality state (self-renewal and readiness to differentiate) of ESCs. However, dormant ESCs and embryos are not the only systems that experience this paradox. Adult stem cells, for example, must stay quiescent to not deplete their finite pool and stay sufficiently responsive to activate and replace tissues when necessary (Cho et al. 2019). A similar case is dormant cancer cells that often arise with the chemotherapeutic treatment of solid tumours (Phan and Croucher 2020).

These dormant cancer cells remain dormant for several years in some cases before reactivating and causing relapses in patients.

We collaborated with the Sigmar Stricker laboratory to isolate satellite cells (muscle stem cells). We performed ATAC-sequencing on these cells and will subject the resulting data to the same footprinting analysis we performed for dormant ESCs (**Figure 42**). Exploring whether the dormancy type bookmarking happens in a cell type-specific manner in other systems would boost our understanding of these systems. In the case of adult stem cells, this understanding could be used to increase their activation in a targeted manner, for example, for tissue regeneration. In the case of dormant cancer cells, a bookmarking mechanism could potentially be targeted to avoid a relapse in patients.

## 4. Methods

### 4.1 Cell lines and culture conditions

Wild-type, *Tet1/2* DKO, and *Tet1Flag/Tet2V5/Tet3HA* ESCs<sup>23</sup> ESCs (E14 cells, a kind gift from the Ian Chambers lab) were cultured without feeders on gelatin-coated plates (0.1%, Sigma-Aldrich G1393). Wild-type KH2, *Dnmt3a/b* DKO, *Dnmt* TKO (from Alexander Meissner Lab), and *Tet1/2/3* TKO ESCs (from Jacob Hanna Lab) were cultured on mitomycin-treated feeders produced in-house. The media was changed every day and cells were passaged every 2-4 day intervals depending on the experiment and cell line. At each passage, cells were dissociated using TrypLE (Thermo Fisher 12604-021) and replated at an appropriate density. Cells were maintained at 37°C in a humidified 5% CO<sub>2</sub> incubator. Cell lines were not authenticated, but genotypes were verified by PCR. Cells periodically tested negative for mycoplasma.

ESC culture media: DMEM/High glucose with Glutamax media (Thermo, 31966047) supplemented with 15% FBS (Thermo, 2206648RP), 1x non-essential amino acids, 1x Penicillin/streptomycin, 1x β-mercaptoethanol, 1000U/mL LIF.

### 4.2 Animal experimentation

All animal experiments were performed according to local animal welfare laws and approved by local authorities (covered by LaGeSo licenses ZH120, G0284/18, G021/19, and G0243/18-SGr1\_G). Mice were housed in ventilated cages on a 12h light/dark cycle and fed ad libitum.

### 4.3 In vitro diapause

To induce dormancy, ESCs or embryos were treated with the mTOR inhibitor INK128 or RapaLink-1 at 200 nM final concentration for the duration specified in individual experiments. To obtain embryos, 10- to 12-week-old b6d2F1 mice were superovulated by intraperitoneal injection with PMSG (5IU/100 μl) on day 0 of the superovulation protocol. On day 2, mice were intraperitoneally injected with HCG 5 IU/100μl. On day 3, mice were sacrificed with CO<sub>2</sub> and cervical dislocation, after which the cumulus-oocyte complexes (COCs) were retrieved. 10 μl of motile sperm was added to each drop of fertilizing CARD Medium (CosmoBio, KYD-003-EX) containing the COCs. After overnight culture, the

obtained 2-cell stage embryos were transferred to a fresh drop of KSOM (Merck, MR-107-D). For all experiments, embryos were used from E3.5 onwards, with the exception of the Bobcat339 conditioning experiment, where blastocysts were treated 12 h prior to reaching E3.5.

#### **4.4 Embryo transfer and in vivo diapause induction**

Blastocysts were transferred into pseudopregnant females that had been previously mated with vasectomized males at E2.5. To induce diapause in vivo, ovariectomy was performed after embryo transfer, as described previously. Females were afterward injected every other day with 3 mg medroxyprogesterone 17-acetate subcutaneously. Diapaused blastocysts were flushed from uteri in M2 media after four days of diapause at EDG7.5 (equivalent day of gestation).

#### **4.5 Flow-assisted cell sorting (FACS)**

Cells were dissociated from plates using TrypLE (Thermo Fisher 12604-021) and washed in DPBS (Dulbecco). Cells were labelled with either Alexa488-SSEA1 antibody (Biolegend, 125610) or Alexa647-AnnexinV antibody (Invitrogen, A23204) in combination with a live/dead cell stain excitable at 405nm wavelength (Invitrogen, L34955), respectively, for 20 minutes in the dark on ice and subsequently washed in PBS containing 2% BSA. Washed cells were resuspended in PBS containing 2% BSA and 5 mM EDTA and kept on ice until further processing. FSC and SSC were used to set the first three gates to separate duplets from singlets by selecting the main population of cells and avoiding cell debris. SSEA1 negative and positive populations were gated based on unstained but otherwise identically treated cells, and dead cells were gated out using the live/dead staining. SSEA1 high and low populations were gated based on the SSEA1 signal intensity of wild-type cells at time point 0h, assigning ~50% of total events to the high and low fractions, respectively.

#### **4.6 Pharmacological treatment of embryos**

Embryos were cultured in KSOM medium (Merck, MR-107-D) in 4-well dishes (Nunc IVF multi dish, Thermo Scientific, 144444) in a volume of 500  $\mu$ l. Embryo survival was evaluated daily under a stereomicroscope, and dead (collapsed) embryos were removed. For pharmacological treatments, Bobcat339 (100  $\mu$ M final, Sigma SML2611), vitamin C (50  $\mu$ M final, Sigma A4403), Rapalink (200 nM final, Hölzel HY-111373), and alpha-ketoglutarate (200  $\mu$ M final, Merck K1128) were used. Recently, it has been shown that Bobcat339's

effectivity is influenced by copper, which was not separated from the inhibitor stock used here (Weirath et al. 2022).

#### **4.7 Survival analysis:**

Embryo survival visualization and statistical testing (log-rank test) were performed in RStudio (version 1.3.1093 with R version 3.6.3) with the survminer (version 0.4.9) package.

#### **4.8 Proliferation curves**

Cells were seeded in 6-well plates (Corning, 3516) at a density of  $10^5$  cells per well (on feeder cells when required, 2.5M per plate). On the following day, INK128 (MedChemExpress, MCE-HY-13328) was added to the medium at a concentration of 200 nM for the paused condition, and the initial number of cells was determined for both conditions on the same day as well as the subsequent days, over the duration of the assay. Cell number was accessed by trypsinizing cells for 5 min at 37°C and subsequently counted using a 1:1 mix of cells and trypan blue on a counting slide (Invitrogen) in Cell countess 3 (Invitrogen).

#### **4.9 Overexpression of wild-type or catalytically-dead TET1 and/or TET2**

Wild-type Tet1 or Tet2 coding sequence was amplified from pcDNA3-Tet1 (AddGene: 60938) and FH-Tet2-pEF (AddGene: 41710) and cloned into a pCAGGS vector. To achieve the desired amino acid changes H1652Y and D1654A (TET1) and H1304Y and D1306A (TET2) that result in catalytic dead enzymes respectively<sup>65</sup>, we used the Q5 Site-Directed Mutagenesis Kit (NEB, E0554S) according to manufacturer's instructions

(TET1 fwd: 5' GGCGATTCACAACATGCACAAC,

rev: 3' TTGTAAGAATGGGCACAAAAATC,

TET2 fwd: 5' AGCGCAGCAGAACATGCCAAATG,

rev: 3' CTGTAGGAATGAGCAGAGAAGTC).

#### **4.10 Generation of Tet1/2 DKO mESCs**

Knock-out of *Tet1* and *Tet2* was performed using guides targeting Exon 4 (GATTAATCACATCAACGCCG) and 13 (GCTTTGCGCTCCCCCAAACGA) and Exon 3 (GAGTGCTTCATGCAAATTCG) and 12 (GCTACACGGCAGCAGCTTCG), respectively. Each guide was cloned into px330 containing the gene for the Cas9 Endonuclease and mCherry, allowing for Flow assisted cell sorting of successfully nucleofected cells. Wild-type

E14 cells were nucleofected with the plasmids using the Lonza 4D Nucleofector. After 48h, cells were single-cell sorted into 96 well plates using the BD FACSAria Fusion. After 8 days clones were screened using two primer pairs for each Tet gene. Primer pair 1 (TET1: fwd: 5'AGCCATAGAAGCCCTGACTC, rev: 3'CGGAGTTGAAATGGGCGAAA, TET2: fwd: 5'CCGAAGCAACCGAACTCTTT, rev 3'ACAAGTGAGATCCTGGTGGG) binds outside the guide targeted region and only produces a PCR product after successful KO. Primer pair 2 (TET1: fwd: 5'CGCCTGTACAAAGAGCTCAC, rev: 3'AGGCTAGTCTCAGTTGGCAG; TET2: fwd: 5'TTCTAATGCCTGTGTTCTCTCA, rev: 3'CAACCTCTTTTGGCTCAGCT) binds at Exon 6 and will only produce a PCR product in case of the respective wild-type gene. KO strategy and PCR screening results can be accessed in Figures 7 and 8 an. Genetic depletion of the Tet genes was confirmed with a western blot (Figure 9) using anti-TET1 (NBP2-19290, Novus Biologicals, 1:1000) and anti-TET2 (Cell Signaling Technology 45010S, 1:1000).

#### **4.11 Immunofluorescence (IF) imaging and quantifications**

ESCs: Cells were seeded as single cells on matrigel coated 8-chamber culture slides (Falcon, Cat: 354108) for 30 min until adherent and subsequently fixed with 4% PFA in DPBS. After fixation, cells were washed 3x and permeabilized using PBS-0.2% Triton-X100 for 10 min at RT. For the labeling with antibodies against 5mC and 5hmC, cells were de-purinated using 2N HCL for 1h followed by a neutralization of 30 min in 0.1M sodium borate. After permeabilization, cells were blocked in DPBS-0.2% Triton-X100 containing 2% BSA and 5% goat serum for 1h at RT. After blocking, cells were incubated with anti-5mC (Diagenode, C15200003; IF 1:100) or anti-5hmC (ActifMotif, 39769; IF 1:200) or anti-TFE3 (Merck, HPA023881) in the blocking buffer overnight at 4°C and subsequently washed three times in PBS-0.2% Triton-X100 containing 2% BSA at RT. After washing, cells were incubated with a secondary antibody in a blocking buffer for 1h at RT. Subsequently, the cells were washed in PBS-0.2% Triton-X100 containing 2% BSA at RT. The chamber was then detached from the slides, and Vectashield containing DAPI (Vectashield, Cat: H-1200) was added to the slides, and slides were sealed with a cover glass (Brand, 470820). The slides were kept in the dark until imaged. Images were acquired with a ZEISS LSM880 microscope at 20x magnification. Images were further processed using Fiji (version 2.3.0). Image quantifications were done with CellProfiler66 (version 4.2.1). Nuclei were set as primary objects, and the IF signal of 5mC and 5hmC was normalized to DAPI signal intensity.

Embryos: Embryos were washed through a series of KSOM drops (Sigma), followed by a series of PBS + 0.4% BSA. Fixation was performed by incubation with 4% PFA for 10 mins. PFA was washed off by a series of washes in PBS + 0.5% TritonX-100 (PBS-T). Embryos were de-purinated using 2N HCL for h, followed by a neutralization of 30min in 0.1M sodium borate. Embryos were then permeabilized in PBS-T for 20 min at room temperature. After permeabilization, samples were washed in PBS-T and blocked in PBS-T + 2% BSA + 5% goat serum for 1 h at room temperature. Primary antibodies were diluted in blocking buffer (PBS-T + 2% BSA + 5% goat serum) overnight at 4°C. Following incubation with the primary antibody, samples were washed three times for 10 min at room temperature in PBS-T + 2% BSA and subsequently incubated with secondary antibodies (1:1000) in PBS-T + 2% BSA + 5% goat serum for 1 h at room temperature. Samples were washed three times 10 min at room temperature in PBS-T. After the last washing step, embryos were transferred to a mounting medium containing DAPI (Vectashield, Cat: H-1200) and further to a glass slide (Roth) and sealed with a cover glass (Brand, 470820). Images were acquired with a ZEISS LSM880 microscope at 20x magnification. Images were further processed using Fiji (version 2.3.0). Image quantifications were done with CellProfiler66 (version 4.2.1). Single nuclei were set as primary objects based on the DAPI signal, and the IF signal of 5mC was normalized to DAPI signal intensity.

#### **4.12 Western blotting**

Samples were mixed with 4× ROTI loading buffer (Carl Roth, K929.2), boiled at 98°C for 5 min, and loaded on 4-15% Mini-PROTEAN®TGX™ precast protein gels (Bio-Rad, 4561083). Proteins were separated by electrophoresis at 70 V for 15 min followed by 100 V for approximately 1 h using 10× Tris/Glycine/SDS running buffer (Bio-Rad, 1610772). Proteins were transferred to a PVDF membrane (Thermo Fisher Scientific, IB24001) using the iBlot 2 dry blotting system (Thermo Fisher Scientific, IB21001) and run at 20 V for 7 min. After blotting, membranes were blocked with 5% milk in TBS-T buffer (Thermo Fisher Scientific, 28360) for 1h at RT. For detection of the protein of interest, membranes were incubated at 4°C overnight with primary antibody (indicated in each method section) in 5% milk in TBS-T buffer, followed by secondary antibody at RT for 1 h. For detection, membranes were incubated with ECL Western Blotting Substrate (Thermo Fisher Scientific, 32106) for 1 min prior to imaging with the ChemiDoc system (Bio-Rad).



### 4.13 RNA-sequencing

Sample preparation: Cells were grown in 10 cm dishes. Pausing was achieved by treating cells with the mTOR inhibitor INK128 (Selleckchem, s2811) at 200 nM. At 0h, 24h, 72h, and 144h, cells were trypsinized and collected using the cell sorting system BD FACSAria Fusion. Wild-type cells were collected first, followed by the Tet DKO cells using the same gating for the respective time point. Total RNA was extracted from 200,000 cells using the Qiagen RNeasy kit (Qiagen, 74004). Samples were spiked in using an ERCC62 RNA spike-in mix (Thermo, 4456740), and 500 ng of RNA was used as input for library preparation. Library preparation was performed using the KAPA RNA HyperPrep Kit with RiboErase (Roche, 8098131702) following the manufacturer's instructions. Libraries were sequenced on a Novaseq600, S4 flow cell, paired-end mode with a desired sequencing depth of 50M fragments per sample.

Analysis: Raw reads were subjected to adapter and quality trimming with cutadapt67 (version 2.4; parameters: `--quality-cutoff 20 --overlap 5 --minimum-length 25 --interleaved --adapter AGATCGGAAGAGC -A AGATCGGAAGAGC`), followed by poly-A trimming with cutadapt (parameters: `--interleaved --overlap 20 --minimum-length --adapter "A[100]" --adapter "T[100]"`). Reads were aligned to the mouse reference genome (mm10) using STAR (version 2.7.5a; parameters: `--runMode alignReads --chimSegmentMin 20 --outSAMstrandField intronMotif --quantMode GeneCounts`)<sup>68</sup> and transcripts were quantified using stringtie (version 2.0.6; parameters: `-e`)<sup>69</sup> with GENCODE annotation (release VM19). For the repeat expression quantification, reads were re-aligned with additional parameters `'--outFilterMultimapNmax 50'`. Differential gene expression analysis was performed on stringtie output using DEseq270 (version 1.38.2).

### 4.14 ATAC-seq

Cells were collected as described above for RNA-seq. The ATAC-seq protocol from Corces et al. 2017 was followed with minor modifications (Corces et al. 2017). In brief: 50,000 cells were spun at 500 RCF at 4°C for 5 min in a fixed angle centrifuge and resuspended in a cold RSB buffer containing 0.1% NP40 and 0.1% TWEEN20 and subsequently incubated on ice for 3 min. Lysis was washed out using 1ml cold RSB-buffer containing 0.1% TWEEN20 but no NP40 and nuclei pelleted at 500 RCF at 4°C for 10 min. The resulting pellet was resuspended in the transposition mix (25 ul 2x TD buffer, 2.5 ul transposase (100nM final,

NEXtera), 16.5 ul PBS, 0.5 ul 1% digitonin, 0.5 ul 10% Tween-20, 5 ul H<sub>2</sub>O) and incubated at 37°C for 30min with 1000 RPM mixing on a standard thermocycler. Samples were then processed with the Zymo DNA Clean and Concentrator-5 Kit (D4014) following manufacturer recommendations and samples eluted in 21µl elution buffer. All libraries were amplified with 8 PCR cycles with i5 and i7 primers from NEB. The final number of cycles was determined following Buenrostro et al. 2015 (Buenrostro et al. 2015). Libraries were sequenced on a Novaseq600, S4 flow cell, paired-end mode with a desired sequencing depth of 50M per sample.

Analysis: Raw reads were subjected to adapter and quality trimming with cutadapt (version 2.4; parameters: --quality-cutoff 20 --overlap 5 --minimum-length 25 --adapter AGATCGGAAGAGC -A AGATCGGAAGAGC) as were their respective input samples. Reads were aligned to the mouse genome (mm10) using BWA with the ‘mem’ command (version 0.7.17, default parameters)<sup>73</sup>. A sorted BAM file was obtained and indexed using samtools with the ‘sort’ and ‘index’ commands (version 1.10)<sup>74</sup>. Duplicate reads were identified and removed using GATK (version 4.1.4.1) ‘MarkDuplicates’ and default parameters. After careful inspection and validation of high correlation, replicates of treatment and input samples were merged respectively using samtools ‘merge.’ Peaks were called using the MACS2<sup>75</sup> peakcall (2.1.2\_dev) function with default parameters.

#### **4.15 Whole Genome Bisulfite Sequencing (WGBS)**

Cells were collected as described above for RNA-seq. Genomic DNA was isolated from 50,000 cells using the Purelink Genomic DNA mini kit (Invitrogen), following the manufacturer's recommendations. Libraries were prepared using the Accel-NGS Methyl-Seq DNA Library Kit following manufacturers' recommendations and sequenced on a Novaseq600, S4 flow cell, paired-end mode with a desired sequencing depth of 300M per sample.

Analysis: Raw reads were subjected to adapter and quality trimming using cutadapt (version 2.4; parameters: --quality-cutoff 20 --overlap 5 --minimum-length 25; Illumina TruSeq adapter clipped from both reads), followed by trimming of 10 and 5 nucleotides from the 5’ and 3’ end of the first read and 15 and 5 nucleotides from the 5’ and 3’ end of the second read<sup>67</sup>. The trimmed reads were aligned to the mouse genome (mm10) using BSMAP (version 2.90; parameters: -v 0.1 -s 16 -q 20 -w 100 -S 1 -u -R)<sup>76</sup>. A sorted BAM file was

obtained and indexed using samtools with the 'sort' and 'index' commands (version 1.10)<sup>74</sup>. Duplicates were removed using the 'MarkDuplicates' command from GATK (version 4.1.4.1) and default parameters<sup>77</sup>. Methylation rates were called using mcall from the MOABS package (version 1.3.2; default parameters)<sup>78</sup>. All analyses were restricted to autosomes, and only CpGs covered by at least 10 and at most 150 reads were considered for downstream analyses.

#### **4.16 CUT&Tag**

Sample preparation: Cleavage Under Targets and Tagmentation (CUT&Tag) on cryopreserved nuclei or freshly derived cells was performed as described previously in Kaya-Okur et al. 2019 (Kaya-Okur et al. 2019) with minor modifications. For cryopreserved nuclei, cells were dissociated using accutase and washed in PBS. Nuclei were extracted by resuspending the cells in ice-cold NE1 buffer (20 mM HEPES-KOH, pH7.5, 10 mM KCl, 0.5 mM Spermidine, 0.1% Triton X-100, 20% glycerol, 1 mM PMSF, 5 mM NaF, 1 mM Na<sub>3</sub>VO<sub>4</sub>) and incubating on ice for 10 minutes. Nuclei were fixed by incubating with 0.1% formaldehyde at room temperature for 2 minutes. 1.25 M glycine was added to stop cross-linking. Fixed nuclei were centrifuged for 4 minutes at 1300x g at 4 °C and were frozen in Wash buffer (20 mM HEPES-KOH, pH 7.5, 150 mM NaCl, 0.5 mM Spermidine, 1 mM PMSF, 5 mM NaF, 1 mM Na<sub>3</sub>VO<sub>4</sub>) with 10% DMSO at -80 °C until further processing. For CUT&Tag on fresh cells, cells were directly resuspended in wash-buffer. For each CUT&Tag reaction, 3.5 µl of Concanavalin A beads (Bangs Laboratories) were equilibrated by washing 2 times in 100 µl Binding buffer (20 mM HEPES-KOH, pH 7.5, 10 mM KCl, 1 mM CaCl<sub>2</sub>, 1 mM MnCl<sub>2</sub>) and concentrated again in 3.5 µl Binding buffer. 1×10<sup>4</sup> cryopreserved nuclei were thawed and bound to the Concanavalin A beads by incubating for 10 minutes with rotation at room temperature. The beads were separated on a magnet and resuspended in 25 µl of cold Antibody buffer (Wash buffer with 0.1% BSA) containing respective primary antibody or IgG (TET1, NBP2-19290, Novus Biologicals, 1:100; TET2, Cell Signaling Technology 45010S, 1:50; TFE3, Sigma HPA023881, 1:50; IgG, Abcam ab46540, 1:100, H3K27ac, 9733S, CST, 1:100; H3K4me3, 9751S, CST, 1:100; H3K4me1, 5326S, CST, 1:100). Primary antibody incubation was done by incubating the beads at 4 °C with gentle nutation overnight. The beads were then separated from the primary antibody on a magnet. Subsequently, the beads were resuspended in 25 µl of Wash buffer containing matching secondary antibody (guinea pig α-rabbit antibody, ABIN101961, Antibodies online, 1:100) and were incubated for 30 minutes at room temperature with gentle nutation. Afterwards, the

beads were separated from secondary antibody and washed once in 200µl of Wash buffer while being kept on a magnet. The 3xFLAG-pA-Tn5 (homemade) preloaded with Mosaic-end adapters were diluted 1:250 in 300-wash buffer (20 mM HEPES-KOH, pH 7.5, 300 mM NaCl, 0.5 mM Spermidine, 1 mM PMSF, 5 mM NaF, 1 mM Na<sub>3</sub>VO<sub>4</sub>) and 25 µl of it were used to resuspend the beads. The beads were incubated for 1 hour at room temperature with gentle nutation and were washed once in 200 µl of 300-wash buffer on a magnet. Tagmentation was performed by incubating the beads in 50 µl Tagmentation buffer (10mM MgCl<sub>2</sub> in 300-wash buffer) for 1 hour at 37 °C. Tagmentation was stopped by adding 2.25 µl of 500 mM EDTA and 2.75 µl of 10% SDS to the beads followed by adding 0.5 µl of Proteinase K (20 mg/ml). After vortexing for 5 seconds, the beads were incubated at 55 °C for 1 hour to solubilize the DNA fragments and then 70 °C for 30 minutes to inactivate the Proteinase K. The beads were removed on a magnet and the DNA were purified using Chimmun DNA Clean & Concentrator (D5205, Zymo Research) following the manufacturer's manual. The final CUT&Tag DNA were eluted in 25 µl of elution buffer. To amplify the NGS libraries, 25 µl of NEBNext® HiFi 2x PCR Master Mix (New England BioLabs) was mixed with 21 µl of the CUT&Tag DNA, 2µl of 10 µM i5- and 2µl of 10 µM i7- unique barcoded primers<sup>72</sup> and the following program was run on a thermocycler:

Sequencing: CUT&Tag libraries were generated by amplifying the CUT&Tag DNA fragments with i5- and i7- barcoded HPLC-grade primers (Buenrostro et al., 2015 Supplementary Table 6) with NEBNext® HiFi 2x PCR Master Mix (New England BioLabs) on a thermocycler with the following program: 72 °C for 5 minutes, 98 °C for 30 seconds, 98 °C for 10 seconds, 63 °C for 10 seconds (14 cycles of step 3-4) and 72 °C for 1 minute. Ampure XP beads (Beckman Coulter) were used for post-PCR cleanup. 55 µl (1.1x volume) of the Ampure XP beads were added to the PCR mix and incubated for 10 minutes at room temperature. The beads were separated and washed two times using 80% ethanol on a magnet. Finally, the CUT&Tag libraries were eluted in 25 µl of Tris-HCl, pH 8.0. The quality of the CUT&Tag libraries was assessed by Agilent High Sensitivity D5000 ScreenTape System and Qubit™ dsDNA HS Assay (Invitrogen). Sequencing libraries were pooled in equimolar ratios and concentrated again using 1.1x volume of Ampure XP beads when necessary. The libraries were sequenced on Illumina next generation sequencer with paired end mode and approximately 5 million fragments per library.

Analysis: Raw reads were subjected to adapter and quality trimming with cutadapt (version 2.4; parameters: --quality-cutoff 20 --overlap 5 --minimum-length 25 --adapter AGATCGGAAGAGC -A AGATCGGAAGAGC) as were their respective input samples. Reads were aligned to the mouse genome (mm10) using BWA with the ‘mem’ command (version 0.7.17, default parameters)<sup>73</sup>. A sorted BAM file was obtained and indexed using samtools with the ‘sort’ and ‘index’ commands (version 1.10)<sup>74</sup>. Duplicate reads were identified and removed using GATK (version 4.1.4.1) ‘MarkDuplicates’ and default parameters. After careful inspection and validation of high correlation, replicates of treatment and input samples were merged respectively using samtools ‘merge’. Peaks were called using the MACS2<sup>75</sup> peakcall (2.1.2\_dev) function with default parameters.

#### **4.17 Pathway expression analysis**

The pathway expression value was defined as the mean expression (TPM) of genes in a given pathway at the indicated time points. KEGG80 pathways containing at least 10 genes were included in the analysis.

#### **4.18 Motif enrichment analysis**

Motif enrichment was performed using Homer (v4.7, 8-25-2014). TET dormancy targets were compared against the mouse genome (mm10) using the following settings: -size given.

#### **4.19 TF footprinting analysis**

ATAC-seq peak regions were called by MACS2 (2.2.7.1) with 75-bp shift and 150-bp extension. Differential TF footprints inside these peak regions were identified by TOBIAS<sup>36</sup> (0.12.11) using Homer motifs (v4.7, 8-25-2014).

#### **4.20 Definition of mESC enhancer sets**

Active and primed enhancer were previously identified in Cruz-Molina et al. 2017 and are defined as follows: active enhancers, genomic regions with p300 enrichment, located within 1 kb of regions enriched in H3K27ac and not enriched in H3K27ac (within 1 kb); primed enhancers, genomic regions with H3K4me1 enrichment and not enriched in H3K27ac or H3K27ac (within 1 kb) (Cruz-Molina et al. 2017).

#### **4.21 Generation of *Tet* KO embryos via Cas9-assisted gene editing**

Control and mutant embryos were generated using a combination of in vitro fertilization and zygotic electroporation, as previously described<sup>82</sup>. In brief, IVF was conducted using oocytes from superovulated B6D2F1 female mice (7-9 weeks old; Envigo) and sperm from F1B6xCAS, as previously described<sup>83</sup>. Pronuclei stage 3 (PN3) zygotes were rinsed with M2 (Sigma) and OptimMEM I (Gibco) medium before electroporation. The electroporation reaction was set up using the Alt-R CRISPR-Cas9 ribonucleoprotein (RNP) complex, as previously described<sup>82</sup>. For each of the *Tet* genes, 3 gRNAs were designed targeting the first few exons, gRNA sequences listed below. Electroporation was performed with the NEPA21 electroporator (NEPAGENE) in a chamber with 5 mm electrode gap (NEPAGENE), and the following settings: 4 poring pulses with a voltage of 225 V, pulse length of 2 ms, pulse interval of 50 ms, decay rate of 10%, and uniform polarity, followed by 5 transfer pulses with a voltage of 20 V, pulse length of 50 ms, pulse interval of 50 ms, decay rate of 40%, and alternating polarity, was used. The electroporated zygotes were rinsed in KSOM drops (Merck) and cultured in KSOM drops covered by mineral oil (Sigma) at 37°C and CO<sub>2</sub> till blastocyst stage. Embryos that had reached the cavitated blastocyst stage were chosen for the re-transfer experiment. A total of 30 blastocysts were transferred bilaterally using pseudopregnant female CD-1 (21-25 g, Envigo) mice 2.5 days post-coitum (dpc). E8.5 stage embryos were isolated from the uteri of foster mice. The embryos were dissected in 1X HBSS (Gibco) on ice after the decidua were carefully removed from the uteri. Embryos were washed in 1X PBS (Gibco) containing 0.4% BSA before being imaged with an Axiozoom (ZEISS) microscope. Images were processed with Fiji.

For qPCR, RNA was isolated with arcturus Pico Pure RNA isolation kit (Biosystems) following the manufacturer's recommendations. The RNA was eluted in 10 uL of elution buffer and was reverse transcribed with High-Capacity cDNA synthesis kit (KAPA biosystems) as per manufacturer's recommendation. 0.5µl of cDNA was used for RT-qPCR with Kapa SYBR 2x master mix. B-actin was used for internal normalization.:

#### **4.22 Guide RNA sequences**

Tet1:

- 1) TCGATCCCGATTCATTCGGG
- 2) TTGGCGGCGTAGAATTACAT
- 3) GATTAATCACATCAACGCCG

Tet2:

- 1) AAGATTGTGCTAATGCCTAA
- 2) GAGTGCTTCATGCAAATTCG
- 3) GCTCCTAGATGGGTATAATA

Tet3:

- 1) GAGCGCGCTGAGCATTGCCA
- 2) TTCTATCCGGGAACTCATGG
- 3) TCGGATTGTCTCCCGTGAGG

Control guide against *Gfp*:

- 1) GAAGTTCGAGGGCGACACCC

#### 4.23 qPCR primers

Tet1:

F 5'ACCACAATAAATCAGGTTACAC, R 5'TCTCCACTGCACAATGCCTT

Tet2:

F 5'GCAATCACACCACCCAGTAGAA, R 5'TCCACGTGCTGCCTATGTAC

Tet3:

F 5'GCCTCAATGATGACCGGACC, R 5'ATGAGTTTGGCAGCGAGGAA

#### 4.24 FLASH

Generation of stable FLASH-tagged cell lines: For endogenous tagging of Tet1 and Tet2 genes with the biotinylation signal necessary to perform the FLASH method, we used a modified plasmid from the CRISpaint toolkit<sup>84</sup> which contains a biotinylation signal followed by FLAG tag and a puromycin resistance gene as the donor plasmid. Guide RNAs targeting the C-terminus of Tet1 (GTTGCGGGACCCTACAATCGT) and Tet2 (GACAACACATTTGTATGACGC), respectively were expressed from the px330 plasmid, co-expressing Cas9. px330 expressing the appropriate guide RNA together with the donor plasmid and the appropriate frame selector plasmid were nucleofected to generate each cell line. Colonies that remained after 10 days of puromycin selection were genotyped using the following primers:

Tet1:

- (F) 5'GGGAGTGTCTGATGTATCCCCCG  
(R) 3'CTCAGCTCATCACTCCGTGTGTTGA

Tet2:

(F) 5'CCAGTCTCTTGCTGAGAACACAGGG

(R) 3'CAGATGCTGTGACCTGTCCCTACG.

Successful tagging of endogenous TET1 and TET2 was confirmed by a streptavidin pull-down followed by Western blotting. Membranes were incubated with HRP conjugated streptavidin (Thermo, N100) to visualize biotinylated TET1 and TET2 proteins.

FLASH was performed according to Ilik et al. 2019. In brief, cells with either Tet1-FLASH-Tag or Tet2-FLASH-Tag or wild-type (control) were crosslinked with 0.15mJ/cm<sup>2</sup> UV-C irradiation, lysed with 1xNLB and homogenized by water bath-sonication. Target protein of interest was pulled-down with paramagnetic beads pre-coupled to antibodies against the protein of interest. After a brief RNase I-digestion, RNA 3'-ends were healed with T4 PNK. Custom-made, barcoded adapters were ligated using T4 RNA Ligase 1 for 1 hr at 25°C. Custom FLASH adapters contained two barcodes and random nucleotides adjacent to the 3'-adapters according to the pattern NNBBNTTTTTTNN (N: random tag nucleotide, T: tag nucleotide, B: RY-space tag nucleotide). Random tags were used to merge PCR-duplicates, regular tags were used to specify the pulldown condition, and semi-random RY-space tags were used to distinguish the biological replicates (RR: replicate A, YY: replicate B, R: purine, Y: pyrimidine). Excess adapters were washed away, negative controls (IgG) were mixed with experimental controls and RNA was isolated with Proteinase K treatment and column purification. Isolated RNA was reverse-transcribed and RNase H-treated. cDNA was column-purified and circularized with CircLigase for 2-16hrs. Circularized cDNA was directly PCR amplified, quantified with Qubit / Bioanalyzer and sequenced on Illumina NextSeq 500 in paired-end mode.

#### **4.25 Immunoprecipitation (IP)-mass spectrometry**

IP: Cells were harvested by trypsinization. Cell pellets were washed once with 1 ml cold PBS and resuspended in 1 ml cold buffer A (10mM Hepes pH7.9, 5mM MgCl<sub>2</sub>, 0.25M Sucrose, 0.1% NP40) per ~5M cells. Samples were incubated for 10 minutes on ice and passed 4 times through an 18G1 needle (BD Microlance 3, 304622). Samples were then centrifuged for 10 min at 2300 rcf and supernatant was discarded (cytosolic fraction). The nuclei pellet was washed once with 1 ml of buffer A and subsequently resuspended in 1ml cold buffer B (10mM Hepes pH 7.9, 1mM MgCl<sub>2</sub>, 0.1mM EDTA, 25% glycerol, 0.5M NaCl). After 30 min of incubation on ice, samples were passed 4 times through an 18G1 needle. Samples



were then sonicated in Bioruptor 300 (Diagenode) with settings 30 seconds on, 30 seconds off for 5 minutes at 4°C. Afterwards samples were centrifuged for 10 min at 2300 rcf to remove precipitate and protein concentration was quantified by BCA Protein Assay Kit (Pierce, 23225). 1 mg of protein was used per pull-down in a minimum volume of 500 µl in IP buffer (20 mM Hepes pH 7.9, 25% glycerol, 0.5M NaCl, 1.5 mM MgCl<sub>2</sub>, 0.2 mM EDTA, 0.02% NP-40). Flag antibody (Merck, F3165) and Dynabeads Protein A (Invitrogen, 10001D) were added (1 mg of beads and ~8 µg of antibody) and the mixture incubated for 2h at 4°C. After pull-down beads were washed 3x in IP buffer and either immediately digested for mass-spectrometry or boiled at 96°C in 30 µl of Leammi-buffer (Roth, K930.1) for Western-blotting.

Mass spectrometry: 135 µl of 100 mM ammonium bicarbonate were added to the washed magnetic beads. This was followed by a tryptic digest including reduction and alkylation of the cysteines. Therefore, the reduction was performed by adding tris(2-carboxyethyl)phosphine with a final concentration of 5.5 mM at 37°C on a rocking platform (700 rpm) for 30 minutes. For alkylation, chloroacetamide was added with a final concentration of 24 mM at room temperature on a rocking platform (700 rpm) for 30 minutes. Then, proteins were digested with 200 ng trypsin (Roche, Basel, Switzerland) per sample, shaking at 1000 rpm at 37°C for 18 hours. Samples were acidified by adding 6 µL 100% formic acid (2% final concentration), centrifuged shortly, and placed on the magnetic rack. The supernatants, containing the digested peptides, were transferred to a new low-protein binding tube. Peptide desalting was performed on C18 columns (Pierce). Eluates were lyophilized and reconstituted in 11 µL of 5% acetonitrile and 2% formic acid in water, briefly vortexed, and sonicated in a water bath for 30 seconds before injection to nano-LC-MS/MS.

Run parameters: LC-MS/MS was carried out by nanoflow reverse phase liquid chromatography (Dionex Ultimate 3000, Thermo Scientific) coupled online to a Q-Exactive HF Orbitrap mass spectrometer (Thermo Scientific), as reported previously. Briefly, the LC separation was performed using a PicoFrit analytical column (75 µm ID × 50 cm long, 15 µm Tip ID; New Objectives, Woburn, MA) in-house packed with 3-µm C18 resin (Reprosil-AQ Pur, Dr. Maisch, Ammerbuch, Germany).

Peptide analysis: Raw MS data were processed with MaxQuant software (v1.6.10.43) and searched against the mouse proteome database UniProtKB with 55,153 entries, released in August 2019.

#### **4.25 Enhancer and L1Md gene contact analysis**

To determine the genes looping with the identified active enhancers and potentially by L1Md elements, we used the publicly available predictions from the Activity-By-Contact model<sup>49</sup>. For gene looping with enhancers, we used the recommended cut off (ABC-score 0.02). For potential L1Md-promoter contacts, the HiC contact probability (>15) provided in the same file for mESCs was used (mESC.AllPredictions.txt).

#### **4.26 Gene knockdowns**

Three shRNAs against TFE3 were cloned into a pLKO.1 plasmid containing a puromycin resistance gene and allowing for doxycycline inducible expression, respectively, resulting in pLKO.1.shTFE3:

shTFE3\_1:ATCCGGGATTGTTGCTGATAT,  
shTFE3\_2:GTGGATTACATCCGCAAATTA,  
shTFE3\_3:AGCTATCACCGTCAGCAATTC.

2 µg of pLKO.1.shTFE3 was co-transfected with 2 µg of equal parts pVSV-G, pMDL, pRSV (packaging vectors) into HEK 293T cells grown to 80% confluency on a 10 cm uncoated culture dish. After 24h hours, cell culture supernatant was collected for 3 consecutive days to enrich for produced viruses. The virus supernatant was concentrated and used to transduce E14 wild-type cells. For transduction, 100,000 E14 cells were mixed with 50 µl of concentrated virus suspension and 10 µg/mL polybrene in a 1.5 ml tube and rotated at 37°C for 1h. Subsequently, cells were plated on 6-well culture dishes and grown for 48h after which puromycin selection was applied for 6 days. Efficient knock-down of TFE3 was confirmed by IF followed by confocal microscopy.

## 5. Bibliography

Arena Roberta, Simona Bisogno, Łukasz Gąsior, Joanna Rudnicka, Laura Bernhardt, Thomas Haaf, Federica Zacchini, et al. 2021. „Lipid Droplets in Mammalian Eggs Are Utilized during Embryonic Diapause“. *Proceedings of the National Academy of Sciences* 118 (10): e2018362118. <https://doi.org/10.1073/pnas.2018362118>.

Becker, Peter B., Siegfried Ruppert, und Günther Schütz. 1987. „Genomic Footprinting Reveals Cell Type-Specific DNA Binding of Ubiquitous Factors“. *Cell* 51 (3): 435–43. [https://doi.org/10.1016/0092-8674\(87\)90639-8](https://doi.org/10.1016/0092-8674(87)90639-8).

Bentsen, Mette, Philipp Goymann, Hendrik Schultheis, Kathrin Klee, Anastasiia Petrova, René Wiegandt, Annika Fust, et al. 2020. “ATAC-Seq Footprinting Unravels Kinetics of Transcription Factor Binding during Zygotic Genome Activation.” *Nature Communications* 11 (1): 4267. <https://doi.org/10.1038/s41467-020-18035-1>.

Bird, Adrian P. 1980. „DNA Methylation and the Frequency of CpG in Animal DNA“. *Nucleic Acids Research* 8 (7): 1499–1504. <https://doi.org/10.1093/nar/8.7.1499>.

Bird, Adrian, Mary Taggart, Marianne Frommer, Orlando J. Miller, and Donald Macleod. 1985. „A Fraction of the Mouse Genome That Is Derived from Islands of Nonmethylated, CpG-Rich DNA“. *Cell* 40 (1): 91–99. [https://doi.org/10.1016/0092-8674\(85\)90312-5](https://doi.org/10.1016/0092-8674(85)90312-5).

„Bischoff, Theodor Ludwig Wilhelm: Entwicklungsgeschichte des Rehes“, Bild 6 von 64 | MDZ“. o. J. Zugegriffen 13. Februar 2024. <https://www.digitale-sammlungen.de/de/view/bsb10231144?page=6>.

Blaschke, Kathryn, Kevin T. Ebata, Mohammad M. Karimi, Jorge A. Zepeda-Martínez, Preeti Goyal, Sahasransu Mahapatra, Angela Tam, et al. 2013. „Vitamin C Induces Tet-Dependent DNA Demethylation and a Blastocyst-like State in ES Cells“. *Nature* 500 (7461): 222–26. <https://doi.org/10.1038/nature12362>.

Bonetti, Alessandro, Federico Agostini, Ana Maria Suzuki, Kosuke Hashimoto, Giovanni Pascarella, Juliette Gimenez, Leonie Roos, et al. 2020. „RADICL-Seq Identifies General and

Cell Type–Specific Principles of Genome-Wide RNA-Chromatin Interactions“. *Nature Communications* 11 (1): 1018. <https://doi.org/10.1038/s41467-020-14337-6>.

Bonev, Boyan, Netta Mendelson Cohen, Quentin Szabo, Lauriane Fritsch, Giorgio L. Papadopoulos, Yaniv Lubling, Xiaole Xu, et al. 2017. „Multiscale 3D Genome Rewiring during Mouse Neural Development“. *Cell* 171 (3): 557-572.e24. <https://doi.org/10.1016/j.cell.2017.09.043>.

Boroviak, Thorsten, Remco Loos, Paul Bertone, Austin Smith, und Jennifer Nichols. 2014. „The Ability of Inner-Cell-Mass Cells to Self-Renew as Embryonic Stem Cells Is Acquired Following Epiblast Specification“. *Nature Cell Biology* 16 (6): 513–25. <https://doi.org/10.1038/ncb2965>.

Buenrostro, Jason D, Paul G Giresi, Lisa C Zaba, Howard Y Chang, und William J Greenleaf. 2013. „Transposition of Native Chromatin for Fast and Sensitive Epigenomic Profiling of Open Chromatin, DNA-Binding Proteins and Nucleosome Position“. *Nature Methods* 10 (12): 1213–18. <https://doi.org/10.1038/nmeth.2688>.

Buenrostro, Jason D., Beijing Wu, Howard Y. Chang, und William J. Greenleaf. 2015. „ATAC-seq: A Method for Assaying Chromatin Accessibility Genome-Wide“. *Current Protocols in Molecular Biology* 109 (1). <https://doi.org/10.1002/0471142727.mb2129s109>.

Bulut-Karslioglu, Aydan, Steffen Biechele, Hu Jin, Trisha A. Macrae, Miroslav Hejna, Marina Gertsenstein, Jun S. Song, und Miguel Ramalho-Santos. 2016. „Inhibition of mTOR Induces a Paused Pluripotent State“. *Nature* 540 (7631): 119–23. <https://doi.org/10.1038/nature20578>.

Bulut-Karslioglu, Aydan, Inti A. De La Rosa-Velázquez, Fidel Ramirez, Maxim Barenboim, Megumi Onishi-Seebacher, Julia Arand, Carmen Galán, et al. 2014. „Suv39h-Dependent H3K9me3 Marks Intact Retrotransposons and Silences LINE Elements in Mouse Embryonic Stem Cells“. *Molecular Cell* 55 (2): 277–90. <https://doi.org/10.1016/j.molcel.2014.05.029>.

Bulut-Karslioglu, Aydan, Trisha A. Macrae, Juan A. Oses-Prieto, Sergio Covarrubias, Michelle Percharde, Gregory Ku, Aaron Diaz, Michael T. McManus, Alma L. Burlingame,

und Miguel Ramalho-Santos. 2018. „The Transcriptionally Permissive Chromatin State of Embryonic Stem Cells Is Acutely Tuned to Translational Output“. *Cell Stem Cell* 22 (3): 369-383.e8. <https://doi.org/10.1016/j.stem.2018.02.004>.

Cabej, Nelson R. 2019. „Epigenetic Control of Reproduction“. In *Epigenetic Principles of Evolution*, 75–117. Elsevier. <https://doi.org/10.1016/B978-0-12-814067-3.00003-X>.

Chambers, Ian, Douglas Colby, Morag Robertson, Jennifer Nichols, Sonia Lee, Susan Tweedie, und Austin Smith. 2003. „Functional Expression Cloning of Nanog, a Pluripotency Sustaining Factor in Embryonic Stem Cells“. *Cell* 113 (5): 643–55. [https://doi.org/10.1016/S0092-8674\(03\)00392-1](https://doi.org/10.1016/S0092-8674(03)00392-1).

Cheng, Saifeng, Markus Mittnenzweig, Yoav Mayshar, Aviezer Lifshitz, Marko Dunjić, Yoach Rais, Raz Ben-Yair, et al. 2022. „The Intrinsic and Extrinsic Effects of TET Proteins during Gastrulation“. *Cell* 185 (17): 3169-3185.e20. <https://doi.org/10.1016/j.cell.2022.06.049>.

Chew, Joon-Lin, Yuin-Han Loh, Wensheng Zhang, Xi Chen, Wai-Leong Tam, Leng-Siew Yeap, Pin Li, et al. 2005. „Reciprocal Transcriptional Regulation of Pou5f1 and Sox2 via the Oct4/Sox2 Complex in Embryonic Stem Cells“. *Molecular and Cellular Biology* 25 (14): 6031–46. <https://doi.org/10.1128/MCB.25.14.6031-6046.2005>.

Cho, Inchul J., Prudence PokWai Lui, Jana Obajdin, Federica Riccio, Wladislaw Stroukov, Thea Louise Willis, Francesca Spagnoli, und Fiona M. Watt. 2019. „Mechanisms, Hallmarks, and Implications of Stem Cell Quiescence“. *Stem Cell Reports* 12 (6): 1190–1200. <https://doi.org/10.1016/j.stemcr.2019.05.012>.

Chua, Gabriella N. L., Kelly L. Wassarman, Haoyu Sun, Joseph A. Alp, Emma I. Jarczyk, Nathanael J. Kuzio, Michael J. Bennett, Beth G. Malachowsky, Martin Kruse, und Andrew J. Kennedy. 2019. „Cytosine-Based TET Enzyme Inhibitors“. *ACS Medicinal Chemistry Letters* 10 (2): 180–85. <https://doi.org/10.1021/acsmchemlett.8b00474>.

Clark, Natalie M., Eli Buckner, Adam P. Fisher, Emily C. Nelson, Thomas T. Nguyen, Abigail R. Simmons, Maria A. De Luis Balaguer, et al. 2019. „Stem-Cell-Ubiquitous Genes Spatiotemporally Coordinate Division through Regulation of Stem-Cell-Specific Gene

Networks“. *Nature Communications* 10 (1): 5574. <https://doi.org/10.1038/s41467-019-13132-2>.

Corces, M Ryan, Alexandro E Trevino, Emily G Hamilton, Peyton G Greenside, Nicholas A Sinnott-Armstrong, Sam Vesuna, Ansuman T Satpathy, et al. 2017. „An Improved ATAC-Seq Protocol Reduces Background and Enables Interrogation of Frozen Tissues“. *Nature Methods* 14 (10): 959–62. <https://doi.org/10.1038/nmeth.4396>.

Coulondre, Christine, Jeffrey H. Miller, Philip J. Farabaugh, und Walter Gilbert. 1978. „Molecular Basis of Base Substitution Hotspots in *Escherichia Coli*“. *Nature* 274 (5673): 775–80. <https://doi.org/10.1038/274775a0>.

Cruz-Molina, Sara, Patricia Respuela, Christina Tebartz, Petros Kolovos, Milos Nikolic, Raquel Fueyo, Wilfred F.J. Van Ijcken, et al. 2017. „PRC2 Facilitates the Regulatory Topology Required for Poised Enhancer Function during Pluripotent Stem Cell Differentiation“. *Cell Stem Cell* 20 (5): 689-705.e9. <https://doi.org/10.1016/j.stem.2017.02.004>.

Dixon, Jesse R., Inkyung Jung, Siddarth Selvaraj, Yin Shen, Jessica E. Antosiewicz-Bourget, Ah Young Lee, Zhen Ye, et al. 2015. „Chromatin Architecture Reorganization during Stem Cell Differentiation“. *Nature* 518 (7539): 331–36. <https://doi.org/10.1038/nature14222>.

Dixon, Jesse R., Siddarth Selvaraj, Feng Yue, Audrey Kim, Yan Li, Yin Shen, Ming Hu, Jun S. Liu, und Bing Ren. 2012. „Topological Domains in Mammalian Genomes Identified by Analysis of Chromatin Interactions“. *Nature* 485 (7398): 376–80. <https://doi.org/10.1038/nature11082>.

Donaghey, Julie, Sudhir Thakurela, Jocelyn Charlton, Jennifer S. Chen, Zachary D. Smith, Hongcang Gu, Ramona Pop, et al. 2018. „Genetic Determinants and Epigenetic Effects of Pioneer-Factor Occupancy“. *Nature Genetics* 50 (2): 250–58. <https://doi.org/10.1038/s41588-017-0034-3>.

Efroni, Sol, Radharani Duttgupta, Jill Cheng, Hesam Dehghani, Daniel J. Hoepfner, Chandravanu Dash, David P. Bazett-Jones, et al. 2008. „Global Transcription in Pluripotent

Embryonic Stem Cells“. *Cell Stem Cell* 2 (5): 437–47. <https://doi.org/10.1016/j.stem.2008.03.021>.

Elbarbary, Reyad A., Bronwyn A. Lucas, und Lynne E. Maquat. 2016. „Retrotransposons as Regulators of Gene Expression“. *Science* 351 (6274): aac7247. <https://doi.org/10.1126/science.aac7247>.

Fan, Rui, Yung Su Kim, Jie Wu, Rui Chen, Dagmar Zeuschner, Karina Mildner, Kenjiro Adachi, et al. 2020. „Wnt/Beta-Catenin/Esrrb Signalling Controls the Tissue-Scale Reorganization and Maintenance of the Pluripotent Lineage during Murine Embryonic Diapause“. *Nature Communications* 11 (1): 5499. <https://doi.org/10.1038/s41467-020-19353-0>.

Fenelon, Jane C., und Bruce D. Murphy. 2017. „Inhibition of Polyamine Synthesis Causes Entry of the Mouse Blastocyst into Embryonic Diapause†“. *Biology of Reproduction* 97 (1): 119–32. <https://doi.org/10.1093/biolre/iox060>.

Fidalgo, Miguel, Xin Huang, Diana Guallar, Carlos Sanchez-Priego, Victor Julian Valdes, Arven Saunders, Junjun Ding, Wen-Shu Wu, Carlos Clavel, und Jianlong Wang. 2016. „Zfp281 Coordinates Opposing Functions of Tet1 and Tet2 in Pluripotent States“. *Cell Stem Cell* 19 (3): 355–69. <https://doi.org/10.1016/j.stem.2016.05.025>.

Field, Andrew, und Karen Adelman. 2020. „Evaluating Enhancer Function and Transcription“. *Annual Review of Biochemistry* 89 (1): 213–34. <https://doi.org/10.1146/annurev-biochem-011420-095916>.

Fu, Zheng, Bingyan Wang, Shumin Wang, Weiwei Wu, Qiang Wang, Yongjie Chen, Shuangbo Kong, et al. 2014. „Integral Proteomic Analysis of Blastocysts Reveals Key Molecular Machinery Governing Embryonic Diapause and Reactivation for Implantation in Mice1“. *Biology of Reproduction* 90 (3). <https://doi.org/10.1095/biolreprod.113.115337>.

Fulco, Charles P., Joseph Nasser, Thouis R. Jones, Glen Munson, Drew T. Bergman, Vidya Subramanian, Sharon R. Grossman, et al. 2019. „Activity-by-Contact Model of Enhancer–

Promoter Regulation from Thousands of CRISPR Perturbations“. *Nature Genetics* 51 (12): 1664–69. <https://doi.org/10.1038/s41588-019-0538-0>.

Gaspar-Maia, Alexandre, Adi Alajem, Eran Meshorer, und Miguel Ramalho-Santos. 2011. „Open Chromatin in Pluripotency and Reprogramming“. *Nature Reviews Molecular Cell Biology* 12 (1): 36–47. <https://doi.org/10.1038/nrm3036>.

Gonzales, Kevin Andrew Uy, Hongqing Liang, Yee-Siang Lim, Yun-Shen Chan, Jia-Chi Yeo, Cheng-Peow Tan, Bin Gao, et al. 2015. „Deterministic Restriction on Pluripotent State Dissolution by Cell-Cycle Pathways“. *Cell* 162 (3): 564–79. <https://doi.org/10.1016/j.cell.2015.07.001>.

Greenberg, Maxim V. C., und Deborah Bourc'his. 2019. „The Diverse Roles of DNA Methylation in Mammalian Development and Disease“. *Nature Reviews Molecular Cell Biology* 20 (10): 590–607. <https://doi.org/10.1038/s41580-019-0159-6>.

Guzman-Ayala, Marcela, Michael Sachs, Fong Ming Koh, Courtney Onodera, Aydan Bulut-Karslioglu, Chih-Jen Lin, Priscilla Wong, Rachel Nitta, Jun S. Song, und Miguel Ramalho-Santos. 2015. „Chd1 Is Essential for the High Transcriptional Output and Rapid Growth of the Mouse Epiblast“. *Development* 142 (1): 118–27. <https://doi.org/10.1242/dev.114843>.

Hamatani, Toshio, Takiko Daikoku, Haibin Wang, Hiromichi Matsumoto, Mark G. Carter, Minoru S. H. Ko, und Sudhansu K. Dey. 2004. „Global Gene Expression Analysis Identifies Molecular Pathways Distinguishing Blastocyst Dormancy and Activation“. *Proceedings of the National Academy of Sciences* 101 (28): 10326–31. <https://doi.org/10.1073/pnas.0402597101>.

Harris, Sarah E., Nadia Gopichandran, Helen M. Picton, Henry J. Leese, und Nicolas M. Orsi. 2005. „Nutrient Concentrations in Murine Follicular Fluid and the Female Reproductive Tract“. *Theriogenology* 64 (4): 992–1006. <https://doi.org/10.1016/j.theriogenology.2005.01.004>.

Heintzman, Nathaniel D, Rhona K Stuart, Gary Hon, Yutao Fu, Christina W Ching, R David Hawkins, Leah O Barrera, et al. 2007. „Distinct and Predictive Chromatin Signatures of



Transcriptional Promoters and Enhancers in the Human Genome“. *Nature Genetics* 39 (3): 311–18. <https://doi.org/10.1038/ng1966>.

Heinz, Sven, Casey E. Romanoski, Christopher Benner, und Christopher K. Glass. 2015. „The Selection and Function of Cell Type-Specific Enhancers“. *Nature Reviews Molecular Cell Biology* 16 (3): 144–54. <https://doi.org/10.1038/nrm3949>.

Hershey, Christine L, und David E Fisher. 2004. „Mitf and Tfe3: Members of a b-HLH-ZIP Transcription Factor Family Essential for Osteoclast Development and Function“. *Bone* 34 (4): 689–96. <https://doi.org/10.1016/j.bone.2003.08.014>.

Hodges, Emily, Antoine Molaro, Camila O. Dos Santos, Pramod Thekkat, Qiang Song, Philip J. Uren, Jin Park, et al. 2011. „Directional DNA Methylation Changes and Complex Intermediate States Accompany Lineage Specificity in the Adult Hematopoietic Compartment“. *Molecular Cell* 44 (1): 17–28. <https://doi.org/10.1016/j.molcel.2011.08.026>.

Hon, Gary C., Chun-Xiao Song, Tingting Du, Fulai Jin, Siddarth Selvaraj, Ah Young Lee, Chia-an Yen, et al. 2014. „5mC Oxidation by Tet2 Modulates Enhancer Activity and Timing of Transcriptome Reprogramming during Differentiation“. *Molecular Cell* 56 (2): 286–97. <https://doi.org/10.1016/j.molcel.2014.08.026>.

Houghton, Franchesca D. 2006. „Energy Metabolism of the Inner Cell Mass and Trophectoderm of the Mouse Blastocyst“. *Differentiation* 74 (1): 11–18. <https://doi.org/10.1111/j.1432-0436.2006.00052.x>.

Hussein, Abdiasis M., Yuliang Wang, Julie Mathieu, Lilyana Margaretha, Chaozhong Song, Daniel C. Jones, Christopher Cavanaugh, et al. 2020. „Metabolic Control over mTOR-Dependent Diapause-like State“. *Developmental Cell* 52 (2): 236-250.e7. <https://doi.org/10.1016/j.devcel.2019.12.018>.

Ilik, Ibrahim Avsar, Tugce Aktas, Daniel Maticzka, Rolf Backofen, und Asifa Akhtar. 2020. „FLASH: Ultra-Fast Protocol to Identify RNA–Protein Interactions in Cells“. *Nucleic Acids Research* 48 (3): e15–e15. <https://doi.org/10.1093/nar/gkz1141>.

Ito, Shinsuke, Ana C. D'Alessio, Olena V. Taranova, Kwonho Hong, Lawrence C. Sowers, und Yi Zhang. 2010. „Role of Tet Proteins in 5mC to 5hmC Conversion, ES-Cell Self-Renewal and Inner Cell Mass Specification“. *Nature* 466 (7310): 1129–33. <https://doi.org/10.1038/nature09303>.

Iyer, Lakshminarayan M., Mamta Tahiliani, Anjana Rao, und L. Aravind. 2009. „Prediction of Novel Families of Enzymes Involved in Oxidative and Other Complex Modifications of Bases in Nucleic Acids“. *Cell Cycle* 8 (11): 1698–1710. <https://doi.org/10.4161/cc.8.11.8580>.

Jachowicz, Joanna W, Xinyang Bing, Julien Pontabry, Ana Bošković, Oliver J Rando, and Maria-Elena Torres-Padilla. 2017. “LINE-1 Activation after Fertilization Regulates Global Chromatin Accessibility in the Early Mouse Embryo.” *Nature Genetics* 49 (10): 1502–10. <https://doi.org/10.1038/ng.3945>.

Jurka, J., V.V. Kapitonov, A. Pavlicek, P. Klonowski, O. Kohany, und J. Walichiewicz. 2005. „Rebase Update, a Database of Eukaryotic Repetitive Elements“. *Cytogenetic and Genome Research* 110 (1–4): 462–67. <https://doi.org/10.1159/000084979>.

Kagey, Michael H., Jamie J. Newman, Steve Bilodeau, Ye Zhan, David A. Orlando, Nynke L. Van Berkum, Christopher C. Ebmeier, et al. 2010. „Mediator and Cohesin Connect Gene Expression and Chromatin Architecture“. *Nature* 467 (7314): 430–35. <https://doi.org/10.1038/nature09380>.

Kamemizu, Chizuru, und Toshihiko Fujimori. 2019. „Distinct Dormancy Progression Depending on Embryonic Regions during Mouse Embryonic Diapause†“. *Biology of Reproduction* 100 (5): 1204–14. <https://doi.org/10.1093/biolre/ioz017>.

Kamiya, Daisuke, Satoe Banno, Noriaki Sasai, Masatoshi Ohgushi, Hidehiko Inomata, Kiichi Watanabe, Masako Kawada, et al. 2011. „Intrinsic Transition of Embryonic Stem-Cell Differentiation into Neural Progenitors“. *Nature* 470 (7335): 503–9. <https://doi.org/10.1038/nature09726>.

Karttunen, Konsta, Divyesh Patel, Jihan Xia, Liangru Fei, Kimmo Palin, Lauri Aaltonen, und Biswajyoti Sahu. 2023. „Transposable Elements as Tissue-Specific Enhancers in Cancers of

Endodermal Lineage“. *Nature Communications* 14 (1): 5313. <https://doi.org/10.1038/s41467-023-41081-4>.

Katz, Jonathan P., Nathalie Perreault, Bree G. Goldstein, Catherine S. Lee, Patricia A. Labosky, Vincent W. Yang, und Klaus H. Kaestner. 2002. „The Zinc-Finger Transcription Factor Klf4 Is Required for Terminal Differentiation of Goblet Cells in the Colon“. *Development* 129 (11): 2619–28. <https://doi.org/10.1242/dev.129.11.2619>.

Kaya-Okur, Hatice S., Steven J. Wu, Christine A. Codomo, Erica S. Pledger, Terri D. Bryson, Jorja G. Henikoff, Kami Ahmad, und Steven Henikoff. 2019. „CUT&Tag for Efficient Epigenomic Profiling of Small Samples and Single Cells“. *Nature Communications* 10 (1): 1930. <https://doi.org/10.1038/s41467-019-09982-5>.

Khoa, Le Tran Phuc, Yao-Chang Tsan, Fengbiao Mao, Daniel M. Kremer, Peter Sajjakulnukit, Li Zhang, Bo Zhou, et al. 2020. „Histone Acetyltransferase MOF Blocks Acquisition of Quiescence in Ground-State ESCs through Activating Fatty Acid Oxidation“. *Cell Stem Cell* 27 (3): 441-458.e10. <https://doi.org/10.1016/j.stem.2020.06.005>.

Kim, J. 2003. „Methylation-sensitive binding of transcription factor YY1 to an insulator sequence within the paternally expressed imprinted gene, *Peg3*“. *Human Molecular Genetics* 12 (3): 233–45. <https://doi.org/10.1093/hmg/ddg028>.

Kinder, Michelle, Cong Wei, Suresh G. Shelat, Mondira Kundu, Liang Zhao, Ian A. Blair, und Ellen Puré. 2010. „Hematopoietic Stem Cell Function Requires 12/15-Lipoxygenase–Dependent Fatty Acid Metabolism“. *Blood* 115 (24): 5012–22. <https://doi.org/10.1182/blood-2009-09-243139>.

Koh, Kian Peng, Akiko Yabuuchi, Sridhar Rao, Yun Huang, Kerriane Cunniff, Julie Nardone, Asta Laiho, et al. 2011. „Tet1 and Tet2 Regulate 5-Hydroxymethylcytosine Production and Cell Lineage Specification in Mouse Embryonic Stem Cells“. *Cell Stem Cell* 8 (2): 200–213. <https://doi.org/10.1016/j.stem.2011.01.008>.

Kolodziejczyk, Aleksandra A., Jong Kyoung Kim, Jason C.H. Tsang, Tomislav Ilicic, Johan Henriksson, Kedar N. Natarajan, Alex C. Tuck, et al. 2015. „Single Cell RNA-Sequencing of

Pluripotent States Unlocks Modular Transcriptional Variation“. *Cell Stem Cell* 17 (4): 471–85. <https://doi.org/10.1016/j.stem.2015.09.011>.

Kreibich, Elisa, Rozemarijn Kleinendorst, Guido Barzaghi, Sarah Kaspar, und Arnaud R. Krebs. 2023. „Single-Molecule Footprinting Identifies Context-Dependent Regulation of Enhancers by DNA Methylation“. *Molecular Cell* 83 (5): 787-802.e9. <https://doi.org/10.1016/j.molcel.2023.01.017>.

Lam, Ulysses Tsz Fung, Bryan Kok Yan Tan, John Jia Xin Poh, und Ee Sin Chen. 2022. „Structural and Functional Specificity of H3K36 Methylation“. *Epigenetics & Chromatin* 15 (1): 17. <https://doi.org/10.1186/s13072-022-00446-7>.

Lan, Jie, Nicholas Rajan, Martin Bizet, Audrey Penning, Nitesh K. Singh, Diana Guallar, Emilie Calonne, et al. 2020. „Functional Role of Tet-Mediated RNA Hydroxymethylcytosine in Mouse ES Cells and during Differentiation“. *Nature Communications* 11 (1): 4956. <https://doi.org/10.1038/s41467-020-18729-6>.

Lee, Jong-Eun, Hyun-Ah Oh, Haengseok Song, Jin Hyun Jun, Cheong-Rae Roh, Huirong Xie, S. K. Dey, und Hyunjung Jade Lim. 2011. „Autophagy Regulates Embryonic Survival During Delayed Implantation“. *Endocrinology* 152 (5): 2067–75. <https://doi.org/10.1210/en.2010-1456>.

Leitch, Harry G, Kirsten R McEwen, Aleksandra Turp, Vesela Encheva, Tom Carroll, Nils Grabole, William Mansfield, et al. 2013. „Naive Pluripotency Is Associated with Global DNA Hypomethylation“. *Nature Structural & Molecular Biology* 20 (3): 311–16. <https://doi.org/10.1038/nsmb.2510>.

Li, Juying, Jun S. Song, Robert J. A. Bell, Thanh-Nga T. Tran, Rizwan Haq, Huifei Liu, Kevin T. Love, et al. 2012. „YY1 Regulates Melanocyte Development and Function by Cooperating with MITF“. Herausgegeben von Marcus Bosenberg. *PLoS Genetics* 8 (5): e1002688. <https://doi.org/10.1371/journal.pgen.1002688>.

Li, Mo, und Juan Carlos Izpisua Belmonte. 2017. „Ground Rules of the Pluripotency Gene Regulatory Network“. *Nature Reviews Genetics* 18 (3): 180–91. <https://doi.org/10.1038/nrg.2016.156>.

Lister, Ryan, Mattia Pelizzola, Robert H. Dowen, R. David Hawkins, Gary Hon, Julian Tonti-Filippini, Joseph R. Nery, et al. 2009. „Human DNA Methylomes at Base Resolution Show Widespread Epigenomic Differences“. *Nature* 462 (7271): 315–22. <https://doi.org/10.1038/nature08514>.

Loh, Yuin-Han, Qiang Wu, Joon-Lin Chew, Vinsensius B Vega, Weiwei Zhang, Xi Chen, Guillaume Bourque, et al. 2006. „The Oct4 and Nanog Transcription Network Regulates Pluripotency in Mouse Embryonic Stem Cells“. *Nature Genetics* 38 (4): 431–40. <https://doi.org/10.1038/ng1760>.

Lorsbach, R B, J Moore, S Mathew, S C Raimondi, S T Mukatira, und J R Downing. 2003. „TET1, a Member of a Novel Protein Family, Is Fused to MLL in Acute Myeloid Leukemia Containing the t(10;11)(Q22;Q23)“. *Leukemia* 17 (3): 637–41. <https://doi.org/10.1038/sj.leu.2402834>.

Lu, Falong, Yuting Liu, Lan Jiang, Shinpei Yamaguchi, und Yi Zhang. 2014. „Role of Tet Proteins in Enhancer Activity and Telomere Elongation“. *Genes & Development* 28 (19): 2103–19. <https://doi.org/10.1101/gad.248005.114>.

MacLean Hunter, Susan, und Martin Evans. 1999. „Non-Surgical Method for the Induction of Delayed Implantation and Recovery of Viable Blastocysts in Rats and Mice by the Use of Tamoxifen and Depo-Provera“. *Molecular Reproduction and Development* 52 (1): 29–32. [https://doi.org/10.1002/\(SICI\)1098-2795\(199901\)52:1<29::AID-MRD4>3.0.CO;2-2](https://doi.org/10.1002/(SICI)1098-2795(199901)52:1<29::AID-MRD4>3.0.CO;2-2).

Maharana, Shovamayee, K. Venkatesan Iyer, Nikhil Jain, Mallika Nagarajan, Yejun Wang, und G. V. Shivashankar. 2016. „Chromosome Intermingling—the Physical Basis of Chromosome Organization in Differentiated Cells“. *Nucleic Acids Research* 44 (11): 5148–60. <https://doi.org/10.1093/nar/gkw131>.

Maiti, Atanu, und Alexander C. Drohat. 2011. „Thymine DNA Glycosylase Can Rapidly Excise 5-Formylcytosine and 5-Carboxylcytosine“. *Journal of Biological Chemistry* 286 (41): 35334–38. <https://doi.org/10.1074/jbc.C111.284620>.

Marks, Hendrik, Tüzer Kalkan, Roberta Menafra, Sergey Denissov, Kenneth Jones, Helmut Hofemeister, Jennifer Nichols, et al. 2012. „The Transcriptional and Epigenomic Foundations of Ground State Pluripotency“. *Cell* 149 (3): 590–604. <https://doi.org/10.1016/j.cell.2012.03.026>.

Masui, Shinji, Yuhki Nakatake, Yayoi Toyooka, Daisuke Shimosato, Rika Yagi, Kazue Takahashi, Hitoshi Okochi, et al. 2007. „Pluripotency Governed by Sox2 via Regulation of Oct3/4 Expression in Mouse Embryonic Stem Cells“. *Nature Cell Biology* 9 (6): 625–35. <https://doi.org/10.1038/ncb1589>.

McCORMACK, J. T., und G. S. Greenwald. 1974. „PROGESTERONE AND OESTRADIOL-17 $\beta$  CONCENTRATIONS IN THE PERIPHERAL PLASMA DURING PREGNANCY IN THE MOUSE“. *Journal of Endocrinology* 62 (1): 101–7. <https://doi.org/10.1677/joe.0.0620101>.

Meissner, Alexander, Tarjei S. Mikkelsen, Hongcang Gu, Marius Wernig, Jacob Hanna, Andrey Sivachenko, Xiaolan Zhang, et al. 2008. „Genome-Scale DNA Methylation Maps of Pluripotent and Differentiated Cells“. *Nature* 454 (7205): 766–70. <https://doi.org/10.1038/nature07107>.

Meléndez-Ramírez, César, Raquel Cuevas-Díaz Duran, Tonatiuh Barrios-García, Mayela Giacomán-Lozano, Adolfo López-Ornelas, Jessica Herrera-Gamboa, Enrique Estudillo, Ernesto Soto-Reyes, Iván Velasco, und Víctor Treviño. 2021. „Dynamic Landscape of Chromatin Accessibility and Transcriptomic Changes during Differentiation of Human Embryonic Stem Cells into Dopaminergic Neurons“. *Scientific Reports* 11 (1): 16977. <https://doi.org/10.1038/s41598-021-96263-1>.

Meshorer, Eran, Dhananjay Yellajoshula, Eric George, Peter J. Scambler, David T. Brown, und Tom Misteli. 2006. „Hyperdynamic Plasticity of Chromatin Proteins in Pluripotent

Embryonic Stem Cells“. *Developmental Cell* 10 (1): 105–16. <https://doi.org/10.1016/j.devcel.2005.10.017>.

Mitsui, Kaoru, Yoshimi Tokuzawa, Hiroaki Itoh, Kohichi Segawa, Mirei Murakami, Kazutoshi Takahashi, Masayoshi Maruyama, Mitsuyo Maeda, and Shinya Yamanaka. 2003. „The Homeoprotein Nanog Is Required for Maintenance of Pluripotency in Mouse Epiblast and ES Cells“. *Cell* 113 (5): 631–42. [https://doi.org/10.1016/S0092-8674\(03\)00393-3](https://doi.org/10.1016/S0092-8674(03)00393-3).

Monteagudo-Sánchez, Ana, Julien Richard Albert, Margherita Scarpa, Daan Noordermeer, und Maxim V.C. Greenberg. 2023. „The Embryonic DNA Methylation Program Modulates the Cis-Regulatory Landscape via CTCF Antagonism“. Preprint. *Molecular Biology*. <https://doi.org/10.1101/2023.11.16.567349>.

Moore, Lisa D, Thuc Le, und Guoping Fan. 2013. „DNA Methylation and Its Basic Function“. *Neuropsychopharmacology* 38 (1): 23–38. <https://doi.org/10.1038/npp.2012.112>.

Morozumi, Yuichi, Fayçal Boussouar, Minjia Tan, Apirat Chaikuad, Mahya Jamshidikia, Gozde Colak, Huang He, et al. 2016. „Atad2 Is a Generalist Facilitator of Chromatin Dynamics in Embryonic Stem Cells“. *Journal of Molecular Cell Biology* 8 (4): 349–62. <https://doi.org/10.1093/jmcb/mjv060>.

Naeslund, Grels. 1979. „The Effect of Glucose-, Arginine- and Leucine-Deprivation on Mouse Blastocyst Outgrowth In Vitro“. *Uppsala Journal of Medical Sciences* 84 (1): 9–20. <https://doi.org/10.3109/03009737909179136>.

Neri, F, D Dettori, D Incarnato, A Krepelova, S Rapelli, M Maldotti, C Parlato, P Paliogiannis, und S Oliviero. 2015. „TET1 Is a Tumour Suppressor That Inhibits Colon Cancer Growth by Derepressing Inhibitors of the WNT Pathway“. *Oncogene* 34 (32): 4168–76. <https://doi.org/10.1038/onc.2014.356>.

Ng, Huck-Hui, und M. Azim Surani. 2011. „The Transcriptional and Signalling Networks of Pluripotency“. *Nature Cell Biology* 13 (5): 490–96. <https://doi.org/10.1038/ncb0511-490>.

Nichols, Jennifer, Branko Zevnik, Konstantinos Anastasiadis, Hitoshi Niwa, Daniela Klewe-Nebenius, Ian Chambers, Hans Schöler, und Austin Smith. 1998. „Formation of Pluripotent Stem Cells in the Mammalian Embryo Depends on the POU Transcription Factor Oct4“. *Cell* 95 (3): 379–91. [https://doi.org/10.1016/S0092-8674\(00\)81769-9](https://doi.org/10.1016/S0092-8674(00)81769-9).

Ono, Ryoichi, Tomohiko Taki, Takeshi Taketani, Masafumi Taniwaki, Hajime Kobayashi, und Yasuhide Hayashi. 2002. „LCX, Leukemia-associated Protein with a CXXC Domain, Is Fused to MLL in Acute Myeloid Leukemia with Trilineage Dysplasia Having t(10;11)(q22;q23)1“. *Cancer Research* 62 (14): 4075–80.

Pantier, Raphaël, Tülin Tatar, Douglas Colby, und Ian Chambers. 2019. „Endogenous Epitope-Tagging of Tet1 , Tet2 and Tet3 Identifies TET2 as a Naïve Pluripotency Marker“. *Life Science Alliance* 2 (5): e201900516. <https://doi.org/10.26508/lsa.201900516>.

Percharde, Michelle, Aydan Bulut-Karslioglu, und Miguel Ramalho-Santos. 2017. „Hypertranscription in Development, Stem Cells, and Regeneration“. *Developmental Cell* 40 (1): 9–21. <https://doi.org/10.1016/j.devcel.2016.11.010>.

Percharde, Michelle, Chih-Jen Lin, Yafei Yin, Juan Guan, Gabriel A. Peixoto, Aydan Bulut-Karslioglu, Steffen Biechele, Bo Huang, Xiaohua Shen, und Miguel Ramalho-Santos. 2018. „A LINE1-Nucleolin Partnership Regulates Early Development and ESC Identity“. *Cell* 174 (2): 391-405.e19. <https://doi.org/10.1016/j.cell.2018.05.043>.

Phan, Tri Giang, und Peter I. Croucher. 2020. „The Dormant Cancer Cell Life Cycle“. *Nature Reviews Cancer* 20 (7): 398–411. <https://doi.org/10.1038/s41568-020-0263-0>.

Phillips, Jennifer E., und Victor G. Corces. 2009. „CTCF: Master Weaver of the Genome“. *Cell* 137 (7): 1194–1211. <https://doi.org/10.1016/j.cell.2009.06.001>.

Piunti, Andrea, und Ali Shilatifard. 2016. „Epigenetic Balance of Gene Expression by Polycomb and COMPASS Families“. *Science* 352 (6290): aad9780. <https://doi.org/10.1126/science.aad9780>.



Ptak, Grazyna E., Emanuela Tacconi, Marta Czernik, Paola Toschi, Jacek A. Modlinski, and Pasqualino Loi. 2012. „Embryonic Diapause Is Conserved across Mammals“. Herausgegeben von Wendy Dean. PLoS ONE 7 (3): e33027. <https://doi.org/10.1371/journal.pone.0033027>.

Rao, Satyanarayan, Tsu-Pei Chiu, Judith F. Kribelbauer, Richard S. Mann, Harmen J. Bussemaker, und Remo Rohs. 2018. „Systematic Prediction of DNA Shape Changes Due to CpG Methylation Explains Epigenetic Effects on Protein–DNA Binding“. *Epigenetics & Chromatin* 11 (1): 6. <https://doi.org/10.1186/s13072-018-0174-4>.

Renfree, M. B., und G. Shaw. 2000. „Diapause“. *Annual Review of Physiology* 62: 353–75. <https://doi.org/10.1146/annurev.physiol.62.1.353>.

Rodrik-Outmezguine, Vanessa S., Masanori Okaniwa, Zhan Yao, Chris J. Novotny, Claire McWhirter, Arpitha Banaji, Helen Won, et al. 2016. „Overcoming mTOR Resistance Mutations with a New-Generation mTOR Inhibitor“. *Nature* 534 (7606): 272–76. <https://doi.org/10.1038/nature17963>.

Saxton, Robert A., und David M. Sabatini. 2017. „mTOR Signaling in Growth, Metabolism, and Disease“. *Cell* 168 (6): 960–76. <https://doi.org/10.1016/j.cell.2017.02.004>.

Schlesinger, Sharon, und Eran Meshorer. 2019. „Open Chromatin, Epigenetic Plasticity, and Nuclear Organization in Pluripotency“. *Developmental Cell* 48 (2): 135–50. <https://doi.org/10.1016/j.devcel.2019.01.003>.

Shanak, Siba, and Volkhard Helms. 2020. “DNA Methylation and the Core Pluripotency Network.” *Developmental Biology* 464 (2): 145–60. <https://doi.org/10.1016/j.ydbio.2020.06.001>.

Shu, Jian, Chen Wu, Yetao Wu, Zhiyuan Li, Sida Shao, Wenhui Zhao, Xing Tang, et al. 2013. „Induction of Pluripotency in Mouse Somatic Cells with Lineage Specifiers“. *Cell* 153 (5): 963–75. <https://doi.org/10.1016/j.cell.2013.05.001>.

Smith, Austin. 2017. „Formative Pluripotency: The Executive Phase in a Developmental Continuum“. *Development* 144 (3): 365–73. <https://doi.org/10.1242/dev.142679>.

Snow, M. H. L. 1977. „Gastrulation in the Mouse : Growth and Regionalization of the Epiblast“. *Development* 42 (1): 293–303. <https://doi.org/10.1242/dev.42.1.293>.

Sookdeo, Akash, Crystal M Hepp, Marcella A McClure, und Stéphane Boissinot. 2013. „Revisiting the Evolution of Mouse LINE-1 in the Genomic Era“. *Mobile DNA* 4 (1): 3. <https://doi.org/10.1186/1759-8753-4-3>.

Sousa, Maria Inês, Bibiana Correia, Ana Sofia Rodrigues, und João Ramalho-Santos. 2020. „Metabolic Characterization of a Paused-like Pluripotent State“. *Biochimica et Biophysica Acta (BBA) - General Subjects* 1864 (8): 129612. <https://doi.org/10.1016/j.bbagen.2020.129612>.

Spruijt, Cornelia G., Felix Gnerlich, Arne H. Smits, Toni Pfaffeneder, Pascal W.T.C. Jansen, Christina Bauer, Martin Münzel, et al. 2013. „Dynamic Readers for 5-(Hydroxy)Methylcytosine and Its Oxidized Derivatives“. *Cell* 152 (5): 1146–59. <https://doi.org/10.1016/j.cell.2013.02.004>.

Stadler, Michael B., Rabih Murr, Lukas Burger, Robert Ivanek, Florian Lienert, Anne Schöler, Erik Van Nimwegen, et al. 2011. „DNA-Binding Factors Shape the Mouse Methylome at Distal Regulatory Regions“. *Nature* 480 (7378): 490–95. <https://doi.org/10.1038/nature10716>.

Stewart, Colin L., Petr Kaspar, Lisa J. Brunet, Harshida Bhatt, Inder Gadi, Frank Köntgen, und Susan J. Abbonozzo. 1992. „Blastocyst Implantation Depends on Maternal Expression of Leukaemia Inhibitory Factor“. *Nature* 359 (6390): 76–79. <https://doi.org/10.1038/359076a0>.

Tahiliani, Mamta, Kian Peng Koh, Yinghua Shen, William A. Pastor, Hozefa Bandukwala, Yevgeny Brudno, Suneet Agarwal, et al. 2009. „Conversion of 5-Methylcytosine to 5-Hydroxymethylcytosine in Mammalian DNA by MLL Partner TET1“. *Science* 324 (5929): 930–35. <https://doi.org/10.1126/science.1170116>.

Takahashi, Kazutoshi, und Shinya Yamanaka. 2006. „Induction of Pluripotent Stem Cells from Mouse Embryonic and Adult Fibroblast Cultures by Defined Factors“. *Cell* 126 (4): 663–76. <https://doi.org/10.1016/j.cell.2006.07.024>.

Taylor, Gillian C.A., Ragnhild Eskeland, Betül Hekimoglu-Balkan, Madapura M. Pradeepa, und Wendy A. Bickmore. 2013. „H4K16 Acetylation Marks Active Genes and Enhancers of Embryonic Stem Cells, but Does Not Alter Chromatin Compaction“. *Genome Research* 23 (12): 2053–65. <https://doi.org/10.1101/gr.155028.113>.

Tran, Khoa A., Caleb M. Dillingham, und Rupa Sridharan. 2019. „The Role of  $\alpha$ -Ketoglutarate-Dependent Proteins in Pluripotency Acquisition and Maintenance“. *Journal of Biological Chemistry* 294 (14): 5408–19. <https://doi.org/10.1074/jbc.TM118.000831>.

Tsompana, Maria, und Michael J Buck. 2014. „Chromatin Accessibility: A Window into the Genome“. *Epigenetics & Chromatin* 7 (1): 33. <https://doi.org/10.1186/1756-8935-7-33>.

Van Der Weijden, Vera A., und Aydan Bulut-Karslioglu. 2021. „Molecular Regulation of Paused Pluripotency in Early Mammalian Embryos and Stem Cells“. *Frontiers in Cell and Developmental Biology* 9 (Juli): 708318. <https://doi.org/10.3389/fcell.2021.708318>.

Van Der Weijden, Vera A., Maximilian Stötzel, Dhanur P. Iyer, Beatrix Fauler, Elzbieta Gralinska, Mohammed Shahraz, David Meierhofer, et al. 2024. „FOXO1-Mediated Lipid Metabolism Maintains Mammalian Embryos in Dormancy“. *Nature Cell Biology*, Januar. <https://doi.org/10.1038/s41556-023-01325-3>.

Visel, Axel, Edward M. Rubin, und Len A. Pennacchio. 2009. „Genomic Views of Distant-Acting Enhancers“. *Nature* 461 (7261): 199–205. <https://doi.org/10.1038/nature08451>.

Watt, F, und P L Molloy. 1988. „Cytosine Methylation Prevents Binding to DNA of a HeLa Cell Transcription Factor Required for Optimal Expression of the Adenovirus Major Late Promoter.“ *Genes & Development* 2 (9): 1136–43. <https://doi.org/10.1101/gad.2.9.1136>.

Weintraub, Abraham S., Charles H. Li, Alicia V. Zamudio, Alla A. Sigova, Nancy M. Hannett, Daniel S. Day, Brian J. Abraham, et al. 2017. „YY1 Is a Structural Regulator of

Enhancer-Promoter Loops“. *Cell* 171 (7): 1573-1588.e28.  
<https://doi.org/10.1016/j.cell.2017.11.008>.

Weirath, Nicholas A., Alexander K. Hurben, Christopher Chao, Suresh S. Pujari, Tao Cheng, Shujun Liu, and Natalia Y. Tretyakova. 2022. “Small Molecule Inhibitors of TET Dioxygenases: Bobcat339 Activity Is Mediated by Contaminating Copper(II).” *ACS Medicinal Chemistry Letters* 13 (5): <https://doi.org/10.1021/acsmchemlett.1c00677>.

Wu, Weixin, Zhangming Yan, Tri C. Nguyen, Zhen Bouman Chen, Shu Chien, und Sheng Zhong. 2019. „Mapping RNA–Chromatin Interactions by Sequencing with iMARGI“. *Nature Protocols* 14 (11): 3243–72. <https://doi.org/10.1038/s41596-019-0229-4>.

Xu, Yufei, Feizhen Wu, Li Tan, Lingchun Kong, Lijun Xiong, Jie Deng, Andrew J. Barbera, et al. 2011. „Genome-Wide Regulation of 5hmC, 5mC, and Gene Expression by Tet1 Hydroxylase in Mouse Embryonic Stem Cells“. *Molecular Cell* 42 (4): 451–64. <https://doi.org/10.1016/j.molcel.2011.04.005>.

Yang, Yiqi, and Gang Li. 2020. “Post-Translational Modifications of PRC2: Signals Directing Its Activity.” *Epigenetics & Chromatin* 13 (1): 47. <https://doi.org/10.1186/s13072-020-00369-1>.

Yin, Yimeng, Ekaterina Morgunova, Arttu Jolma, Eevi Kaasinen, Biswajyoti Sahu, Syed Khund-Sayeed, Pratyush K. Das, et al. 2017. „Impact of Cytosine Methylation on DNA Binding Specificities of Human Transcription Factors“. *Science* 356 (6337): eaaj2239. <https://doi.org/10.1126/science.aaj2239>.

Ying, Qi-Long, Jason Wray, Jennifer Nichols, Laura Batlle-Morera, Bradley Doble, James Woodgett, Philip Cohen, und Austin Smith. 2008. „The Ground State of Embryonic Stem Cell Self-Renewal“. *Nature* 453 (7194): 519–23. <https://doi.org/10.1038/nature06968>.

Yoshinaga, K., und C. E. Adams. 1966. „DELAYED IMPLANTATION IN THE SPAYED, PROGESTERONE TREATED ADULT MOUSE“. *Reproduction* 12 (3): 593–95. <https://doi.org/10.1530/jrf.0.0120593>.

Zaret, Kenneth S., and Jason S. Carroll. 2011. „Pioneer Transcription Factors: Establishing Competence for Gene Expression“. *Genes & Development* 25 (21): 2227–41. <https://doi.org/10.1101/gad.176826.111>.

Zhang, Xinchao, Yue Zhang, Chaofu Wang, and Xu Wang. 2023. „TET (Ten-Eleven Translocation) Family Proteins: Structure, Biological Functions and Applications“. *Signal Transduction and Targeted Therapy* 8 (1): 297. <https://doi.org/10.1038/s41392-023-01537-x>.

Zhu, Fugui, Qianshu Zhu, Dan Ye, Qingquan Zhang, Yiwei Yang, Xudong Guo, Zhenping Liu, et al. 2018. „Sin3a–Tet1 Interaction Activates Gene Transcription and Is Required for Embryonic Stem Cell Pluripotency“. *Nucleic Acids Research* 46 (12): 6026–40. <https://doi.org/10.1093/nar/gky347.5>. Bibliography